Contribution des propriétés du micro-environnement sur l'adhésion cellulaire

Kalpana Mandal

UNIVERSITÉ DE GRENOBLE

THÈSE

Pour obtenir le grade de

DOCTEUR DE L'UNIVERSITÉ DE GRENOBLE

Spécialité : **Physique pour les sciences du vivant**

Arrêté ministérial : 7 aout 2006

Présentée par

Kalpana Mandal

Thèse dirigée par **Prof. Antoine Delon**
et codirigée par **Dr. Martial Balland**

préparée au sein **Laboratoire interdisciplinaire de Physique**
et de **l'Ecole doctorale de Physique**

Role of ECM Physical Properties on Force Distribution and Cell Internal Organization

Thèse soutenue publiquement le **(26th September 2012)**,
devant le jury composé de :

Prof. Atef Asnacios
University Paris-Diderot, Rapporteur

Dr. Olivier Theodoly
Aix Marseille University, Rapporteur

Prof. Bertrand Fourcade
Joseph Fourier University, Grenoble, Examinateur

Asst. Prof. Martial Balland
Joseph Fourier University, Grenoble, Examinateur

Prof. Antoine Delon
Joseph Fourier University, Grenoble, Directeur de thèse

Asst. Prof. Martial Balland
Joseph Fourier University, Grenoble, Co-Directeur de thèse

Acknowledgement:

First of all, I would like to thank my supervisor Dr. Martial Balland for his guidance, support,enthusiasm throughout my Ph.D. program. It was always encouraging to discuss science with him. He provided all the best possible environment to make my experiments work. I would like to acknowledge Dr. Irne Wang for her guidance, patience and valuable involvement during the period of my graduate research. I had many great discussions with her which helped me a lot in understanding many things in a better way. I would like to convey my sincere regards and respect to Dr. Lionel Bureau for sharing his knowledge with me. It was very nice working with him. I acknowledge financial support from Nanoscience Foundation.

My sincere thanks Dr. Antoine Delon for his support. I convey my deep regards to Dr. Olivier Destaing for his generous help by providing all biological samples. I would like to thank Dr. Beniot Ladoux for his involvement. I would like to thank Dr. Manual Thery for sharing knowledge with us.
I would specially like to thank to Jessie Sitbon for helping me in all administrative matter. I would like to thank Mr. Phillipe for all the technical support he provided. I would like to thank all my co-colleagues in the lab Dr. Aurlien Pennec, Dr. Jean-Claude Vial, Mrs. Mike Kloster Landsburg, Dr. Charles-Edouard Leroux, Ms Rachel Milloud, Dr. Ananda Kumar soshee, Mr. Michal Garcia, Dr. Madhu Priya, Dr. Dipanwita Biswas for all the supports in and outside the lab. I would like to thank my former colleague friends Jie Gao, Qingzong Tseng, Edith, Aparna and Valentina. It has been a very good stay in Grenoble during my PhD work. I would like to thank all my friends in Grenoble who made my stay memorable.

I would sincerely thank my very special friends Monamie Sanyal and Shreya Ghatak. I will always cherish the moments I have spent with them.
I gratefully acknowledge my Late didima for always motivating me to move forward. I am greatful to my parents for their understanding, unconditional support

and believe on me. Lovingly, I acknowldge my brothers; borda, mejhda and bhai, sister in law and tora for their love,care and encouragement. My thesis would have not been possible without the constant support I get from my family. I would like to acknowledge Anupam for his love, care, encouragement and support, courage he gave me.

Abstract

Cells ability to sense the mechanical properties of their microenvironment is a critical feature for tissue homeostasis. Current evidences suggest a bidirectional relationship between extracellular matrix physical properties and cell mechanical force generation in that process. To probe this complex functional mechanism, using single cell micropatterning, we have investigated how cell maintains mechanical integrity as they are submitted to biomechanical stimuli such as stifness or geometry changes in their local microenvironment. By quantifying cellular traction forces on 2D deformable micropatterned substrate, we were able to highlight the process by which cells maintain a mechanical balance by remodeling their own internal organization. Moreover, a direct comparison between cell traction forces developed on 2D micropatterned substrates with 3D micropillar systems gave us new insights in the characteristics of cell force generation in response to substrate topography. Finally, we have shown that cell architecture and intracellular organization can also be controlled by creating thermoresponsive PNIPAM micropattern which can also be used as microactuator to induce cell detachment, providing a new tool to the lab on chip field.

Résumé

La capacité des cellules à sentir les propriétés physiques de leur environnement est un facteur déterminant de l'homéostasie tissulaire. Des découvertes récentes mettent en avant un couplage direct entre les forces de traction cellulaires et les propriétés physique de la matrice extracellulaire dans ce processus. En utilisant la microscopie de traction de forces sur substrats micropatternés nous avons pu, en jouant sur des propriétés physique du substrat d'adhérence comme la rigidité ou la géométrie, mettre en évidence la capacité des cellules à moduler leur architecture interne afin de réguler leur état de tension mécanique. De plus nous avons, dans le cadre de cette thèse, développé une nouvelle technique de micropatterning permettant de créer des réseaux organisés de cellules adhérentes. Cette nouvelle technique repose sur l'utilisation d'un polymère thermosensible permettant de contrôler le détachement physique de cellules adhérentes.

Contents

1. An introduction to cell mechanics: a Physics view

1.1. Introduction:

It has emerged as an active area of research among biophysicists that adherent cells are able to sense the physical properties of extracellular matrix, especially substrate stiffness and geometry which influences the process of biomechanical regulatory mechanism [1, 2, 3, 4]. *In vivo*, cells adhere on a substrate called the extracellular matrix (ECM) [5, 6] which provides a substrate for cell anchorage, serves as a tissue scaffold, guides cell migration during embryonic development and wound repair, plays a key role in tissue morphogenesis [7, 8, 9]. Moreover, the extracellular matrix does not only provide a substrate for cell but, is also responsible for transmitting environmental signals to cells, which ultimately affects cell proliferation, differentiation and apoptosis [10, 11].

Forces, exerted or sensed by the cell, are further translated into biochemical signals. The ability of cells to integrate information from their environment is well known as mechanotransduction involving reciprocal integration of mechanical stimuli into biochemical signals. This property is mostly based on the activation of a family of transmembranous proteins that can create a dynamic mechanical continuum between the extracellular matrix and the cell internal architecture (such as cell cytoskeleton) [12]. Moreover, the plasticity of the mechanotransduction process is reinforced by the ability of transmembrane proteins like integrins to generate intracellular signalling in response to their mechanical activation. The physical properties

such as stiffness of the microenvironment that cell experiences needs to be taken into account when trying to understand the complex nature of cell signaling integrity. A stiffer matrix causes force-dependent aggregation and clustering of integrins resulting in elevated Rho-ROCK dependent cytoskeletal tension, which amplifies the formation and stabilization of focal adhesion assembly [13]. Thus mechanosensitive feedback modulates cell architecture, which in turn [14] affects cell functions in diverse processes such as migration, proliferation, differentiation, apoptosis and is crucial for organ development and homeostasis [15, 16, 17]. Improper regulation of biomechanical feedback loop, often caused by mutations or misregulation of proteins, that disturb cellular or extracellular mechanics, may lead to cancer progression and metastasis [18].

A variety of approaches (such as microcontact printing, micropillar method) have been made over last few years to make the link between ECM physical properties and cell internal architecture and their related forces [19, 20, 21, 22]. These studies provide great insights regarding the development of traction force at the cell ECM interface but, they impose numerous limitations. A major limitation arises from the morphological heterogeneity that cells adopt on these substrates. It becomes more complex to elucidate the relation between cytoskeletal architecture and cellular traction forces and that ultimately makes statistical analysis difficult. Moreover, *in vivo* cells encounter geometrical boundary conditions imposed by both ECM geometry and other cells which is not respected in classical culture. Thus, the underlying mechanism behind the way cell senses, redistributes and transmits forces in response to ECM geometry remains not fully understood. This thesis provides a new insight into the basic mechanisms behind the mechanotransduction process by linking cytoskeletal architecture, cell internal organization and cytoskeletal generated force by using traction force microscopy on micropatterned substrate.

Here we start by describing our model system: an eukaryotic cell. The schematic of our model system is given below in figure 1.1. The figure illustrates a cell adhering on a substrate via focal adhesion, forming connection to its internal cytoskeleton.

Next a short description of cellular internal structure is given. Finally we describe the existing mechanical relation between intracellular structure and force generation at the cell-ECM interface.

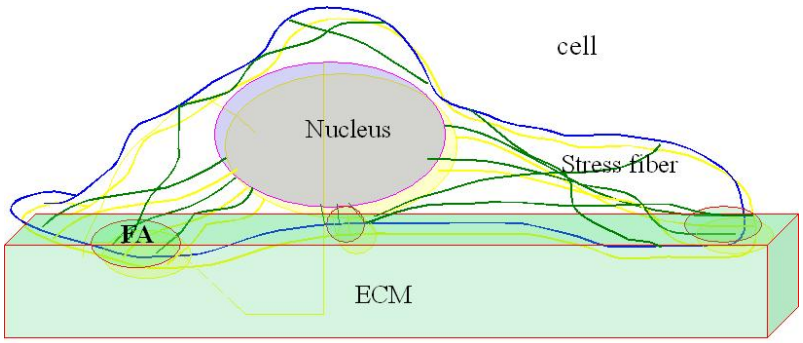

Figure 1.1.: *Schematic of Eukaryotic Cell and its environment.*

1.2. Cell internal architecture: the cytoskeleton

Cell cytoskeleton is a highly dynamic and complex fibrillar network. These cell cytoskeletons is polymer like structural mesh, which is responsible for maintaining cell architecture, internal tension balance and plays a crucial role in organelle positioning [23]. This dynamic meshwork reorganizes its structure during diverse cellular processes including cell division, migration, cell adhesion and intracellular transport. These reorganizations finally lead to specific arrangements of organelles within the cell which at larger scale participate to tissue organization.

The dynamic assembling and disassembling properties of the cytoskeleton polymers allow cell to feel and respond to changes in their micro-environment [24]. External signals propagate through these filaments from ECM (or neighbouring cells) to cell interior. The cytoskeleton is made up of three kinds of protein filaments, namely microtubules(MT), intermediate filaments (IFs) and actin filaments(AFs).

Many different proteins, called motor proteins, ensuring filament crosslinking and sliding are associated with each type of filaments. These molecular motors enable cells to generate tension and thus reorganize or adapt their shape within a living

tissue. Figure[1] 1.2 shows individual filament of all three types. Here is a description of each type of filament.

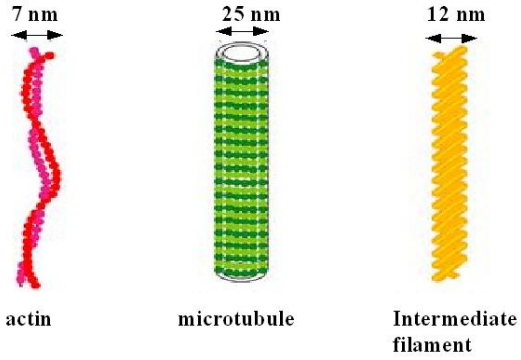

Figure 1.2.: *Schematic of single cytoskeleton filaments actin(red), MT(green), IF(yellow).*

1.2.1. Microtubules

Microtubules (MTs) are cylindrical polymers found in every eukaryotic cell. Microtubules are made of polymerized tubulin and form tubular shaped polymer mostly radially distributed from the centrosome (microtubule organizing center) to the plasma membrane. MT are strongly involved in maintaining cell structure, providing platforms for intracellular transport and spindle formation during mitosis. The basic structural properties like the number of protofilaments (microtubule basic brick), the radius of the tube, filament helical pitch have been well determined by electron microscopy by Chretien et al. 1995; [25]. Moreover, MTs play an important role in cell polarity by positioning the centrosome and in many types of cell interphase[23, 26], thanks to different motor protein interactions such as dynein.

1.2.2. Intermediate filaments

The intermediate filaments (IFs) are considered to be the most stable component of the cell cytoskeleton [27]. Many studies suggested that the dynamical IF network is involved in maintaining cell shape and rigidity, and serve to anchor in place several

[1] http://www.accessexcellence.org/LC/BEOn/data/phasethree/0030-beon/submission.php

organelles, including the nucleus and desmosomes. Intermediate filaments are also involved in formation of the nuclear lamina [28, 29]. IF form an heterogeneous family of cytoskeletal proteins such as vimentin, desmin, neurofilaments, and nestin which are expressed in mesenchymal, muscular, and neuronal tissues, respectively. It has the ability to self-assemble into 812 nm wide filaments [30]. Two central α-helical rod domain associate in parallel to form an elongated, extended coil-coil dimer and tetramer in similar fashion as shown in figure 1.3 [31]. When eight tetramers associate laterally, it results in a formation of a unit-length filaments (ULF) which has the ability, when associated to sustain extremely large deformation. Typically unit filaments (ULFs) are 60 nm long and 15 nm in diameter [32].

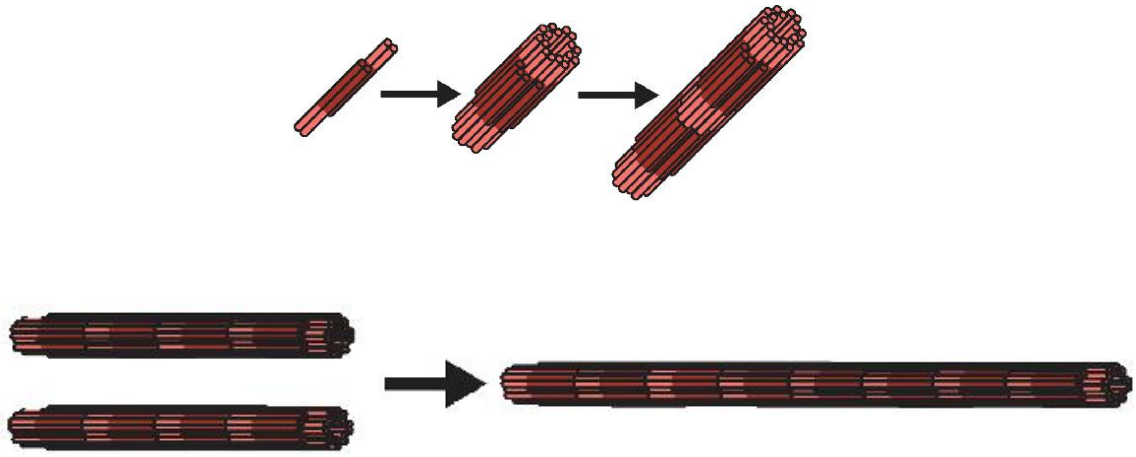

Figure 1.3.: *Intermediate Filament from single dimer to single filamental structure[31].*

1.2.3. Actin filaments

Actin filaments are long semi-flexible polymer like chain consisting of repeating subunit of actin monomers (G-actin). A single actin filament is 7-9 nm in diameter and is formed by directional actin polymerization which gives rise to (+) and (-) end of the filament (F-actin). ATP hydrolysis of G-actin helps conformational change which favors the disassembly of G-actin at the (-) end of actin filaments. The orientation of individual actin filament is a force-driven evolutionary process. The filaments are linked to the plasma membrane through the membrane-spanning proteins, allowing signals from the extracellular matrix to be transmitted to the

cytoskeleton, and vice versa. Actin is able to generate forces by two mechanisms. Firstly, by polymerization and depolymerization, actin filament promotes cell motility [33]at the leading edge of the cell and also subcellular structural movement [34]. Secondly, by interacting with myosin II, actin generates forces that lead to cell contractility [35]. It has been shown that, in cell migration, acto-myosin interaction generates contractile forces to move forward and retract at the back of the cell

The dynamics of actin cytoskeleton regulates many important cellular processes, including cell motility, cell division, cytokinesis, cell contractility and cell shape. Figure 1.4 shows actin network inside REF52 cell, labeled in green by F-actin immunostaining.

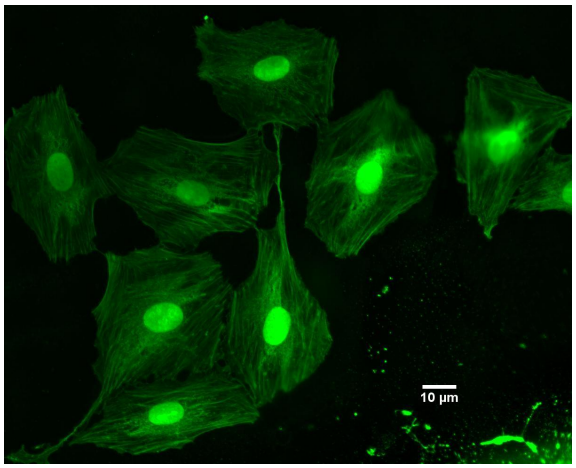

Figure 1.4.: In the actin cytoskeleton of REF52 cells, labelled with GFP-conjugated phalloidin (green).

1.3. Cell interaction with the extracellular matrix

The connection between cells and the underlying ECM are mediated by two types of integrin-dependant junctions: focal adhesion and hemidesmosomes. Focal adhesions are linked to the actin cytoskeleton while hemidesmosomes are linked to the intermediate filaments. As actin filaments are responsible for the generation of cellular traction forces here we focus on cell - ECM interaction through focal adhesions.

Adhesion receptors act as mechanosensors where physical signals (forces sensed or exerted by the cell) are converted into biochemical ones and are then propagated along the linked network of actin filaments and associated proteins by forming a physical linkage to the ECM with cell. Both this physical linkage and the mecanochemical transduction regulate many cell mophological behaviour including actin organization and cell microenvironmental adaptation Etc. Cells constantly probe the physical properties of their microenvironment through mechanotransduction processes involving continuous and bidirectional [8, 36] transduction of cytoskeleton generated forces in dynamic reorganizations of adhesive structures. Nevertheless, the precise mechanisms by which mechanical forces lead to eventual biochemical and molecular responses remain undefined. Now we try to focus on the main components which are involve in this bidirectional mechanism.

1.3.1. The extracellular matrix:

Extracellular matrix (ECM) is a complex structure, composed of many structural and nonstructural proteins assembled into an organized meshwork to give cell a support. *In vivo* extra cellular matrix provides a substrate for cell anchorage and behave as a tissue scaffold and maintains connectivity within tissue [37]. *In vivo* ECM is made and oriented by the cells within it. Moreover, different cell types are associated with different structures of ECM by changing organization, amount and type of proteins [38]. In tissue cell experiences 3D environment with different stiffness, geometry and signaling. Cell interaction with the extracellular matrix has dramatic effect on cell morphology. Numerous studies show the influence of ECM on cell by imposing geometrical restriction or by playing with biomechanical properties of the ECM on tissue mimicking model [39, 40, 41]. It has been shown by Engler et al. that by changing the stiffness of the substrate stem cell fate lineage specification can be controlled [4]. Indeed, monitoring for tissue stiffness is widespread technique in diseases screening like tumors [42, 43]

It is well known that ECM remodels the cell behavior and morphology. Conversely, cell also feeds to organize the ECM proteins which secreted from cell within by

exerting tension on the matrix [44]. Secreted proteins play a diverse role in regulating cell proliferation, migration and differentiation in vertebrate development [37]. The extracellular matrix contains a number of proteins (fibronectin, lamin, collagen) having multiple domains, and each of it has specific binding sites[45].

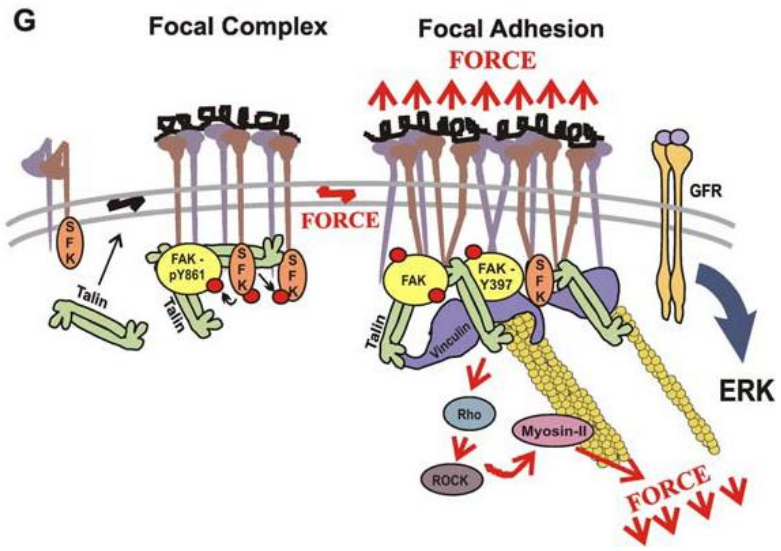

Figure 1.5.: FAs : Schematic of focal adhesion and focal complex. (Paszek et. al)

1.3.2. Cell - ECM linkage : focal adhesion and focal complex

Focal adhesions (FAs) are complex macromolecular structures which cross-link the extracellular matrix to the cell interior via membrane bound receptors [46]. Adhesions are mediated by transmembrane protein such as integrin superfamily(alpha, beta integrin) and molecular adaptors like paxillin, vinculin, tallin and many other proteins that make the link with the actin cytoskeleton. FAs are flat, elongated structures that are several square microns in area, and are often located near the periphery of cells [2]. These highly dynamic structures act as mechanosensor which play an important role in cell signaling or information processing, enabling cell to sense numerous extracellular signals that convey biochemical, mechanical and geometrical signals of the ECM (reviewed in [4]). In many primary processes like cell migration, morphogenesis, wound healing, focal adhesions play a leading role.

Initially, when cell starts adhering on the substrate, adhesion sites evolve from dot like structure of less than $1\mu m$ in diameter called nascent adhesions. These nascent adhesion sites are known to mature in focal complex. Focal complexes are short - lived structures, containing integrin [47], vinculin and paxillin. Their formation is induced by the Rho-family GTPase Rac. Focal complexes normally develop into focal adhesions (see figure 1.5) as a consequence of the activation of Rho [48, 49] or following the application of external force [13].

It is widely presumed that FA size is modulated by force to mediate changes in adhesion strength at different levels of cellular tension. Consistent with this idea, several studies have found a direct correlation between FA size and local traction force, indicating that the force per unit area, or stress, remains constant during FA maturation [13, 20]. However, other measurements have illustrated a more complex dependence. Recent study reported an inverse link between size and traction stress in the front of migrating cells, but found no such relationship in the cell rear [50]. Moreover, it has been shown that small FAs (1μm) exhibit variable levels of stress [51], and extremely large supermature FAs exert a high stress [52]. Conversely, a recent study [53] shows that a strong correlation between adhesion size and traction force exists only during the initial stages of myosin-mediated adhesion maturation and growth. However, for mature adhesions, no correlation between traction stress and size has been observed.

Adhesion assembly and maturation are highly dependent on the ECM environment which is believed to incite intracellular structural rearrangements that in turn foster the recruitment of additional proteins (growth) and induce signaling cascades leading to actin polymerization [54]. Transition of the focal complexes into focal adhesions is accompanied by transition of the associated actin mesh into densely packed straight bundles of filaments known as stress fibers [3]. Relation between focal adhesion with actin or force still remains in debate. Such knowledge is crucial for our understanding of force transmission at FAs and cellular mechanosensing. Next section contains more about the cell matrix interactions and its effect on cytoskeletal organization.

1.3.3. ECM-adhesion-cytoskeleton interactions

In tissue, biomechanical regulatory process are tightly regulated by maintaining cell shape and internal architecture [17, 23, 36]. ECM influence on cell internal organization has nicely been shown by Thery et al. [40]. Using glass micropatterning, they showed that ECM geometry, focal adhesion and actin are functionally linked. This work particularly revealed an intrinsic ability of cell to self-organize into a very reproducible manner in response to a given ECM geometry. Moreover, this bidirectional [55] interaction leads to change dynamically structure and molecular properties of adhesion sites in response to cytoskeletal reorganizing signals. These changes are mainly driven by the actomyosin contractile machinery of the cells, or by forces applied externally to the cells [56]. Thus, matrix stiffness (exogenous forces) and cytoskeletal tension (endogenous forces) functionaly cooperate in a mechano-circuit that modulates phenotypic transformations in cells.

1.4. Cell mechanics: force generation and mechanotransduction

Cells sense, process and respond to mechanical and other biophysical cues from the ECM using an interconnected hierarchy of mechanochemical systems that include adhesion receptors, cytoskeletal networks and molecular motors as shown in the schematic 1.6. The integrated mechanics and dynamics of these systems enable cells to control their shape and generate forces. Understanding how forces are sensed or generated by cells and translated by proteins is one of the main question in the field of cell mechanics. Acquiring knowledge about the role played by forces on cell and tissue behavior, requires finding what factors contribute to force generation in cell.

In adherent cells, forces get generated by the following two mechanisms: continuous assembling and disassembling of actin fibers and acto-myosin contractile machinery which is mainly driven by myosin II interaction with actin. These forces are transmitted through adhesion sites to the underlying substrate, resulting in its deformation.

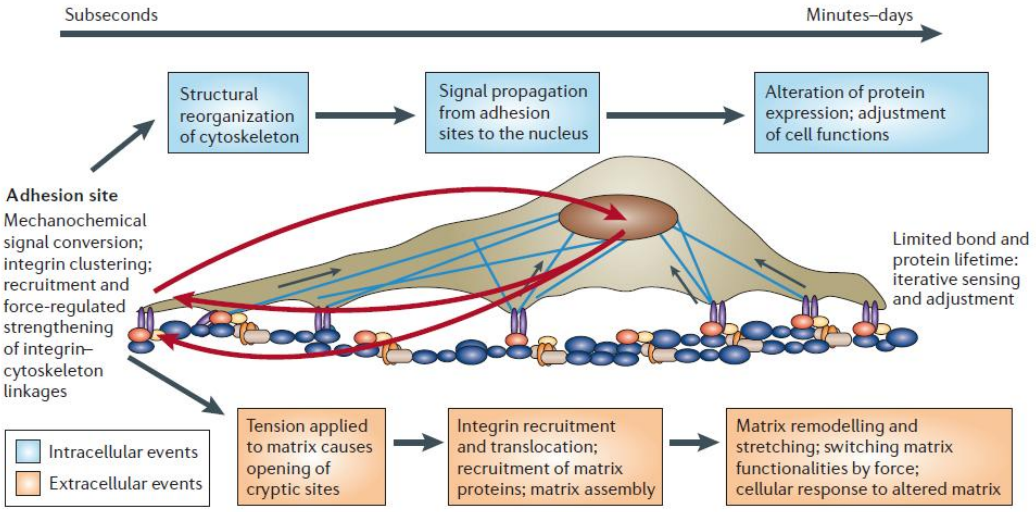

Figure 1.6.: Cellular processes of mechanosensing and responses:[1]

Studies have pointed out that cellular traction forces exerted on the ECM or at the cell-cell adherent junctions controls the maturation or disassembly of adhesion molecules and initiates intracellular signaling cascades which leads to alter many cellular behaviors [57, 13, 24]. Moreover it is assumed that different cell types can optimize their function at different matrix rigidities. Cells ability to sense the mechanical properties of their microenvironment is a critical feature [19] for tissue homeostasis, a process which is supported by a bidirectional relationship between cytoskeletal architecture and mechanical forces generated by cells as can be seen in figure 1.6. Schematic explains the intracellular and extracellular response of mechanotransduction. Applied forces on the substrate recruits adhesion proteins which further alters the ECM. This mechanical stimuli propagates to cell interior as biochemical signal which leads to reorganization of cell cytoskeleton and protein regulation. As a result cell morphology, behavior and function changes. It thus appears really important to make the link between cytoskeletal architectures and cellular traction forces in order to probe the fundamental processes underlying cell mechanosensitivity. Many different ways to measure or estimate forces has been proposed till the date such as micropipette aspiration, Traction force microscopy method, Micropillar method, [22, 21]. In this present work, we try to shed light on the link between force and cell organization to probe mechanotransduction by using

TFM technique.

1.5. Objectives and specific goals

Many interesting development have been made towards the understanding of cell sensitivity to physical cues such as geometry, topography etc. One of the most obvious missing information concerns the role of the extracellular matrix geometry on tension distribution inside the cell and its influence on the intracellular organization.

In this thesis, we focus on the role of the extra cellular matrix geometry on cell adhesion, internal organization and traction forces distribution by combining use of traction force microscopy and micropatterning techniques. More precisely, we study how different shapes of the adhesive micropatterned ECM affect cell force distribution both locally and globally at the single cell level. We try to see the correlation of actin network organization with paxillin and centrosome distribution. Some of the measurements have yielded intriguing insights into cellular response to geometrical stimulation.

Chapter 2 contains a description of the experimental methods and approaches used in this work. In this chapter we give details about our micropatterning technique and our traction force microscopy algorithm for data analysis.

Chapter 3 is divided into two parts. In the first part we focused on how geometrical modulation of the ECM influences traction force distribution, and also localization of focal adhesion at the single cell level. We have measured cell traction force using different micropatterned shapes on 2D soft polyacrylamide gel embedded with nano beads. We showed that ECM geometry affects local stresses while whole cell contractile energy appears to be conserved.

In a second part, we try to compare cell traction forces developed when cells are on a continuous 2D micropatterned substrate with discrete 3D micropillar array of "equivalent" stiffness. We also have investigated how forces and focal adhesions

varies with rigidity modulation of the extracellular matrix in both these two cases.

Chapter 4 tries to explore a potential relation in between traction forces orientation and cell internal organization. We studied a strong correlation in between cell internal organization such as focal adhesion with centrosome positioning which suggests a potential role of actin in centrosome centration. This is, to our knowledge the first evidence of that process.

Chapter 5 describes an alternative approach to the design of micropatterned surfaces on PNIPAM polymer brushes having thermoresponsive properties for single cell studies. In the first part we characterize polymer brush (length and density) and pattern creation on synthesized polymer. Next we study cell adhesion dependence on brush thickness, length and polymer lower critical temperature. Finally, we discuss temperature-dependent swelling properties of PNIPAM and their potential application in cell detachment.

2. Tools and techniques for biomechanics

2.1. Introduction

There are many studies going on in biomechanics from single molecular level to tissue engineering where a large number of cells as a whole is studied. Most of these studies use the tools of mechanics in order to correlate the structural or functional response of biological samples to force measurements such as in adhesion, migration [58], differentiation and apoptosis. Nowadays more and more groups are focusing their attention on this ability of cells to respond to physical cues of their microenvironment, a process called mechanotransduction.

Many different techniques have been developped or adapted to the field of cell mechanics in order to probe cell mechanotransduction aspects. The technologies used in that field relies on one basic bioengineering principles that ensures that precise forces are imposed or measured onto biological objects in a well defined environment. Both local and global approaches are used to apply calibrated forces onto living cells [17]. In case of techniques such as AFM, Optical Trapping, magnetic tweezers a local (smaller than the cell size) probe is used to exert forces to the cells. A great advantage of these techniques are to apply tunable solicitations to individual cells. However, lack of understanding the system as a whole is major inconvenience of these techniques. On the other hand, in case of global approaches [59, 60], there can be some lack in describing the details of the individual microstrustural elements as it is usually assumed to be averaged over large scale areas. Hereby it has to be

noticed that the spatial organization of cells within tissues is very important for their function and thus, one of the most difficult part to study cell mechanics is that in classic culture like glass or plastic petri dish, where cell internal and external arrangements are highly variable from cell to cell. Statistical analysis of any cell morphology and their coupling with cell mechanical properties is thus very difficult. Hence, it appears necessary to have a control on cell architecture to quantify cell biomechanical properties statistically. It is challenging to many biomedical and tissue-engineering applications to control cell adhesion and cell internal organization in order to describe as precisely as possible cell mechanical behavior.

Another way to approach this problem is not to apply calibrated solicitations to the cells but to directly measure traction forces developped by individual cells in relation to their structure and shape, which may allow local as well as global insight of a systematic understanding. The main goal of my work is to be able to relate local and global cell internal structures to cellular traction forces. For that purpose, we propose to design a set-up that will combine single cell micropatterning with traction force microscopy.

Micropatterning is a high-throughput method with a wide range of applications, such as tissue engineering, cell based drug screening, and fundamental cell biology studies [23]. This tool has been used to arrange living cells in a regular manner giving access to statistical tools (image averaging) and to localize spatial distribution in cell based biosensors and transducers. By using standard patterning techniques, cell microenvironment geometry can easily be modulated. Hence, cell internal organization also becomes reproducible. Moreover, the number of structures fabricated at once on the same substrate can reach several tens of thousand allowing a "statistical" approach in the observations and measurements under similar experimental conditions. The use of Traction Force Microscopy technique enable us to calculate forces exerted by the cell on the substrate it is subjected to adhere. Thus by designing micropatterns on soft substrates it is possible to correlate cell internal organization with cell force distribution in a statistical approach.

2.2. Experimental design

2.2.1. Mask design

To address the question: how ECM geometry influence cellular traction forces distribution, different micropatterns shapes have been designed in the work.
To create adhesive micropattern of a specific design, a quartz photomask mask need to be fabricated. There are many software used to design photomasks such as Klayout , Autocad, CleWin. For our work, mask designing software CleWin has been used. To design different ECM geometry, different types of patterns are required for the mask design. For some of our shapes, we have preserved the same projected area to ensure that cell pre-stress will be the same. Single shapes are designed in

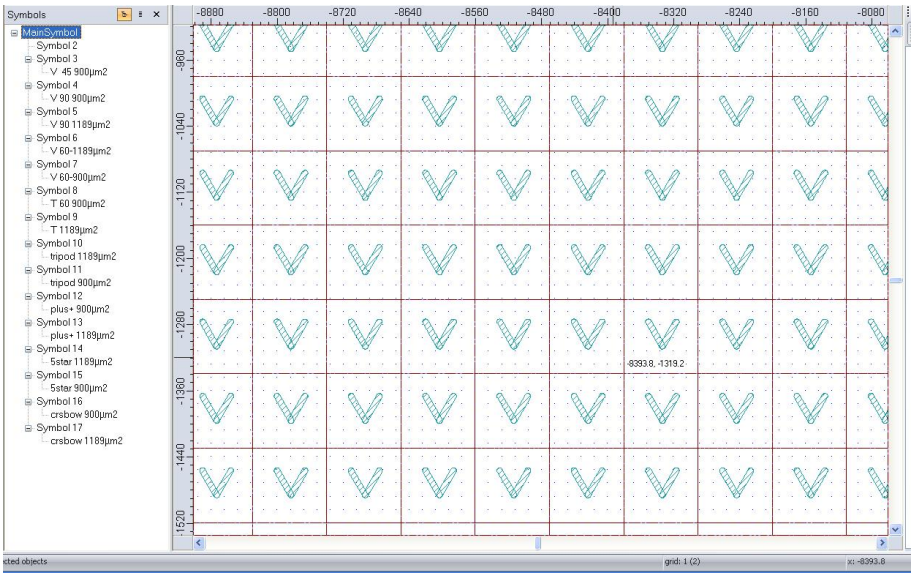

Figure 2.1.: Mask designed by CleWin: designed V shape shown in the image of triangular area is about $900\mu\ m^2$ with bar width $7\mu m$

one layer. To create an array of 2D micropattern, particular shapes are grouped and arranged (as shown in figure 2.1) into a regular array in a different layer. Different layers are useful to specify to the mask manufacturer which parts of the mask should be opaque for the uv light exposure (that will ultimately lead to adhesive ECM islands creation). Numbers are etched in a regular interval to create a matrix reference on the whole coverlsip to avoid any ambiguity among cells when they are

arranged on the array (especially useful while working with fixed samples).
Then, the designed mask (a GDSII file) is send to the mask manufacturing company (Toppan Photomasks inc.,Texas USA) for implementation of design on chromium quartz photomask.

2.2.2. Micro-fabrication and utilization

Microfabrication is a very useful approach in cell mechanics as well as in fluid mechanics. The main interest relies on the microfabrication that it gives researchers to design model environment with fixed boundary conditions (micropatterns, microwells, micropillars etc.). By designing artificial environment, cell internal organization and multi-cellular assemblies can thus be designed "at will" allowing to study cell morphological behavior statistically. Moreover, *in vivo* cells are constrained mechanically and geometrically. Single cell micropatterning to some extent, can thus mimick those conditions which are not possible in classic culture where cells are plated on an homogeneous layer of ECM proteins and hence, adopt any kind of morphology[10].

There are mainly two ways to create 2D micropatterns. Firstly, micro-contact printing [61, 62] which is a widely used method that use elastomeric microstructure stamps made of polydimethylsiloxane (PDMS) to deposit ECM proteins on different kind of substrates (glass coverslips, hydrogels). A common alternative to PDMS stamping is the use of UV light activation, through a photomask to a specific region of the substrates that can further be modified chemically so as to link different types of proteins as shown by Azioune et al. [63, 64].
Another methodology has been developed in our group by using PNIPAM polymer brushes with thermoresponsive properties that give an extra feature to single cell micropatterning (details described in chapter 5). [41]

In this thesis, the technique we have used relies on UV irradiation of the sample, which is a thin layer of polyacrylamide hydrogel. This technique avoids a large number of steps and is less time consuming compare to other existing patterning

techniques. There are many different interest of working with polyacrylamide gel:

1. Polyacrylamide (PAA) is a soft elastic material allowing experimentalist to measure cellular tractions forces.
2. PAA is very transparent so that imaging through the gel is possible.
3. PAA is very easy to prepare.
4. PAA is mechanically very stable and mechanical properties can easily be tuned.
5. PAA material is biocompatible.

Here is a brief description of our polyacrylamide micro-patterning procedure:

2.2.2.1. Gel preparation:

Fabricated chromium quartz mask can directly be used for patterning. An acrylamide gel pre-mix (PBS/acrylamide/bis-acrylamide) can directly be polymerized onto the quartz mask by placing a drop of pre-mix in between the mask and a silanized coverslip [see protocol annexA3]. This gel pre-mix is pre-doped with 200nm fluorescent beads [treated with PLL-PEG(Follow AnnexA1)]. Beads are added only for TFM measurement. Required stiffness of the gel can be achieved by controlling over the relative concentration of acrylamide and cross-linker bis-acrylamide.

After polymerization, next step is to activate the polyacrylamide hydrogel by using a deep UV light exposure below 200nm (ref: UVO- CLEANER, Jelight Conmany,Inc.). This deep UV irradiation creates a local plasma in illuminated regions that oxidize the gel surface. As it is not possible to conjugate ECM proteins directly to the gel, this gel oxidation allows us to indirectly cross-link protein with the activated part of the polyacrylamide gel. After irradiation, EDC and NHS chemicals are mixed at a proper concentration and molarity (see annex A3) to cross link PAA with ECM proteins. Schematic diagram 2.2 shows the gel preparation steps. As previously described, only the pattern part is transparent and exposed to deep UV light (rest of the mask is opaque). Fluorescent ECM protein conjugation with the

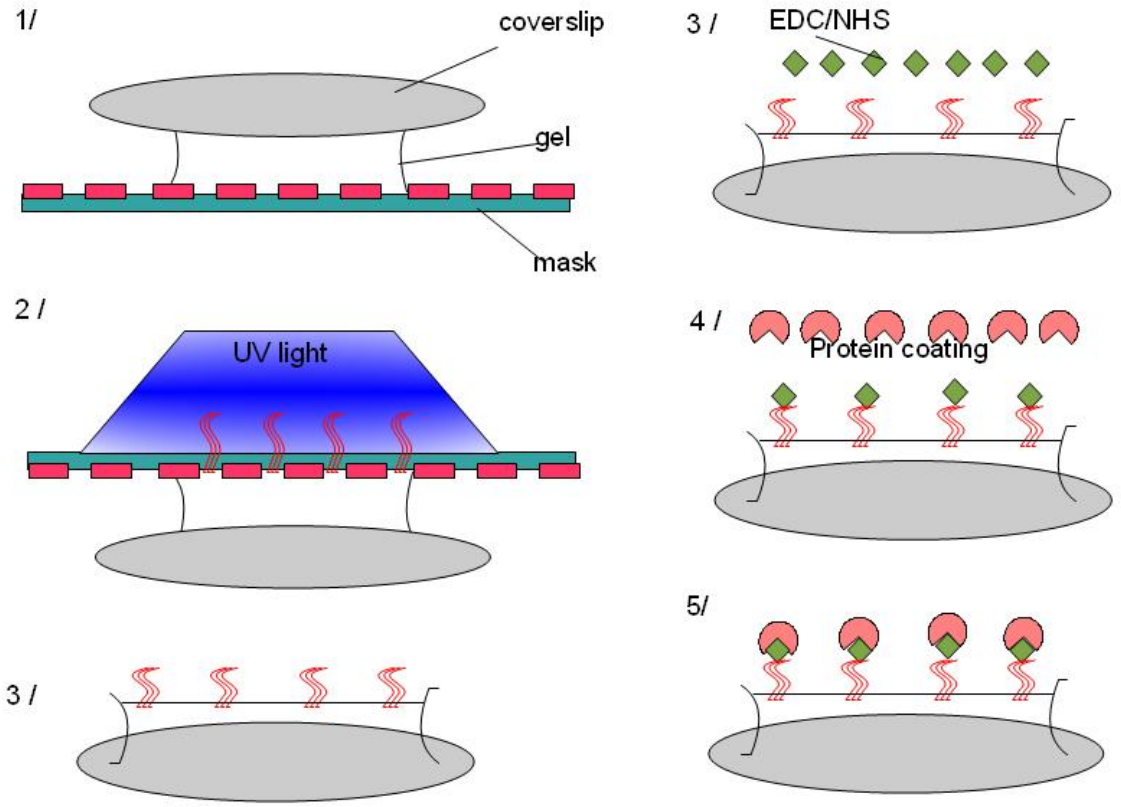

Figure 2.2.: schematic of the experimental procedure to create pattern on acrylamide gel.

gel results in a monolayer of coating (as shown in figure 2.3) on the activated part of the gel which can easily be detectable under fluorescence microscope and which is ready for cell culturing.(For the details of the protocol see Annex).

This micropatterning technique is well suited to study biological phenomenon as it has the ability to produce stable patterns on transparent polymeric substrates in a biocompatible manner. The success of the technique relies on the fact that it has one to one transfer of any kind of 2D patterning. Micropattern spatial resolution can reach up to 2μm (as shown by the elliptical dot in figure 2.3) in this technique. Moreover, the incorporation of nano beads in the gel enable us to calculate cell traction force distribution in response to ECM geometry.

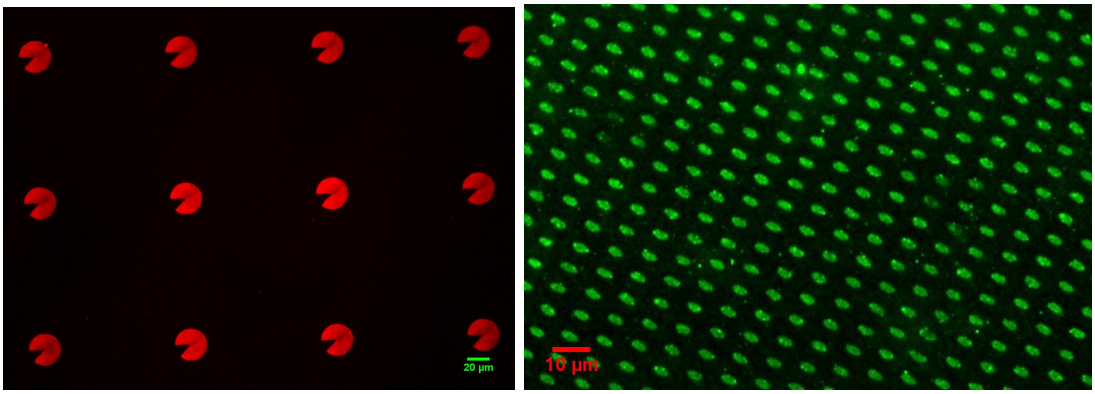

Figure 2.3.: Fluorescently labeled protein coated micropattern (red) on polyacrylamide hydrogel; Regular array of oval shape dot (green) structure : major and minor axis are 2 and 3 μm.

2.2.2.2. PAA micropattern characterization :

Protein conjugation efficiency has been checked by looking at the micropattern fluorescence intensity while changing UV illumination time for 2min, 3min, 3.5min, 4min respectively. The figure 2.4 below, shows the effect of UV exposure time on protein conjugation. Here optimum time for UV irradiation is 4mins, resulting in good protein coating as required for the experimental analysis.

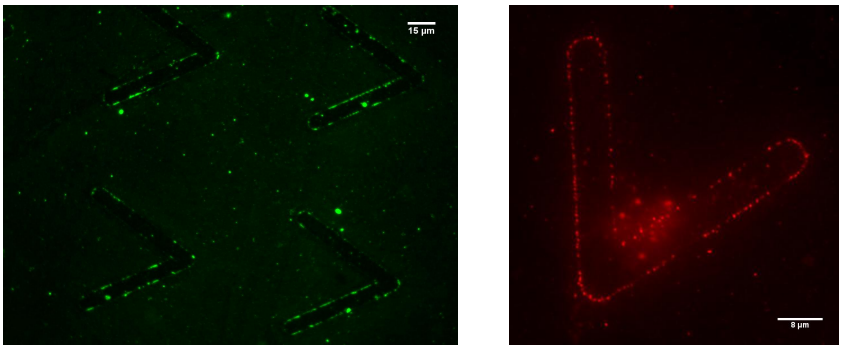

Discussions:

- PAA micropatterning technique presents advantages in comparison to micro-contact printing it avoids many steps and can be performed in less than 3hrs.
- Patterning technique is applied to PAA hydrogels in which rigidity can be

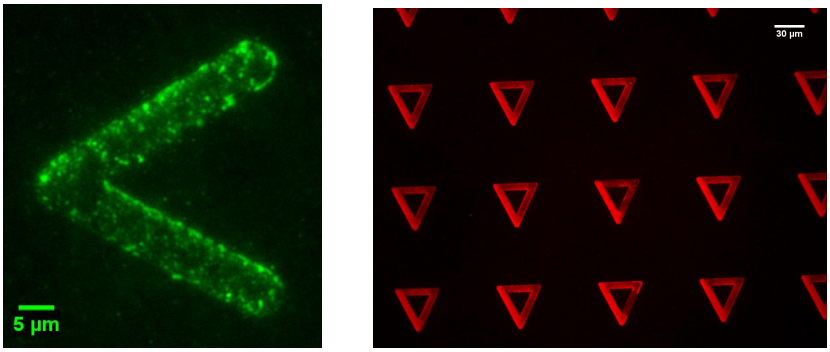

Figure 2.4.: Images showing influence of UV activation time (2,3 min and then 3.5 , 4min) on protein coating.

modulated to very low Young modulus around 0.5 Pa and higher up to 40 KPa (as tried) by controlling the concentration of the chemicals used for polymerization pre-mix as per experimental requirement.

- This technique uses one to one transfer i.e the pattern can directly be achieved from the mask itself ensuring a very high spatial resolution allowing to control cell internal organization at the subcellular level
- The patterning process is efficient at large scales. The great interest of this technique is thus to fabricate tens of thousands of patterns once at a time on the same coverslip

2.2.2.3. Cell culture :

Before culturing cells on the PAA micropatterned substrates, washed with sterile Phosphate Buffer Saline(PBS) 1X with 7.4pH extensively. Coverslip carrying micropatterns are mounted on a cell observation chamber. Cells on the classic petri dish, are trypsinized and seeded to the micropattern with a specific density as required for each experiment(≈50 000 cells/coverslip). Since micropatterns are ECM protein coated, cells start adhering only on the patterns. Figure 2.5 shows HSF1 cells, fully spread on the pattern. However some "extra-cells" in between the patterns have to be washed off with fresh media/PBS after 30 minutes of adhesion. When cells are fully spread on the projected area of each shape, the observation

chamber is being taken for experimental observation under the "TFM" microscope. At that time, cell culturing media is replaced by imaging media without Phenol red in order to prevent photochemical reaction in the media. Moreover as the pattern is stained in Cy3, retrieving phenol red from the media gives a better contrast for pattern images. In some cases, the micropattern sample, bearing cells is taken for fixation to stain either actin, paxillin or tubulin.

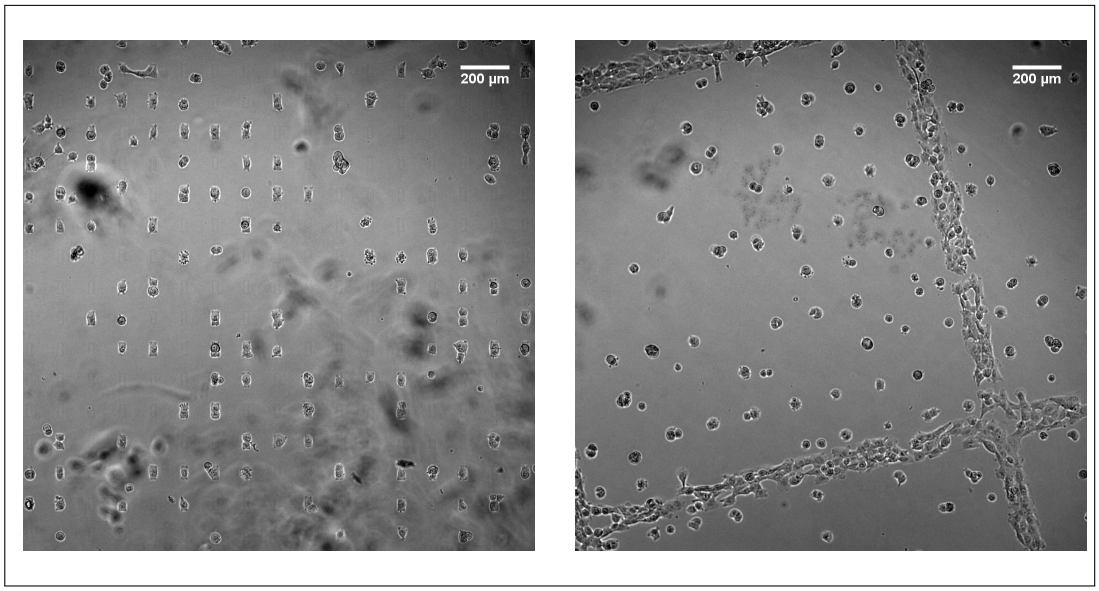

Figure 2.5.: Bright field images of cells, arranged in a regular manner on the protein coated micropattern: Images taken by phase contrast olympus microscope with 4X objective.

2.2.3. Fluorescence Microscopy

Fluorescence microscopy is a commonly used imaging technique in biological specimen investigation. The main interest of this technique is that instead of looking to the whole cell, special parts of interest can be visualized by using protein antibodies linked with fluorophores that in turn attach to targeted features of investigation. The discovery of green fluorescent protein in the early 1960s ultimately heralded a new area in cell biology by enabling investigators to apply molecular cloning methods, fusing the fluorophore to a wide variety of protein and enzyme targets, in order to monitor cellular processes in living systems using optical microscopy and related

methodology.

The basic task of the fluorescence microscope is to let excitation light radiate the specimen and then sort out the much weaker emitted light to make up the image. First, the microscope has a filter that only lets through radiation with the desired wavelength that matches your fluorescing material. The radiation collides with the atoms in your specimen and electrons are excited to a higher energy level (see figure[1] 2.6).

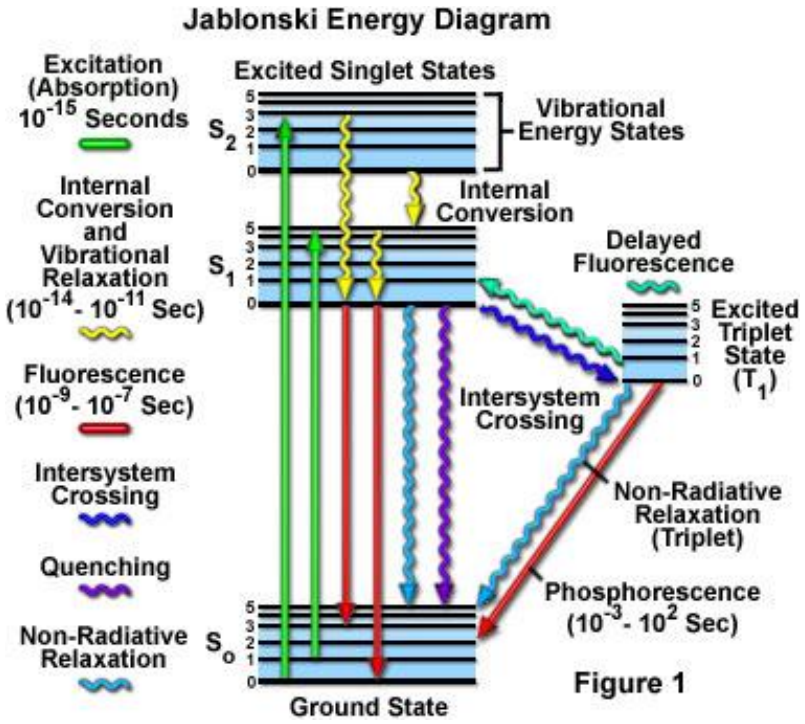

Figure 2.6.: Diagram shows mechanism of a molecule to Fluoresce. Typical excitation and fluorescence specification of a given fluorophore has been shown.

When they relax to a lower level, they emit light. To become visible, the emitted light is separated from the much brighter excitation light in a second filter. Here, the fact that the emitted has a longer wavelength is used. The fluorescing areas can be observed in the microscope and shine out against a dark background with high contrast. Practically, in a fluorescence microscope a multispectral arc-discharge lamp is generally used so that specific wavelength can be selected by bandpass excitation filter. Light from the source passes through the excitation filter and then

[1] [http://www.olympusmicro.com/primer/java/jablonski/jabintro/jablonskijavafigure1.jpg]

it reflects from the dichroic mirror surface. The dichroic mirror has the property to reflect the short wavelengths coming from excitation light onto the specimen. It is transparent for the longer wavelength emitted from the specimen. The emission light gathered by the objective lens passes back through the dichroic mirror and is subsequently filtered by a barrier (or emission) filter, the latter one is used to block the unwanted excitation wavelengths (schematic shown in figure 2.7). Thus, by choosing the right set of fluorophores and filters it becomes possible to observe separately different fluorescent objects and this for different sub-cellular structures at the same time. That point is very important for our application as we need for a single run of experiment to take bead images, pattern images in different fluorescence channels.

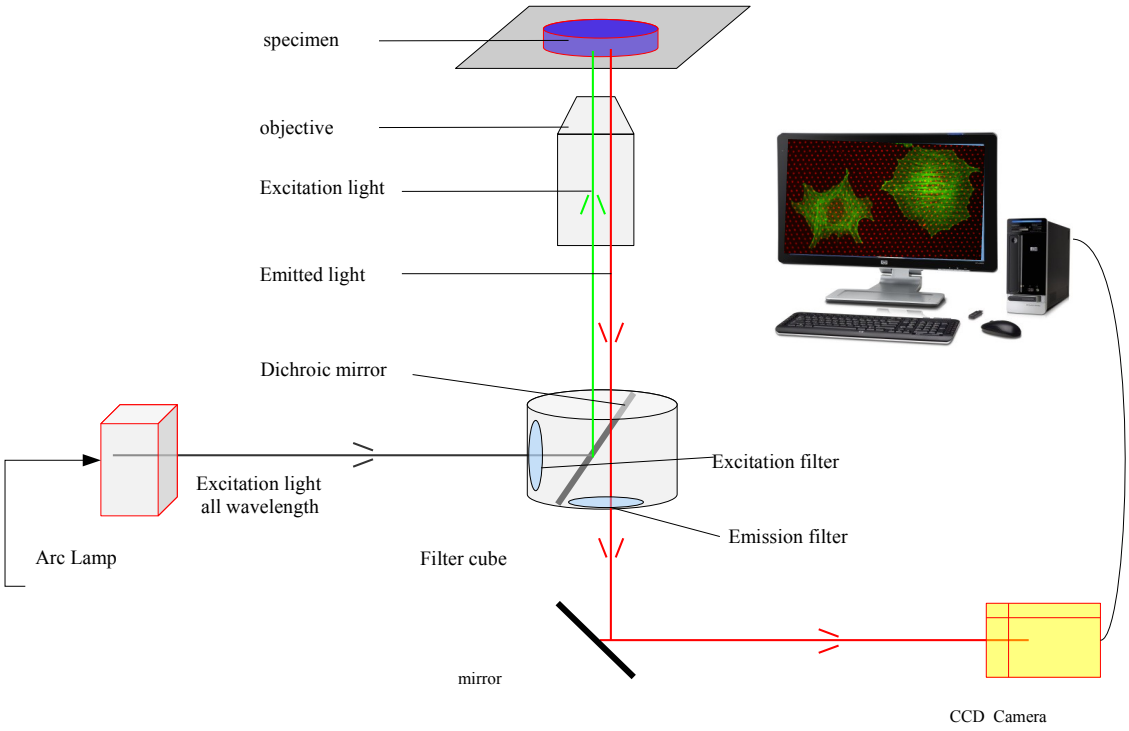

Figure 2.7.: Schematic ray diagram of the Fluorescence Microscope imaging technique.

When a molecule (a fluorophore) is excited at its specific absorption wavelength it goes from a ground state to its excited state (see figure 2.6). Afterwards there is a spontaneous emission of light during transition of the molecule from its lowest

vibrational energy level of an excited state S1 back to the ground state under a mechanism called fluorescence.

Photobleaching:

A common problem in fluorescence microscopy is the phenomenon of photobleaching. It occurs when a fluorophore permanently loses the ability to fluoresce due to photon-induced chemical damage and covalent modification. Photobleaching may results from different possible mechanism, but it is assumed to be linked to a transition from the excited singlet state to the excited triplet state. The excited triplet state is relatively long-lived and is chemically more reactive. The average number of excitation and emission cycles that occurs for a particular fluorophore before photobleaching is dependent upon the molecular structure and the local environment.

Fluorophores used in our experiment are listed in table[2] [**?**]

Fluorophore	Excitation	Emission	Target
	nm	nm	
FITC	495	519	Actin
Texas Red	589	615	centrosome
DAPI	345	455	Nucleus,paxillin
GFP	488	507	Actin
CY3	512	570	Pattern
CY5	650	670	Actin,beads
YFP	508	524	Paxillin,beads

Moreover, in our experimental conditions, during gel preparation, fluorescently labeled beads gets bleached when exposed to deep UV light, this creates a problem in bead detection while quantifying displacement fields. Thus in our experiments

[2]The annotated wavelength corresponds to the peak value of the excitation/emission spectra of the respective fluorophore spectra.

beads fluorophores are chosen in order to minimize photobleaching.

2.2.4. Imaging tools and development

For image acquisition the Nikon ECLIPSE Ti Series inverted microscope has been used. Phase contrast imaging has been done on an Olympus CKX41 inverted microscope.
Typical objectives used for all experiments are : 10X, 20X air, 40X air , 60X oil (for fixed samples imaging, a 1.5 multiplier has been used).
An automated filter wheel is mounted with the Nikon microscope containing 5 bandpass filter cubes at a time. Each filter cube contains one excitation filter , one dichroic mirror and one emission filter. For bright field imaging an upright illuminator is placed on top of the microscope. For fluorescence imaging an Arc lamp Nikon (C-HGFIE refno 670384) is used. Images are acquired by CCD camera (CoolSnap ES Roper Scientific).

A proper culture environment is very important for live-cell imaging experiments. Maintaining a proper temperature(37°C) environment for cell on the microscope stage is fundamental. For that purpose a thermalization chamber has been developed in the lab. Live- cell imaging chamber is also very critical part of the experiment. A large variety of designs are available in the market giving cell friendly environment for long term cell imaging. A useful good chamber should be

- easily sterilizable and chamber material should not be toxic for the cell.
- an unit isolated from the laboratory environment.
- properly covered during experiment to minimize evaporation or contamination.
- the culture chamber should be simple enough to allow physical manipulation of the cells like changing media during experiment.

Initial experiments are done with a workshop made chamber which turned out to be toxic for cells. After mounting the coverslip onto the chamber within 10 mins

cells are dead. Later on, the chamber has been used for long time imaging is a POC-R model from Zeiss.

2.2.5. Image acquisition and processing

For all our image acquisitions, the software Micromanager (μ-manager) has been used in order to automatize the system for multi-positioning acquisition (including Z-stack acquisition and auto-shutter). For a typical TFM experiment, when cells are nicely spread on the micropattern, images of cells in brightfield, beads and patterns are acquired. To measure the displacement field induce by cellular traction forces on the hydrogel a pair of bead images need to be acquired : one image when cells are on the pattern and another one when cells are detached from the substrate in order to obtain the relaxed state of the gel (cells are detached from the substrate by simply adding water which results in cell lysis). Sample images for TFM has shown in figure 2.8. It has to be noticed that for bead images, a Z- stack is acquired because the beads are in a plane which is under the cell surface. Among all Z stack images of the beads, only the best focus image is selected for TFM calculation. These "best focus" images are important to calculate the displacement field accurately.

For each coverslip 50 to 60 positions (corresponding to 50 to 60 cells) are usually acquired. Acquired images are then renamed and their contrast is usually enhanced for all image sets for further processing.

2.3. Cell traction measurement and development

When cells are adhered on the substrate it exerts tensile stress by acto-myosin contractile machinery and also by constant polymerization and depolymerization of actin. These forces are transmitted to the substrate via adhesive structures such as focal adhesion (Balaban et al. 2001)[20, 7]. Traction forces play a pivotal role in cell shape maintenance, migration, wound healing, mechanical signal generation or many other cellular functions [65].

Numerous different techniques that enable experimentalist to quantify cellular traction forces, which have been developed over the last few years[21, 66, 67]. Trac-

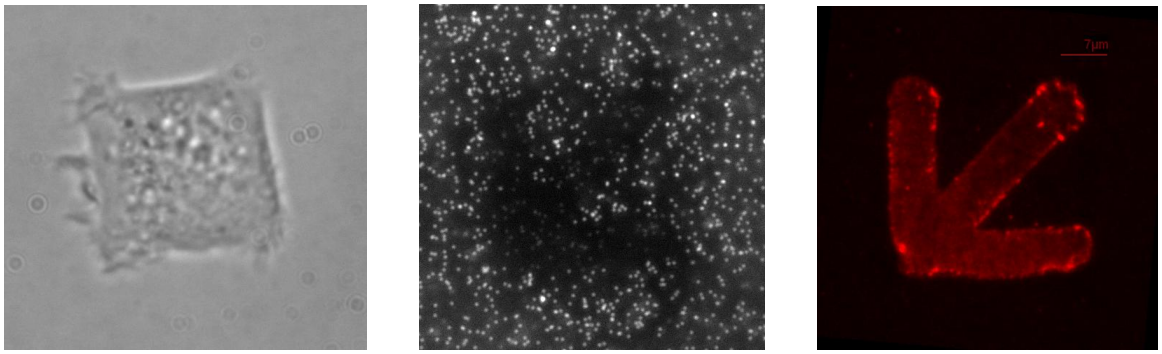

Figure 2.8.: Typical images are acquired for TFM experiment: from left: cell under bright field, beads (200nm) under the pattern in YFP, fibronectin coupled with fibrinogen, coated on Pattern in Cy3 channel respectively

tion forces developed by cells are roughly in the nN range (Choquet al. 1997) on adhesion sites possessing areas of micrometer square or less [16, 52]. In particular, these have been characterized by different methods based on the deformation of elastic planar substrates [50, 51, 57, 69, 70].

Among all these techniques, TFM (Dembo al.1996) remains the most widely used method to precisely quantify and localize mechanical forces generated by single adherent cell [22, 69, 71, 68, 72, 73]. TFM studies provided great insights regarding the development of traction forces at the cell-ECM interface. In this study we have chosen to work with a particular version of traction force microscopy called Fourier Transform Traction Cytometry (FTTC).

The objective of Traction force microscopy technique is to calculate forces (F) exerted on a continuous substrate from its deformation measurements. To do that experimentalists need to solve an inverse problem, which is ill-posed owing to the presence of noise. From this inverse problem solution they are able to calculate traction forces at each adhesion sites by using linear elasticity theory.

Here we have used linear theory of elasticity to calculate the cellular stress field[74]. For FTTC calculation we have considered the substrate homogeneous and linear elastic semi-infinite half space as the prepared polyacrylamide gel has to be thick

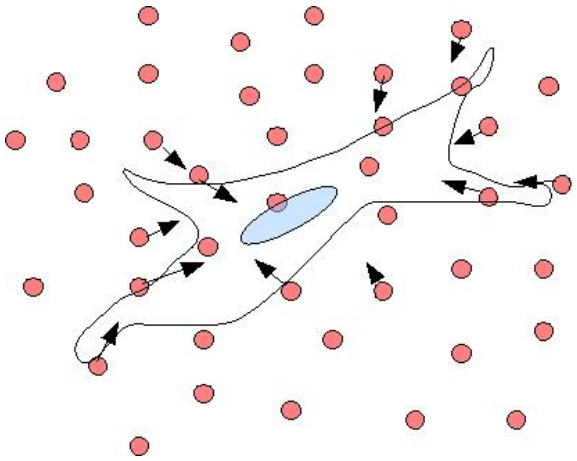

Figure 2.9.: Cell traction force exerted on the substrate.

enough for this assumption. Both lateral distance over which displacement is measured and the lateral dimension of force or deformed area should be small with respect to the substrate thickness to approximate semi- infinite elastic continuum to finite one. Thickness or our gel is 70 - 80 μm as considered for all experiment. The displacement vector induced by cellular forces at any point can be written as u_i on the elastic substrate as convolution form :

$$u_i(\mathbf{x}) = \int G_{ij}(\mathbf{x} - \mathbf{x}')f_j(x')d\mathbf{x}' \tag{2.1}$$

where u_i and f_j includes x and y component for the displacement and force respectively. The force field includes forces from all other point x' apart from the applied point of force. G_{ij} is the Green's tensor in response which is response to point traction in two dimensional plane of substrate, can be written as

$$G_{ij}(r) = \frac{1+\nu}{\pi E}\left[(1-\nu)\frac{\delta_{ij}}{r} + \nu\frac{x_i x_j}{r^3}\right] \tag{2.2}$$

or can be written as

$$G_{ij}(r) = \frac{1+\nu}{\pi E r^3}\begin{bmatrix} (1-\nu)r^2 + \nu x^2 & \nu xy \\ \nu xy & (1-\nu)r^2 + \nu y^2 \end{bmatrix} \tag{2.3}$$

where $r = \sqrt{\mathbf{r}.\mathbf{r}} = \sqrt{x^2 + y^2}$

E is the young modulus ν is the Poisson's ratio of the substrate under consideration.
Green's function for the system under consideration has the following property:

1. It has singularity at the origin
2. It varies as 1/r

Which makes inverse problem more complicated to solve to extract force since it has long range effect for the 1/r factor. Mathematically three standard methods have been established to calculate force from displacement field :

1. Boundary element method (BEM) [22].
2. Fourier transform traction cytometry (FTTC) [69].
3. Traction reconstruction with point forces (TRPF) [75].

BEM technique is based on inverting a large number of linear equations in real space. Hence it requires long computational time but, a very high resolution can be reached. FTTC method solves the inverse problem in Fourier space which turns out to change the previous convolution (2.1) in a simple matrix multiplication making the computation easy and very less time consuming. Some recent advances of the technique called TRPF has been shown by Schwarz et al [68]. TRPF gives a better accuracy in point force measurement but, it requires a prior knowledge of focal adhesion placements that turns out to add microfabrication steps in the experimental set-up. Comparative study conducted by Sabbas et al demonstrates that FTTC, when combined with a proper regularization parameter and filtering, is comparable with results obtained by using BEM [75].

For our cell traction calculation, as one of our goal is to provide statistical measurements, we have chosen to implement an home-made FTTC algorithm as it is

computationally inexpensive (Thanks to Dr. Irene Wang for developing the code). We have developed a Fast Fourier Traction Cytometry software which includes a combination of Particle Image Velocimetry (PIV) and Particle tracking for displacement field measurements.

2.3.1. Displacement field extraction

To determine cell-induced displacement field, the very first step of the analysis is global correction of stage drift using images of beads before (stressed) and after (relaxed) killing cell. Drift correction is achieved by cross correlating the two images. Position of the max /peak of cross-correlation corresponds to the global translation. After determining this maximum cross-correlation in between stressed and non-stressed bead images, translation is corrected and bead images are resized at the same dimension

In the first step of displacement field analysis, we perform to PIV calculation, stressed and relaxed bead images are overlapped and subdivided into small windows. Here all the small window sizes are kept constant, typical size of 64 or 128 pixels. Between the corresponding pair (stressed and relaxed) of bead images, cross-correlation is obtained [75, 76]. Mean displacement is calculated from the peak of the the maximum cross-correlated images [7, 69, 72], then each bead displacement is mapped using particle tracking in each sub-window. Schematic diagram ?? shows displacement field calculation.

So the new displacement for each bead is:

$$[U^{'}x^{'}]_i = U_i(x) + X_i \tag{2.4}$$

Where i gives corresponding PIV window. X_i gives the average displacement in each case and the value of X_i is constant for the all beads on the same PIV window.

This calculation needs to determine the bead identity as the displacement can be measured when initial and final position of the beads are known. PIV requires a large enough window to yield accurate values. Therefore, it is compromise between resolution and accuracy.

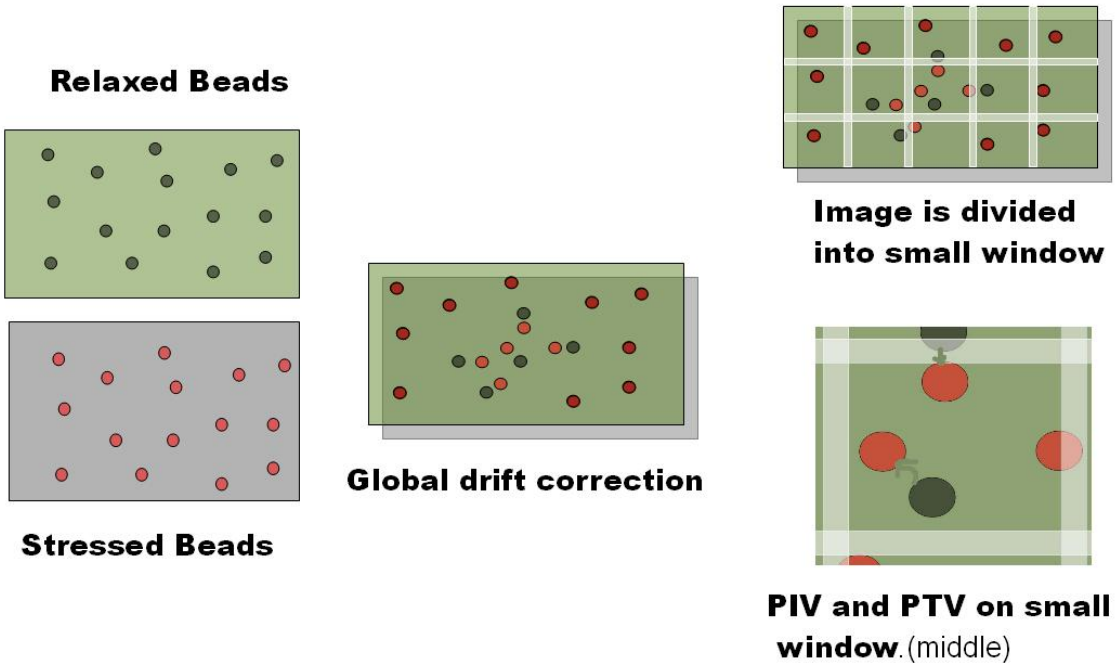

Figure 2.10.: Schematic diagram shows displacement field determination by Particle Image Velocimetry and particle tracking.

During particle tracking there will be no ambiguity for a single beads with their neighbour in the radius of bead displacement as large displacement is already corrected. For the accuracy of the measurement it require good bead density to have good spatial resolution. These two step processes (PIV and Particle tracking) helps to track the beads more accurately.
A grid is designed on the displacement field in regular interval. By interpolation we find field vector on each node of the mesh which is shown in the image 2.12

2.3.2. Traction field determination

As previously described by Bulter et. al 2002 [69] we use Fourier transform (FT) to solve the inverse problem. Thus matrix convolution equation becomes a simple matrix multiplication. $\widetilde{G}(k)$ is moreover diagonal in Fourier space. After Fourier

transform eq(1) becomes

$$\widetilde{u}(k) = \widetilde{G}(k) * \widetilde{f}(k) \tag{2.5}$$

Where $\widetilde{u}$, $\widetilde{G}$,$\widetilde{f}$ are the displacement field, Green's tensor, and force field respectively in Fourier space. And k is the wave vector in the fourier space.

$$\widetilde{f}(k) = \widetilde{G}^{-1}(k) * \widetilde{u}(k) \tag{2.6}$$

$$\widetilde{G}_{ijk} = \frac{2(1+\nu)}{E}\left[\frac{\delta_{ij}}{k} - \frac{\nu_{ij}k_ik_j}{k^3}\right] \tag{2.7}$$

$$= \frac{2(1+\nu)}{Ek^3}\begin{bmatrix} (1-\nu)k^2 + \nu k_y^2 & \nu k_x k_y \\ \nu k_x k_y & (1-\nu)k^2 + \nu k_x^2 \end{bmatrix} \tag{2.8}$$

where $k^2 = {k^2}_x + {k^2}_y$;

It is easy to calculate $\widetilde{G}^{-1}(k)$ since it is diagonal in Fourier space.

Then displacement field $\widetilde{u}_{ik}$ is calculated by Fourier transform. Since we have obtained the displacement field in regular mesh, it fulfills the requirement of the Fast Fourier transform. Force field is calculated in fourier space by multiplying displacement with the inverse of the Boussinesq Green function. It has been shown before that inverse problem is "ill-posed" in the presence of noise and spatial resolution of force can be achieved by adapting a regularization scheme. [53, 68]

With regularization fourier transform equation becomes :

$$\widetilde{f}(ik) = \left[\sum_{lj}\left\{\sum_{m}\widetilde{G}_{ml}\widetilde{G}_{mi} + \lambda^2\widetilde{H}_{il}\right\}^{-1}\widetilde{G}_{jl}\widetilde{u}_{(j)}\right]_k \tag{2.9}$$

For the regularization kernel $H_{ij}(\mathbf{x},\mathbf{x}')$ 0th order regularization has been chosen. Finally force is mapped into real space by inverse fast Fourier transform. After calculation then it is transformed back to the real space by inverse Fourier transform to map traction force field.

Here is an example of classical traction force calculation with MEF cell cultured on non pattern polyacrylamide gel substrate by using our technique as described before (see figure 2.11 and 2.12) .

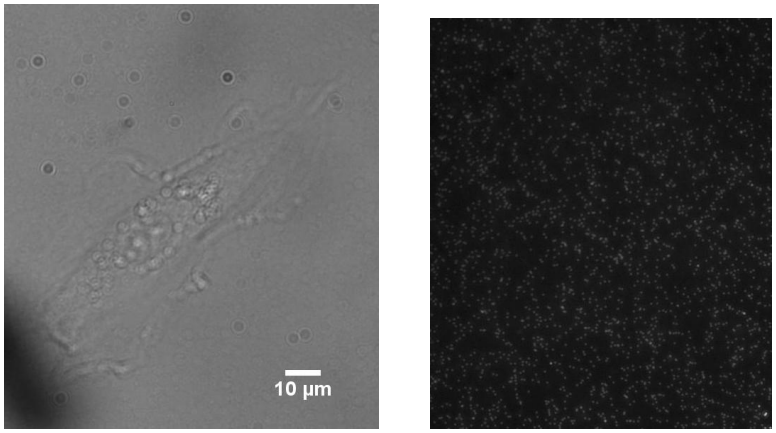

Figure 2.11.: Cell (left) in bright field, cultured on 5 kPa soft substrate and bead (right) images under the cell, taken in fluorescence chanel.

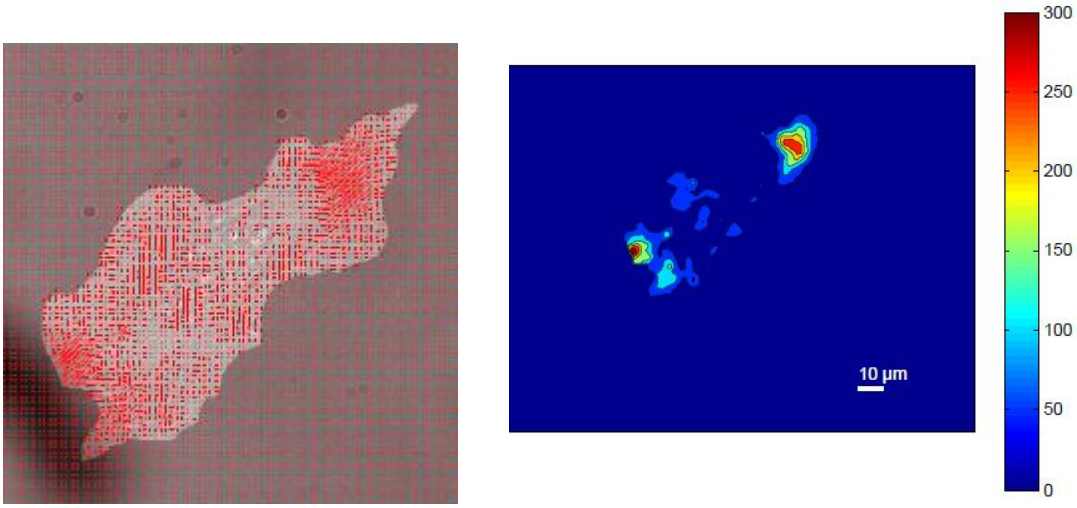

Figure 2.12.: Cell force map (left) shows calculated force by arrow at each point and traction contour (right), color bar shows the intensity of stress exerted by the cell (in Pa).

To understand more about cell-substrate interaction contractile or strain energy is also calculated by integrating the traction force times the displacement over the

whole area of an individual cell.

The way to measure the contractile strength is the strain energy or contractile energy U, is equal to the net force applied by the cell to the substrate by integrating over the whole projected surface area of cell, the element of the shear moment matrix can be written as :

$$U = (1/2) \int \vec{f}(\vec{r}).\vec{u}(\vec{r})dxdy$$

The FFTC technique we have implemented has the advantages that : It is computationally not intensive. It needs few seconds to analyze force field. Utilizing PIV and PTV in FTTC technique results in a good accuracy in displacement field determination. Following chapters show combining use of TFM and micropatterning technique to compute force exerted by cells on the micropatterned substrate for answering fundamental question in cell biophysics.

3. Influence of ECM physical properties on force generation and mechanotransduction

3.1. Introduction

In vivo cells maintain predefined and reproducible shapes and architectures, which play a critical role in cellular and tissue functioning. Extra cellular matrix, on which cells adhere, provides a variety of biochemical signals that influence cellular behaviour including cell adhesion, migration and differentiation but it also provides scaffold for cells that strongly influences cell architecture and their related intra-cellular tension [1]. Understanding how the physical properties (geometry, rigidity etc.) of the extra-cellular matrix influences cell shape, internal organization and signaling remains a major question in cell biology[77]. Recently a large number of microfabrication techniques such as micropatterning has expound the ability to artificially reconstruct internal conditions (geometrical constraints, soft substrates) experienced by cells *in vivo*[78].

In this chapter we will probe the existing relation between cell shape and cell force generation in response to ECM physical properties by using a combination of cell micropatterning and traction force microscopy on soft substrates. This chapter is divided into two parts. In the first part of this chapter, we have investigate the effect of micron-scale ECM geometry influence on spatial force distribution at the single cell level. Observation on cell traction force distribution is based on the utilization

of micropatterns with different subcellular geometrical shapes while ensuring individual cells to have exactly the same envelope. We have shown that single cells are able to regulate their contractile energy at the global scale by spatially redistributing actin generated forces and adhesion sites in response to the geometry of the ECM.

In the second part of this chapter we explore how matrix stiffness influences the process of cell rigidity sensing that is known to have diverse effects on cellular behaviour including motility, proliferation, adhesion and differentiation [4, 79, 80, 81]. In this second part, we compare forces developed in continuous 2D substrate with micropillar 3D substrate, having same arrangement by using a previously described elastic model [82] that allowed us to evaluate the equivalent Young modulus of a microtextured surface with the one of a continuous hydrogel. In particular, we study the forces developed by REF52 cells on a micro-post array in comparison to those measured on micro-patterned substrate with different substrate rigidities. By correlating forces with focal adhesion assembly, we delineate how mechanotransduction process gets stimulated in response to stiffness changes.

Part I.

3.2. Role of the ECM geometry in cell traction force distribution

Substrate rigidity, ECM-ligand specificity, and topography influence cellular traction forces and ultimately on cell behaviour. In particular, does the cell regulate its tension locally or globally is still a question that remains unsolved. To address this question we have used Traction force microscopy on a set of 3 different micropatterns enabling us to control cell shape while changing their underlying ECM geometry.

3.2.1. Experimental approach

As a model system we have used Mouse Embryonic Fibroblasts (MEF) for these experiments. Each micropattern has been designed so as to isolate single cells on a square envelope of projected surface area of 900 μm^2 using adhesive bars of 7 μm width on 5kPa hydrogels. Micropatterns are coated with a mix of ECM proteins composed of fibronectin conjugated with fluorescent fibrinogen. ECM protein concentration are kept constant throughout all the experiments (20 μg/mL). Previous studies [40] have shown that, on micropattern created on glass substrate, cells tend to form actin bundles over non adhesive regions. Micropatterning technique on soft hydrogel enable us to determine traction forces, besides controlling cell shape. It provides control on cellular organization in response to substrate modulation.

Figure 3.1.: *Image of Protein coated micropatterns(red), created on polyacrylamide hydrogel U, H and Arrow respectively. Fluorescence images are acquired in Cy3 channel.(scale bar 10 μm)*

We design 3 shapes (U/H/Arrow) based on this construction rule so as to compare the effect of one, two independent or two connecting actin bundles on cell force distribution. Figure 3.1 shows the selected set of fibronectin coated patterns conjugated with fibrinogen that have been prepared for TFM experiments. Images show that the non-activated part of the polyacrylamide gel (black background) highly prevents protein conjugation (red fibrinogen) which gives a highly contrasted background.

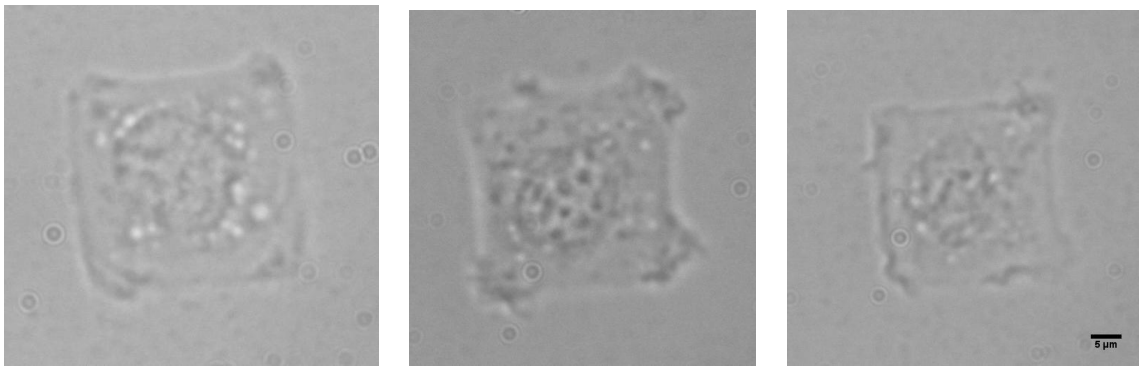

Figure 3.2.: *Bright field image of mouse embryonic fibroblast MEF) cells plated on U, H and arrow shapes micropatterns, following square envelope irrespective of underlying geometry.*

Thus when cells are plated on elaborated substrates, they adhere only on the protein coated part and confined themselves in the restricted geometry. Hence, cell shape is well controlled as shown in the bright field image of single cells in figure 3.2.

3.2.2. Investigating cell internal structure organization in response to ECM geometry

Micropattern imposes boundary condition on cell spreading and cell internal architecture. Confinement of cell shape on adhesive micropatterns of different geometry regulates many cellular processes including cell morphology. In order to investigate the actin stress fiber and focal adhesion spatial distribution in response to ECM geometry, cells are plated on our selected shapes and fixed after 2-3 hrs when they are

fully spread. Subsequently actin fibers and focal adhesions are labeled and immunofluorescence images are carried out.

In particular, on chosen set of shapes, cells do not migrate and display a stable shape with ruffling activity upon adhesive sides. Remarkably this steady state was characterized as on glass substrates, by convex cell shape. Actin fibers (stained with Phalloidin alexa-488) formed an organized and spatially accumulated network at the periphery of the square envelope. Most remarkably, we find that the actin cytoskeleton on soft micropatterns forms bundles along both adhesive and non-adhesive edges in discordant with the case when cells are plated on micropattern created on hard substrate (glass coverslips) as shown by Thery et al. [40]. Actin cytoskeleton also tends to form concave fibers at the nonadhesive boarder. Figure 3.3 shows single MEF cell actin network on U, H and arrow micropattern shape.

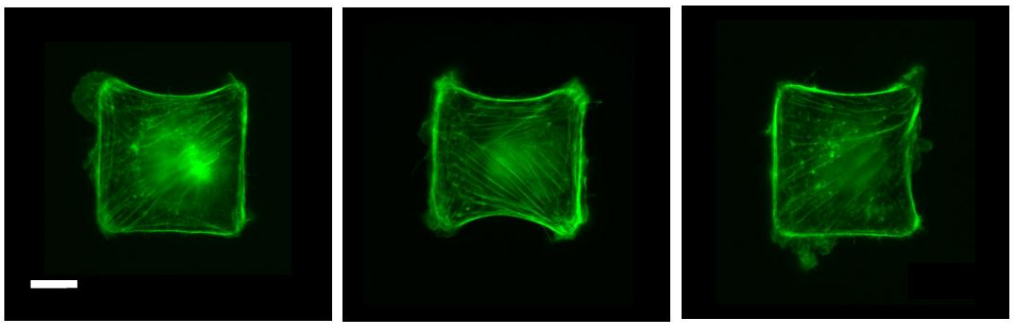

Figure 3.3.: *Actin fiber (green) distribution of single MEF cell plated on U, H and arrow shape micropatterns on polyacrylamide hydrogel substrate, respectively : fibers formed on both over adhesive and nonadhesive boarder of each shape. Images acquired: 60X oil objective.(scale bar 10 μm)*

Actin cables are not significantly larger upon nonadhesive edges than adhesive ones. Moreover, on soft micropattern, actin fiber appears to reach smaller curvature above nonadhesive edges in comparison to those observed on glass substrates. This last result may point out the major role of substrate stiffness in actin reinforcement and spatial organization. Here we would suggest that, on glass micropatterns, cells are probably overstimulated in their contractile regime leading to an increase in

actin fiber curvature. To demonstrate more clearly the role of ECM geometry in actin cytoskeleton organization, the average distributions of actin are obtained by averaging individual images over tenth of cells on each micropattern. A Matlab program has been developed in the lab to average actin or any kind of staining images over many cells. In particular, to compare size and intensity of fibres as well as focal adhesions without the influence of intercellular variation, the indivudal images are normalized in same intensity scale so that the integrated fluorescence over the cell is the same for all cells. The number of cells considered for averaging for each shape are 12, 11, 10 respectively. The obtained average actin images confirm the reproducibility of the localization of actin cable within a single cell. Averaged images show enrichment upon the periphery of the cell envelope as visible in figure 3.4.

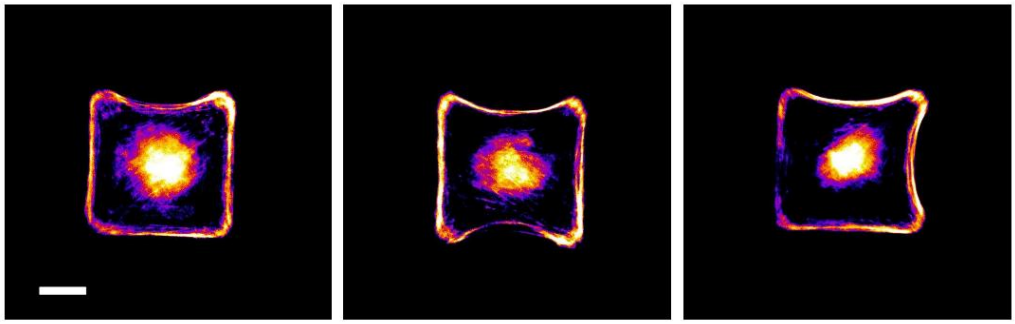

Figure 3.4.: *Average actin image ("Fire map")of MEF cell plated on U, H and Arrow shape micropatterns on polyacrylamide hydrogel substrate.(scale bar 10 μm).*

As suggested by Thery et al [40] the following question now arises: Does the development of such stress fiber organization driven locally by the geometry of adhesive conditions or governed globally at the level of single cell, by the equal distribution of a limited amount of contractile elements? Therefore, it appears necessary to investigate the relation between specific cytoskeletal organizations and cellular traction development within single cell.

It has been demonstrated that the size of focal adhesions (FA's) on which actin cables are anchored, is proportional to tension within the cable [13, 16, 83, 84]. Thus

imaging paxillin (adhesion marker) should give us a first estimation of the tension distribution within adhesive boundary conditions imposed by the micropatterns.

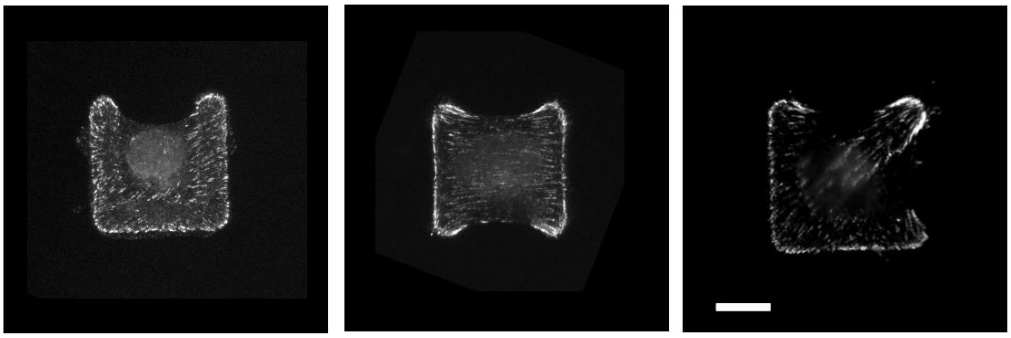

Figure 3.5.: *Fluorescence images of paxillin of single MEF cell plated on U, H and Arrow shape micropatterns on polyacrylamide hydrogel substrate. Images acquired: 60X oil objective (scale bar 10 μm).*

As observed in our experiments, focal adhesions, revealed by paxillin immunolabelling, are distributed around the pattern periphery with a higher concentration at cell apices where actin fiber cables attach as shown in figure 3.5. To further confirm the spatial distribution of FAs, we use the same averaging strategy as for actin fiber network quantification. The number of cells considered for paxillin averaging are 14, 21, 12 for U, H and arrow shapes respectively. Similar remodeling of focal adhesion has been observed (see figure 3.6) as previously described on hard substrate by labeling vinculin [40].

In response to different micropattern geometries, actin architecture and focal adhesion distribution are correlated. As shown in the schematic 3.7 below, the image of stress fibers are anchored to ECM via the focal adhesions in a reproducible manner as previously shown by other groups [6, 85, 86, 87]

However the literature for investigating the correlation between actin, FA and force is sparse [88, 89]. Therefore, we are interested in quantifying traction forces generated by acto-myisin contractile mechanism.

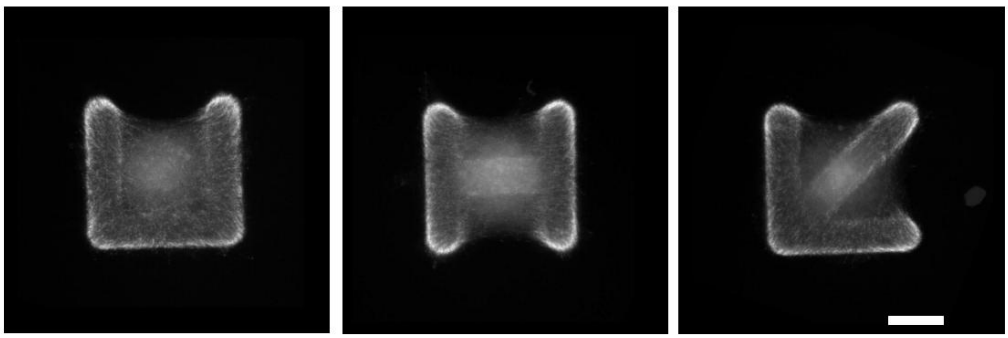

Figure 3.6.: *Average paxillin images over several MEF cells :Images show adhesions on U, H and Arrow patterns respectively. (scale bar 10 μm).*

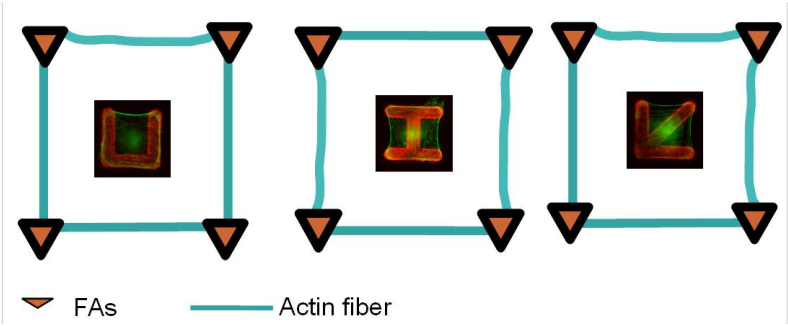

Figure 3.7.: *Schematic of stress fiber - focal adhesion coupling distributed over the projected area envelopes. (scale bar 10 μm).*

3.2.3. Cell traction force quantification in response to ECM geometry

In this sub-section, we will focus on how traction forces are spatially distributed in relation to previously observed actin filaments and paxillin organizations. To answer this question we quantify the force exerted by the cell both locally and globally on the ECM.

When cells are fully spread on the micropatterned substrate they are generally very flat (thickness in z direction is in the range of few micrometers). Therefore, force exerted on the substrate by the adherent cell, is considered to be tangential to the substrate as previously described by Schwarz et al. [68]. Force quantification has been done on polyacrylamide hydrogels embedded with fluorescent nano-beads as described in chapter2 and ANNEX. In order to maintain same experimental con-

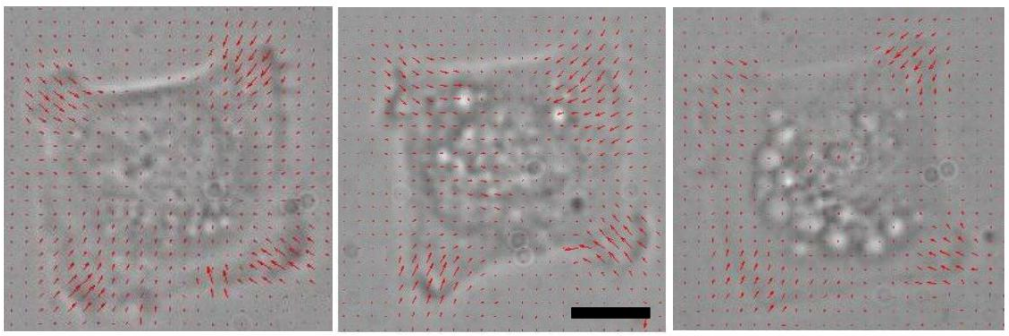

Figure 3.8.: *Single cell displacement vector map for U, H and arrow (↓): Forces are highly concentrated on the corner of the projected area envelope.(scale bar 10 μm).*

ditions (same cell passage/ same substrate), micropatterns are prepared in such a way that all the shapes are in the same bearing coverslip.

Displacement field of the soft substrate induced by cellular traction forces are determined by using stressed and relaxed images of the beads (see chapter2). Typical traction vectors for a single cell are shown in figure 3.8. Stress magnitude calculated for single cell by FTTC are shown in figure 3.9

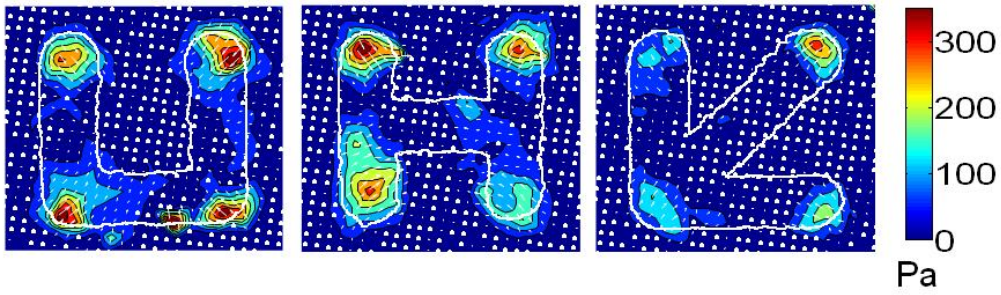

Figure 3.9.: *Traction contour map of a single cell on each micropattern shape (U, H, Arow).*

3.2.3.1. Average traction force distribution

Traction forces are calculated on individual cells, and the obtained stress maps are averaged over several cells to get a statistical distribution of force for each shape U,

H and arrow (number of cells per shape: 53, 58, 63 respectively). Figure 3.10 shows the average force contour map for each shape. The color code bar on the left side of the image shows the corresponding stress values (in Pa).

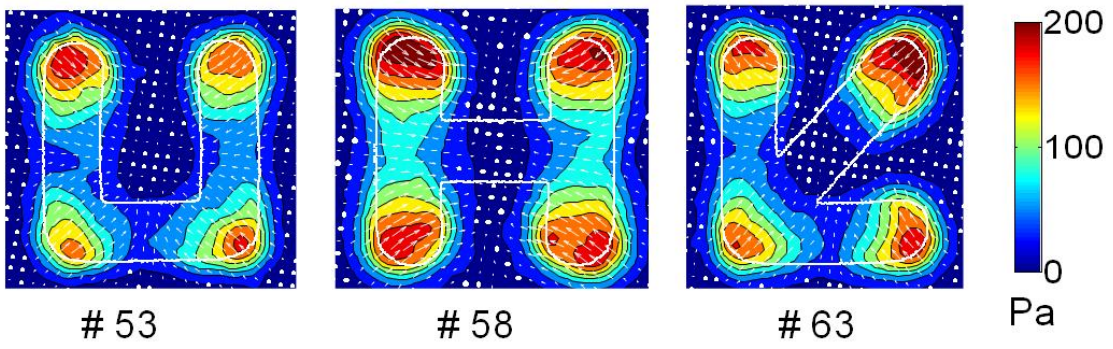

Figure 3.10.: *Average Traction contour map over large number of cells on each shape (U, H, Arow).*

It is clear from the average contour force map (as shown in figure 3.10)that forces are highly concentrated at each corner of the square envelope which is in good agreement with actin and paxillin distributions. In order to conclude we further proceed to total contractile energy calculation for each shape, averaged over the same number of cells used in stress calculation. Total contractile energy has been calculated by integrating over the same projected area envelope for each shape (see details in chapter 2).

$$U = (1/2) \int \vec{f}(\vec{r}).\vec{u}(\vec{r})dxdy \tag{3.1}$$

No significant difference in total contractile energy has been observed among all 3 shapes, having same square envelope as shown in figure 3.11.Therefore, we suggest that the cell regulates its internal tension globally so as to maintain a fixed amount of contractile energy for a given set of shapes, having same envelope, by spatially redistributing adhesive clusters and their related contractile elements. Probing local force distribution may reveal the effect of global tension regulation on local cellular traction forces and their relation with adhesive structural distribution.

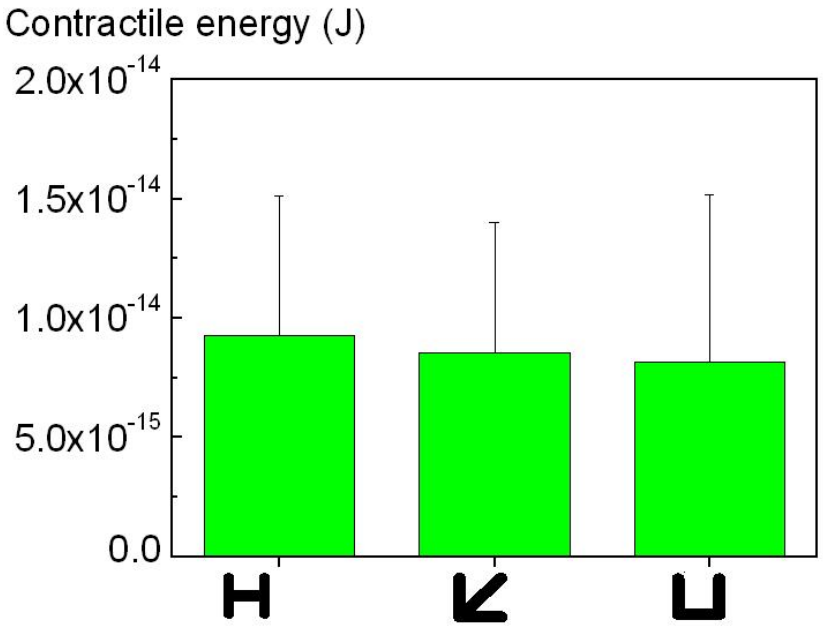

Figure 3.11.: *Average of total contractile energy developed by cells on U, H and arrow shape micropatterns.*

3.2.3.2. Local force distribution

To get a better insight on spatial redistribution of cellular traction forces in response to ECM geometry, we calculate average force on each corner of the pattern by averaging force on a circle of diameter 18μm on each pattern corner and normalized with respect to total force produced by cell. Results are presented in figure 3.12.

In all the cases, we found that the forces tend to be relatively higher at the point where nonadhesive fibers are connected, suggesting that tension along the non adhesive fibers are higher in comparison to adhesive ones. This argument is clear when we compare corner number 1 and 3 histogram bars with 2 and 4 on U shape. However, in the shape with symmetrical corners i.e H shape, forces are not equally distributed. These differences is certainly related to intercellular variability and calculation errors. Interestingly, we found that on arrow, two non adhesive fibers contacting at corner 3 lead to a local increase in traction forces. For the same shape, at corner 1 and 4 local forces are little higher as compared to corner 2 but lower than the corner 3 as expected (non adhesive vs adhesive fibers). These results confirm

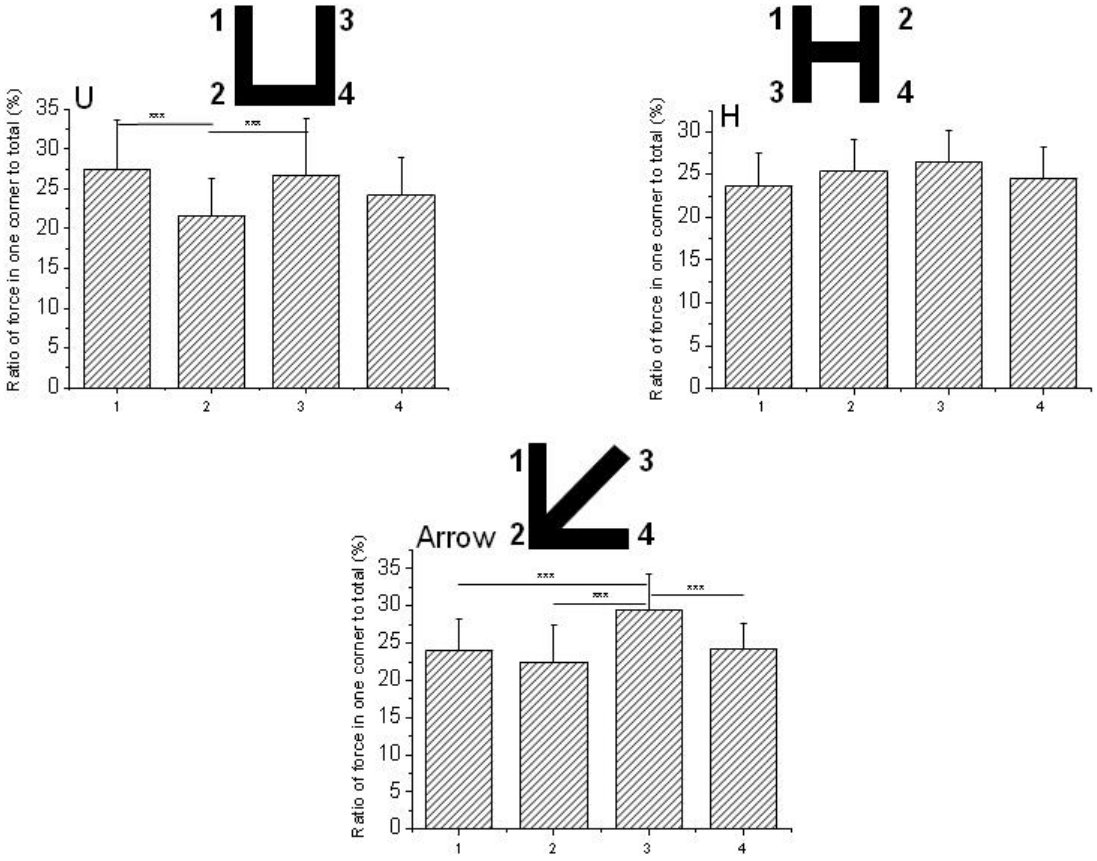

Figure 3.12.: *Local force distribution on each corner averaged over many cells(U=53, H=58, arrow=63) for each shape.*

that stress fiber strength along edges depends on local adhesiveness (ability of cells to form or contact numerous fibers).

3.2.4. Conclusion and Discussion

In this study, we have systematically investigated the influence of micron scale ECM geometry on cellular traction force distribution. Observations on force distribution is based on the use of a micropatterning technique combined with traction force microscopy. Results show that, for a given set of shapes having same projected area and square envelope while changing the underlying ECM geometry, total contractile energy is preserved. This contractile energy regulation in response to ECM geometry is achieved through local force redistribution. The observation on spatial

distribution of traction force measurement are co-localized with focal adhesion. An asymmetric distribution of focal adhesion throughout the pattern, while enriched upon the corners of the envelope is observed in correlation with actin fiber organization. Actin cytoskeleton remodels organization in response to ECM geometry. Most strikingly fibers are assembled and oriented both along adhesive and non adhesive edges of the cell envelope. Results obtained on soft substrate are dissimilar with results obtained earlier on hard substrate pattern. Moreover, tension in fiber along nonadhesive boarder are higher than the adhesive ones. Furthermore, actin structures are correlated with associated force distributions. Henceforth, local distribution shows higher stress value at the end of the nonadhesive fiber despite, having same total contractility. We thus can conclude that cells think globally but act locally.

Part II.

3.3. Towards a direct comparison of micropillar array with TFM on micropatterned substrates

To provide quantitative force measurements, experimentalists have mainly focused on designing tunable substrates in a variety of topography, geometry and rigidity that would enable both high spatial resolution measurements of substrate deformation and biocompatible functionalization. Traction force microscopy and micropillar (micropost) array are the two main methods that largely participated in describing cell rigidity sensing. However, TFM is based on experiments using continuous flexible hydrogel while micropillar studies are based on the utilization of discrete microtextured surfaces. Forces can directly be measured in Micropillar method from the deflection of the pillar. Hence, no approximation to be assumed so as solving inverse problem. However these technique lacks high resolution imaging. But the question arises now does it experiences physiological condtions like in tissue?

In this part, we will try to compare two techniques by designing continuous 2D micropatterned substrates, that will mimick 3D micropost arrays, on which we will measure forces exerted by Rat Embryonic Fibroblasts and that for different substrates rigidities.

3.3.1. Experimental approach

Traction force microscopy experiments are performed on continuous hydrogel, patterned in a regular array of circular protein coated dots mimicking the geometry and arrangements of array of micropillars used in related studies [82]. For both experiments, Rat Embryonic Fibrobasts (REF52)[kindly provided by Dr. Benoit Ladoux (University, Paris7)] are used. Cells are maintained at 37°C in a humidified atmosphere of 5% CO2 and 95% air in Dulbeccos modified Eagle medium (DMEM) containing 10% bovine calf serum. REF52 cells are plated few hours before microscopy experiments. Gel used for traction force microsopy experiments are patterned following a previously described procedure [87]. For details of the exper-

imental procedure and protocols see chapter2 and ANNEX.

A freshly prepared 2D soft substrates coated with protein (fibronectin)is shown in figure 3.13.

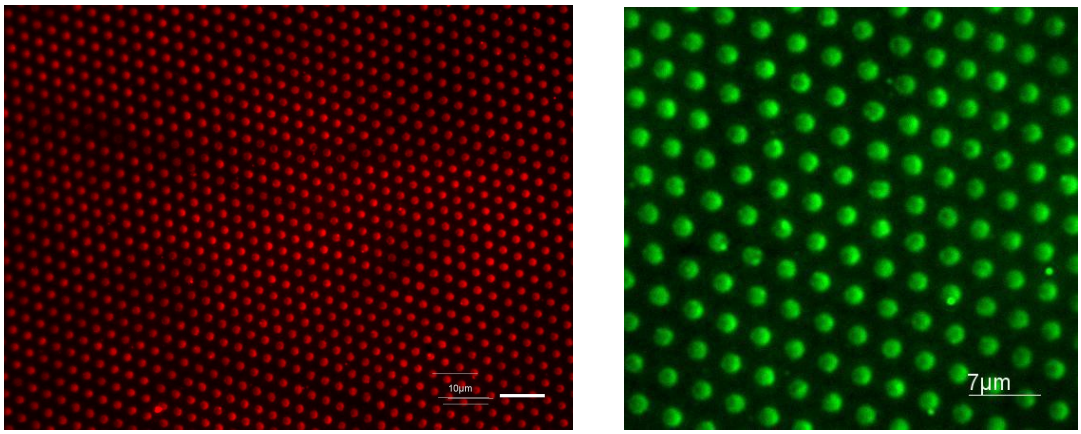

Figure 3.13.: *Circular array of 2D protein coated dots on a polyacrylamide hydrogel. Typical size of a dot is two micrometers. Images are taken in Cy3 Channel in epifluorescence microscopy with 20X and 40X air objectives respectively.*

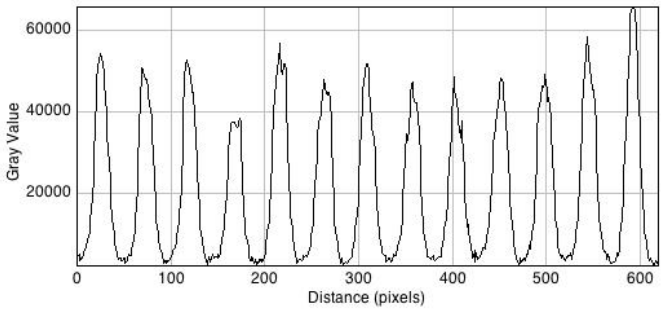

Figure 3.14.: *Intensity line profile of circular dot array indicates a strong contrast.*

Line profile of fluorescent intensity of the pattern image shows a high signal to noise ratio (figure 3.14) which implies a high spatial resolution achieved at micron scale via photo lithography. Figure 3.13 also shows a homogeneous protein distribution on the dot pattern. Here, size, center to center distance and arrangement of the dots fully correspond to micropost array structures.

In order to compare forces, substrates are designed for three different rigidities 7, 19.6, 40 kPa by changing the relative concentration of acrylamide and bis acrylamide in solutions (see chapter 2 for experimental details). REF52 cells permanently expressing YFP-paxillin, are plated on the protein coated substrate, engrafted with beads. Fully spread cells (see figure 3.15) are taken for observations or fixation 4 hours after plating.

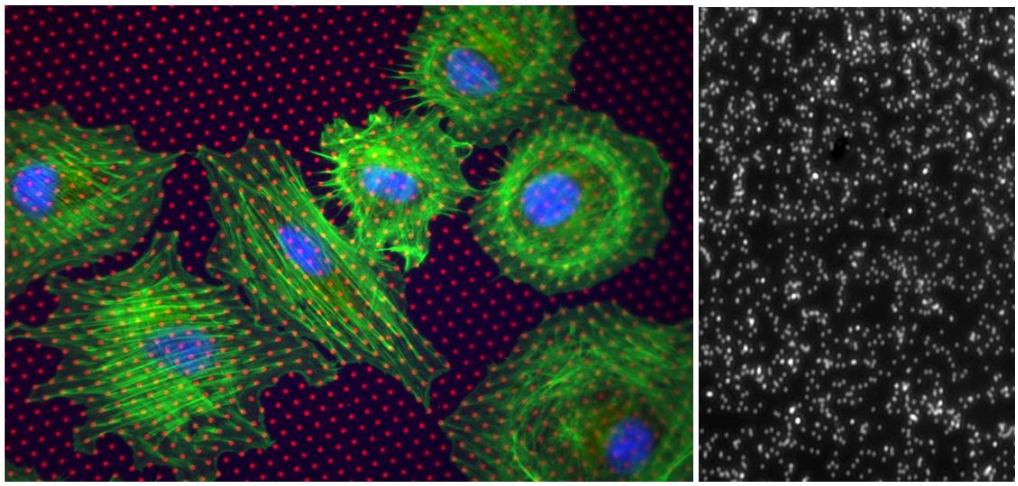

Figure 3.15.: *Typical image of REF52 cell adhering on circular dot microarray(left) Actin in green. Typical fluorescent image of embedded beads(right) in a 20KPa hydrogel. Bead images are taken in GFP channel with 40X air objectives with 1.5X microscope magnification.*

3.3.2. Traction force measurement

Force calculation on continuous substrate are performed using FTTC algorithm. First part of the TFM calculation is same as chapter 2. Substrate displacements are determined from images of fluorescent beads with and without the cell. After correcting experimental drift, images are divided into 6.72 μm square windows. First, average displacements are determined by cross-correlating on each pair of sub-images which are shifted accordingly. Then the fluorescent beads are tracked to obtain a displacement field with high spatial resolution. The final displacement field is obtained on a regular grid with $0.84\mu m$ spacing using linear interpolation. Force

reconstruction is conducted with zeroth-order regularization [75] in FTTC with the assumption that the substrate is a linear elastic half-space. The problem of calculating the stress field from the displacement is first solved in Fourier space and then inverted back to real space. The final stress field is obtained on a grid with 0.84 μm spacing.

To determine traction force vectors on individual adhesion dots in order to compare with the micropillar substrate, we need to integrate the stress field on each dot. Hence, we need position of the dots. First step is to acquire fluorescent images of the dot pattern simultaneously with the bead images. Pattern image is cross-correlated with a model dot which is a disk with a top hat intensity profile. A detection of local maxima in the correlated image provides the center of each dot. Working on the cross-correlated image makes the method less sensitive to inhomogeneities of fluorescence emission on the dots surface, which may cause localization errors. Finally, the overall traction force on each dot was obtained from the stress field by multiplying the stress value by the unit grid area and integrating over the dot surface ($3.5\mu m^2$). These typical distribution of traction forces can be compared to forces measured on micropillar substrates. All calculations and image processing are performed in Matlab. Figure 3.16 shows a typical force distribution for a single REF52 cell plated on a micropatterned polyacrylamide hydrogel so as to mimick a micropost array experiment.

3.3.2.1. Force distributions on different rigidities

Many studies have shown that cell adhesion forces are strongly influenced by physical properties of the extracellular matrix (ECM) [90, 91]. To compare how ECM stiffness is sensed by cells in continuous vs discrete substrate, we have plated REF52 cells on three different rigidities under the same experimental conditions. Cell traction forces are then calculated for more than 10 cells for each rigidity. All different substrates have the same protein concentration (20 μg/ml). Statistical distribution of forces, for all three different Young's moduli, are plotted in figure 3.17.

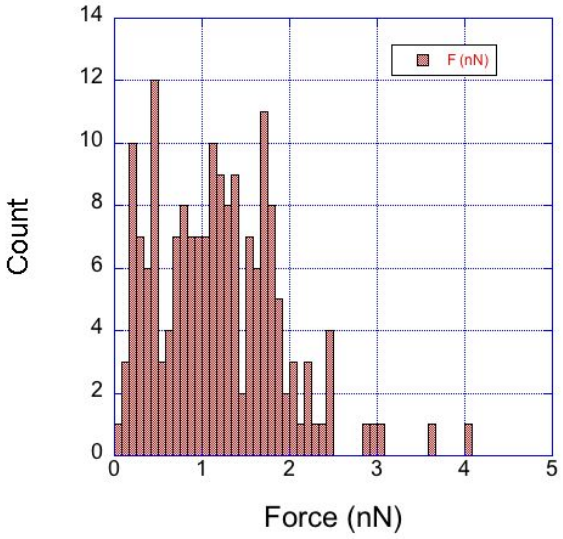

Figure 3.16.: *Statistical distribution of force per circular dot on a 7 kPa rigid gel for a single REF52 cell.*

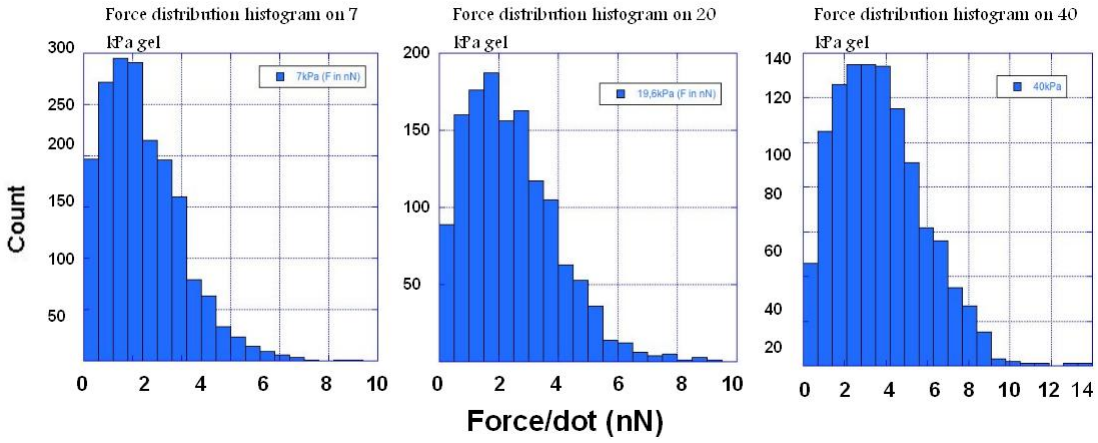

Figure 3.17.: *Statistical distribution of force developed by REF52 cells on dot micropattern with substrate rigidity 7, 19.6, 40 kPa.*

Increasing the substrate rigidity leads to a clear shift of the distribution towards higher forces as shown in figure 3.18. To get a clear view on that point we plotted the average force (per dot) exerted by the cells for different Young's modulus of the micro-patterned substrates where a strong correlation with the surface stiffness is exhibited as previously described by other groups [16, 82].

Indeed we observe (in figure 3.19) that increasing substrate stiffness of the un-

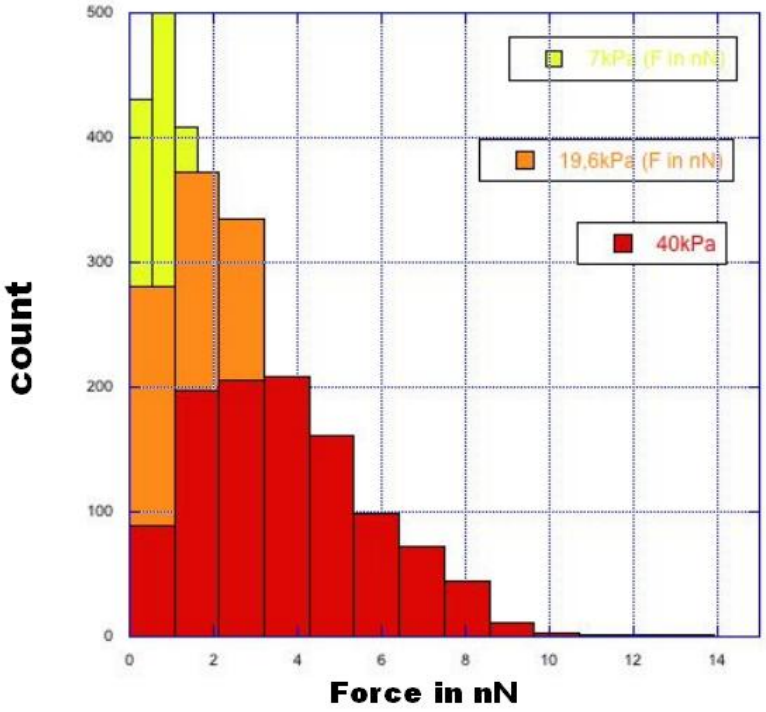

Figure 3.18.: *Histogram shows the shift of peak of the statistical distribution of traction force as rigidity increases.*

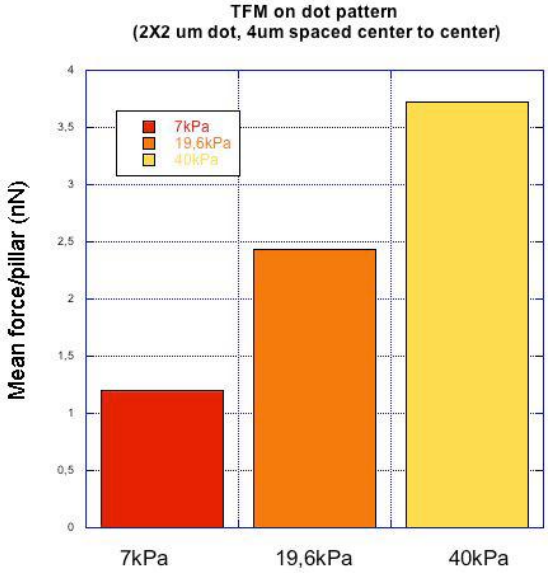

Figure 3.19.: *Histogram shows force comparison in different rigidities: Mean value of the force has been plotted.*

derlying hydrogel from 7 to 40 kPa enhanced the total cellular traction forces by approximately 50 to 60 % .

More precisely, we observe a linear increase of the average force per dot from 1.2nN to 3.7nN for moduli varying from 7 to 40kPa. This result highlights the ability of cells to sense the rigidity of their microenvironment. However, we did not reach the "classical" saturated regime of the maximal force exerted by cells.
In addition, previous studies have shown that cell rigidity sensing is often associated with different organization of their actin cytoskeleton and focal adhesion. In order to investigate the role of morphological cellular changes in the force transmission process, we next analyze the size distribution of focal adhesions as a function of substrate rigidity.

3.3.3. Focal adhesion size depends on substrate stiffness

FA's play an important role in cell mechanotransduction. To investigate the significance of focal adhesion behavior in rigidity sensing, we have quantified the adhesion area of prominent residents at focal contacts, known as paxillin, transfected with YFP on our model system, REF52 cells. We probe mechanotransduction using paxillin expression of REF52 cells in response to changes of polyacrylamide substrate Young's modulus. Paxillin expression on the circular array of adhesive dots is shown in figure 3.20. In paxillin images, we observe well-defined focal contacts localized with micropattern adhesive structures confining adhesions on micro dots. On individual dots, paxillin exhibits an elongated architecture directed toward the cell center as shown in figure 3.21(left).

We quantify the area of each focal adhesion assembly. To perform this analysis all image intensities have been normalized and thresholded to an arbitrary but identical value. FA's areas are measured for at least 10 cells per rigidity using Image J particle tracking plugin. Focal contact quantification method is schematically represented in figure 3.21. Mean focal adhesion areas are determined using FA's size distributions (typically 100 FA's per cell) measured on more than 10 cells. Results are presented in figure 3.22(right).

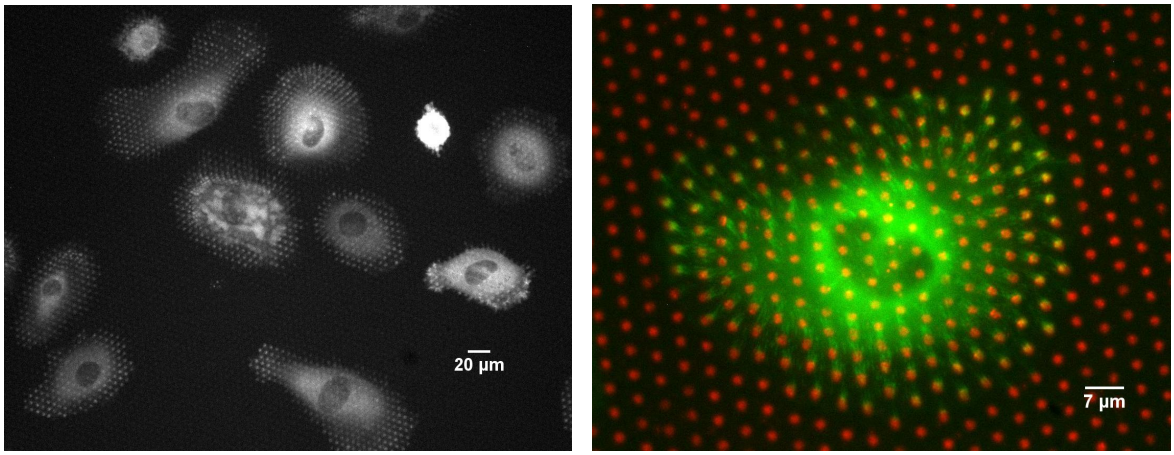

Figure 3.20.: *Paxillin adhesion distribution on regular array of circular dot. Right Paxillin (green) overlapped with protein coated pattern (red): Images acquired by 20X (left) and 40X (right) air objectives in YFP channel.*

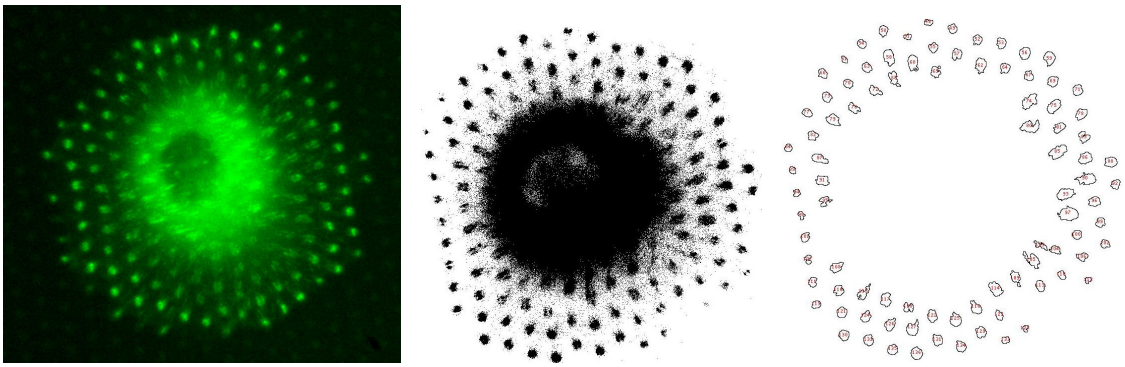

Figure 3.21.: *Paxillin adhesion area quantification: paxillin(YFP); Intensity thresholded image of paxillin (middle); binarized area of each adhesion assembly(right).*

As expected from previous studies [13, 20, 82] the size of FAs increases with increasing substrates stiffness. This result also appears to be highly linked with the previous force measurement (figure 3.18) and further suggests that focal contact growth is force induced. To study correlation between focal adhesion size and force, we plotted average force per dot along x-axis with mean focal adhesion area per circular dot along y-axis for all tested rigidities as shown in figure 3.23. Each point in the plot represents different rigidities from 7 to 40 KPa. It should be noted that

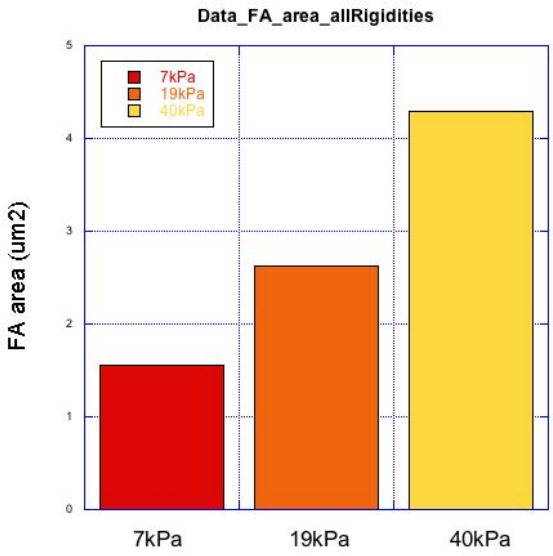

Figure 3.22.: *Mean focal adhesion area (determined by averaging over 500 circular dot) increases, in response to increasing stiffness from 7 to 40 kPa.*

each point in the plot has been obtained from an average over hundreds (500) of FA

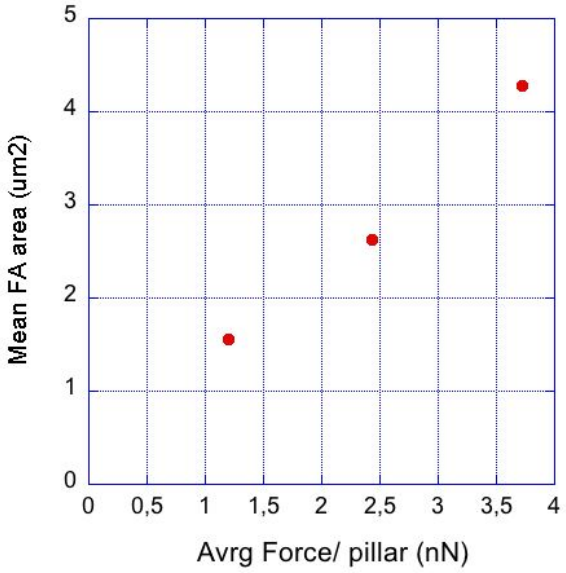

Figure 3.23.: *Mean focal adhesion area variation with average force per circular dot for 7 , 19.6 and 40 kPa rigid substrates.*

The result depicted in figure 3.23 shows a linear relationship between force and

focal adhesion growth in the lower rigidity regime. Thus, the force applied by the cell on its substrate is closely linked to the assembly of the adhesion sites. Moreover, forces exerted at single focal adhesion in fibroblasts are found to be of the order of a few nN. These two observations are consistent with previous estimations [13, 20, 82].

3.3.4. A few comparison on micropillar/patterned hydrogel

At the date of writing this report, REF52 force statistics on micropillars have not been performed. However Ghibaudo's paper in Soft Matter [82] allowed us to extract informations so as to compare our two experiments. Ghibaudo and colleagues propose "an elastic model that estimates the equivalent Young's modulus, E_{eff}, of a micropillar substrate". This model leads to the following equation:

$$E_{eff} = \frac{9 * k}{4\Pi * a} \tag{3.2}$$

where k is the spring constant of a micropillar and where a corresponds to either the size of FA or the radius of the pillars. As in both experiments we used 1 micrometer radius pillars, the relation between E_{eff} and k is E_{eff}=0.7×10^6k. Thus by using this simple relation , we want to compare our results on 7, 20 and 40kPa respectively we have to consider forces and FA measurements done on micropillars of stiffness of 10, 28.5 and 57 nN/micrometer respectively. Figure 2/C of Ghibaudo et al. enables us to have some estimation of corresponding rigidity associated forces. Our observations are summarized in the following table.

E kPa	E_{eff} kPa	k(10^6) nN/μm	F_{pillar} nN	F_{dot} nN
7	7	10	2	1.2
20	20	28	4	2.6
40	40	57	7	3.7

Table 3.1.: Force comparison on discrete (MDCK cell) and continuous(REF52 cells) substrate.

Taking Ghibaudo's model into consideration, this table 3.1 highlights the fact that our cells exert less forces for comparable stiffnesses. However, forces increases 50 to 60 % with increasing substrate rigidity. This force variation may be a consequence of using different cell type. Nevertheless, the difference is really significant. In one of his recent papers [5], Denis Discher ask the following question; "How deeply do cells feel?". After reminding that cell-induced deformation of ECM propagates a finite distance into the matrix and is invariably accompanied by cell deformation, he proposed that this deformation propagation "probably contributes to the feedback mechanisms that regulate cell contractility and help to maintain a basal level of cell pre-stress (tension)".

A micropillar surface does not have the same mechanical behavior as a semi-infinite elastic substrate. Each micropillar may be considered as a small independent spring. The Green's tensor of the micro indented surface is therefore extremely localized, whereas the Green's tensor of a semi-infinite elastic solid decreases as 1/r, where r is the distance between the applied force and the location of displacement. Therefore, continuous substrate allows deformation to propagate throughout long distances while pillars restrict deformation propagation to the pillar itself. Consequentely, biomechanical feedback loop induced by substrate deformation does not occur anymore (as each pillar is independent from the others) leading the cells to reach higher tension levels. This argument would explain largely the observed differences between the two set ups.

Finally we remove the adhesive constraints imposed by the substrate by studying same cells on homogeneous substrate. We compared tractions forces exerted by REF52 cells plated on 7kPa micropatterned substrates versus 7kPa homogeneously coated ones. In non-patterned substrate, average stresses are determined from local stress integrating over whole cell surface. Then to compare with force per circular dot we multiplied average force with circular dot area,

$$P = \frac{\int pds}{s}, \tag{3.3}$$

Where P = average stress; p = stress on small area ds ; s = total surface area under the cell. Force (F) per circular dot can be written as

$$F = P * S, \tag{3.4}$$

S = area of the circular dot.

Results obtained are presented in figure 3.24 histogram where $< F >$ is average force per circular dot area.

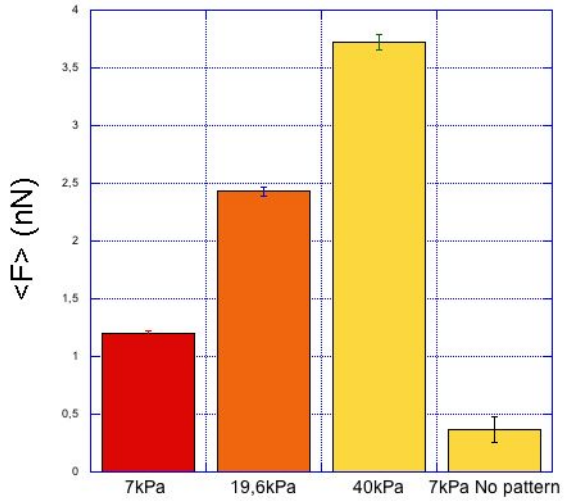

Figure 3.24.: *Force comparison on pattern vs non-pattern substrate of rigidity 7 to 40 kPa.*

We found that lying on substrates of identical rigidities, cells exert significantly higher forces on micropatterned hydrogels. This observation is consistent with our previous findings on single cell micropatterns in which cells tend to form large contractile fibers above non adhesive regions leading to local increase in cellular traction forces. Result is not surprising since focal adhesions are localized on the dots while for homogeneous substrate adhesion are not biased. Therefore, in average force calculation whole cell area is considered as shown in eq. 3.3

3.3.5. Conclusion and Discussion

By coupling hydrogel micropatterning with Traction Force microscopy using Fast Fourier Traction Cytometry algorithm , we are able to correlate forces that single

REF52 cell develop with the focal adhesion size by measuring paxillin. Moreover, culturing the cells on 7, 20, 40 kPa hydrogels, shows a linear correlation of substrate rigidity with cell traction force in the lower rigidity regime. In this regime we find linear relationship between force per adhesive area with focal adhesion size. Using quantitative approach we were able to compare our observations with the results obtained on discrete substrate such as on micro-pillars. Although, different cell types are used for force comparison, our observation show a reduced cell contractility on continuous substrate which may be due to the fact that the micropillars do not allow cell to sense long range deformations which may lead to increase basal tension in the absence regulating feedback. Finally our findings may suggest that substrate texture plays a major role in transmission of cell induced deformation and ultimately in cell rigidity sensing.

4. Spatial correlation between actin generated forces and centrosome positioning

4.1. Introduction:

Cell responds to physical cues of their microenvironment, such as stiffness and geometry of the ECM [40, 92]. More precisely, geometrical features such as shape of the substrate are known to affect cell traction force and adhesive structural organization as we have shown in the previous chapter. However, little is known about the effect of distribution and orientation of traction forces on cell internal organization. To elucidate force distribution influence on organelle distribution, we will discuss the potential relation between spatial force distribution and centrosome positioning in this chapter. We try to correlate traction force with centrosome distribution.

Centrosome is the main microtubule organizing center (MTOC) of the animal cell as well as a regulator of cell-cycle progression. It has been suggested by Michel Bornens that the centrosome is"suspected from the start to have a role in cell symmetry breaking and the maintenance of cell polarity"[26]. Interestingly, when adherent cells are free to spread on a substrate, the centrosome self organizes at the geometrical center of the cell. The precision of this centrosome centering have been nicely demonstrated when cells were cultured on a glass substrate where cell shape was confined [23, 26]. Thus, centrosome positioning at the cell center appears to be tightly regulated and to be a fundamental event in cell polarity establishment. The

microtubule network plays a leading role in centrosome positioning. However, it still remains unexplored how actin generated forces are linked to centrosome positioning. In this chapter we have investigated the relation between cellular traction forces and centrosome positioning in response to different ECM geometry.

4.2. Experimental Details

4.2.1. Micropattern design:

Four geometrical shapes are designed for the study. The chosen shapes are V, T and ⅄ (tripod), having the similar triangular envelopes and plus (+) has square a envelope.

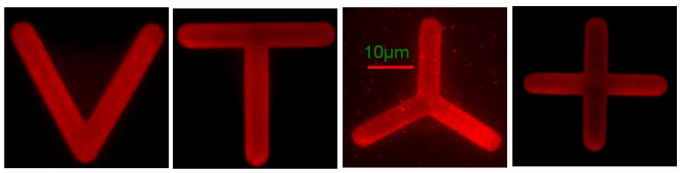

Figure 4.1.: *Fluorescent image of the fibronectin coated micropatterns (red-fibrinogen conjugation) taken with magnification factor of 60X.*

Figure 4.1 shows fibronectin coated pattern conjugated with fibrinogen in red. Projected area given to each cell is nearly $900\mu m^2$. Ligand binding sites onto the substrate is maintained constant for all patterns throughout the experiments by maintaining fibronectin/fibrinogen concentration.
For experimental setup details see chapter 2 and protocols in ANNEX A.

4.2.2. Cell culture on micropattern:

When cells are plated on micropatterns, it takes about 30mins to 1 hr for the cells to fully spread on each shape in a restricted manner such as imposed boundary condition are respected. Figure 4.2(top panel) shows bright field image of MEF cells, spanning over the whole triangular envelope. Images are acquired after 2hrs of plating. When cells are on the soft pattern, forces exerted on the substrate by cell

contractile mechanism induce substrate deformation as shown in figure 4.2(bottom panel).

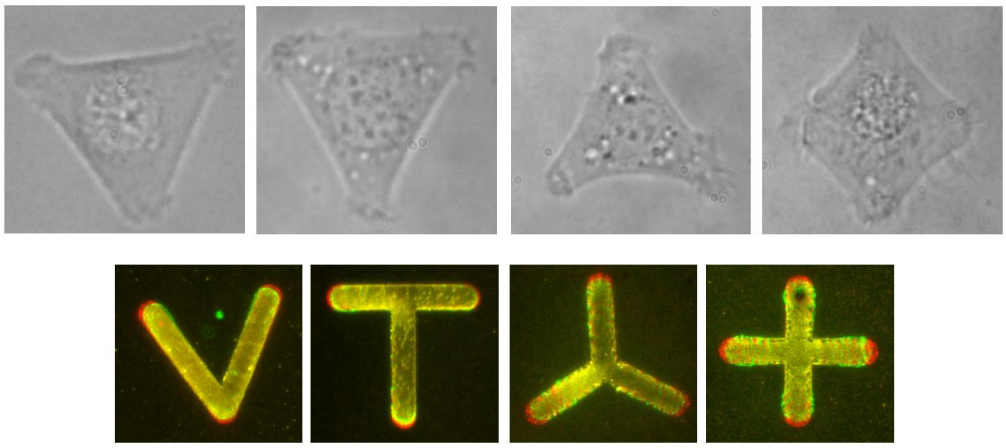

Figure 4.2.: *Bright field image of MEF cells on fibronectin coated micropatterns (top). Overlapped images (bottom) of stressed(green) pattern with relaxed(red) pattern.*

4.3. Cell internal organization in response to ECM geometry

Recent work by Terenna et al. has shown that the actin cytoskeleton is responsible for cell polarity and growth where microtubule network determines polar direction [96, 95]. However very few studies in the literature show a correlation among actin organization , focal adhesions with centrosome positioning [93].

Here, we mainly focus on the actin cytoskeleton, focal adhesion and centrosome distribution on the patterned cell to elucidate the complex function of integration among cell shape, mechanics, architecture and polarity.

4.3.1. Actin architecture

To visualize cell cytoskeleton organization on a given pattern, actin cables are revealed by phalloidin immuno-staining. When MEF cells are fully spread, after 2-3

hrs of plating, cells are fixed and stained. Reproducible fiber bundles are enriched upon both adhesive and nonadhesive area which connects the extreme edges of the pattern. Figure 4.3 (upper panel) shows non intersecting actin fibers formed by a single cell on V, T, Tripod and plus micropatterns. The space between the adhesive bars are filled with sparse actin fibers.

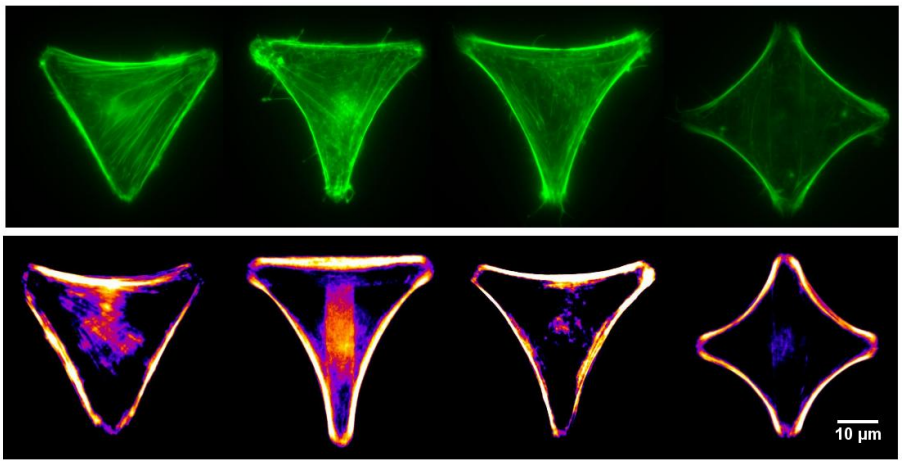

Figure 4.3.: *Actin fibers(green) organized inside single MEF cells plated on V, T , Tripod, Plus shapes (top panel). Images acquired: 60X oil objective. "Fire color map" of actin fiber cables averaged over several cells on the respective shapes (bottom panel).*

Actin stained images have been averaged over several cells on each micropattern(V = 10; T= 15; Tripod= 20; Plus= 15). All images are normalized to the same intensity scale.

Averaged actin images are shown in figure 4.3 (bottom Panel). Color code in "fire map" shows a higher concentration of actin ($purple \rightarrow yellow$) densely accumulated along the periphery of the triangular envelope. Fiber network is concave over non adhesive region and in contrast, fibers are mostly straight along the adhesive edge of the pattern, which is in agreement with our previous findings (chapter 3).

These formation of actin bundles can stimulate the formation of focal adhesion since actin fibers are strongly coupled with adhesion sites as we have seen in chapter 3. To establish strong correlation between actin and FA, it is important to reveal FA distribution.

4.3.2. Focal Adhesion distribution in response to ECM geometry

Focal adhesions not only provide the linkage between ECM and the actin cytoskeleton. It also act as a microsensor in biomechanical signaling. FAs are mainly mediated by integrin clustering which connects actin cytoskeleton in an integrated manner to generate both stable and transient adhesive structures. Focal adhesion formation has an effect on cytoskeletal architecture which in turns induce mechanical forces that reciprocally work as feedback to influence focal adhesion size, protein localization, and cytoskeleton remodeling. Thus it is interesting to investigate the role of focal adhesion in centrosome positioning.

Focal adhesions are revealed by paxillin immuno-labelling. Cells on the 4 different shapes are prepared such a way that all are in a single $24 \times 24mm^2$ coverslip to maintain same experimental conditions.

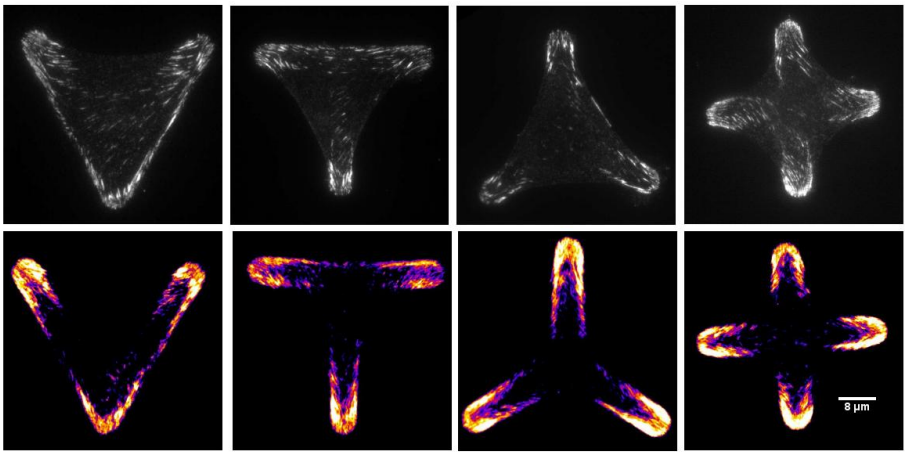

Figure 4.4.: *Focal adhesion distribution(upper Pannel) in a single cell, are revealed by Paxillin in YFP channel. "Fire map" of average paxillin image shows adhesion enriched area on the pattern. Images acquired: 60X oil objective.*

An anisotropic distribution of paxillin has been observed on all micropatterns. Each individual adhesion sites, i.e paxillin, presents an elongated shape which is oriented along the fiber direction i.e the direction of pulling force [Figure 4.4(upper pannel)]. Paxillin in cells plated on the micropattern are accumulated with a greatest density along the edges of the envelope periphery. The distribution is very

similar to those observed on glass substrates for identical shapes [40].

To better understand focal adhesion distribution, we averaged paxillin image over several cells for all shapes (V = 8; T= 14; Tripod= 13; Plus= 19). All images are normalized in the same intensity scale. Average paxillin image as shown in figure4.4 (bottom panel) are preferentially localized at the extreme edges of adhesive pattern in agreement with previous studies [40, 97, 98]. No adhesion has been observed at the center of the micropattern. Paxillin distributions are strongly co-localized with force as FA contacts developed with force [97]. Accumulation of FAs at the extremities of the actin fiber cable provides link between FA and actin network. This proves that cell shape changes the organization of actin cytoskeleton that in turn governs focal adhesion formation. Next we focus on the centrosomes are distributed on different shapes to correlate with adhesion and actin organization.

4.3.3. Centrosome distribution:

Centrosome is a subcellular organelle, which plays a key role in cell division, migration, polarization etc. It has been shown before that centrosome plays an important role in defining cell polarity. To investigate the role of centrosome in cell centering and cytoskeletal organization, we first plated cells on the individual micropatterned substrates. To elucidate the precise position of the centrosome, γ-tubulin(yellow) has been stained as shown in figure 4.5 (top panel) in yellow. The brightest spot in γ-tubulin images shows centrosome position of a single MEF cell.

Several centrosomes are plotted on different micropattern in a single image window as shown in figure 4.5. However, on V and T micropattern centrosome distribution is off-centered with respect to the geometrical center by localizing the distribution in the upper region of T shape and lower region of V-shape. Now the question arises whether centrosome could be regulated by adhesion geometry. In order to find a correlation we calculate the center of mass(COM) $\vec{r}_{com}$ of average paxillin images

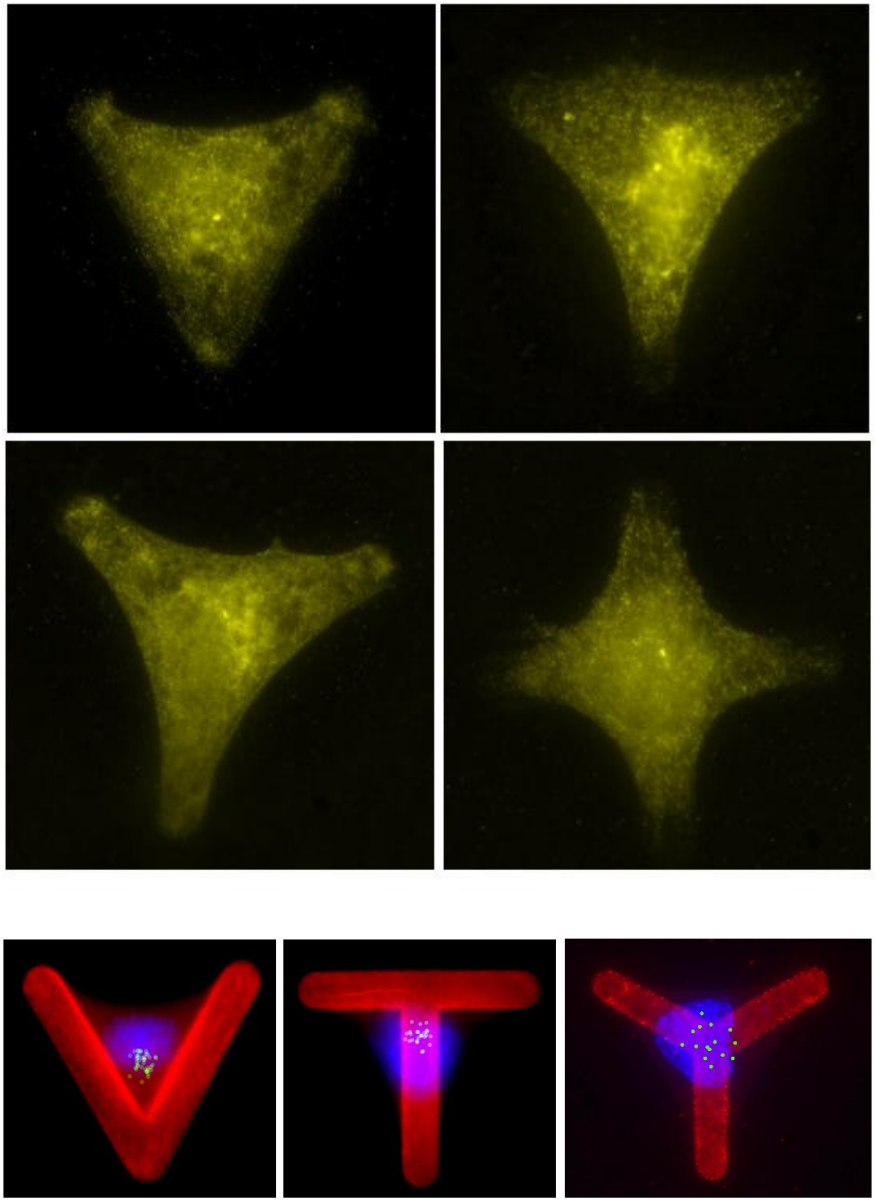

Figure 4.5.: *γ−tubulin stained in GFP(top): Bright spot in the middle is the centrosome. Distribution of the centrosomes(blue) plotted on a pattern(red).60X oil objective.(V = 23, T = 40; tripod = 12).*

by,

$$\vec{r}_{com} = \frac{\int_S I(\vec{r})\vec{r}dS}{\int_S I(\vec{r})dS} \tag{4.1}$$

Where $\vec{r}_{com}$ is the position of the center of mass; I($\vec{r}$) is the fluorescence intensity at the position $\vec{r}$;

$\vec{r}$ is the position of the considered small area dS, S is the total surface area.

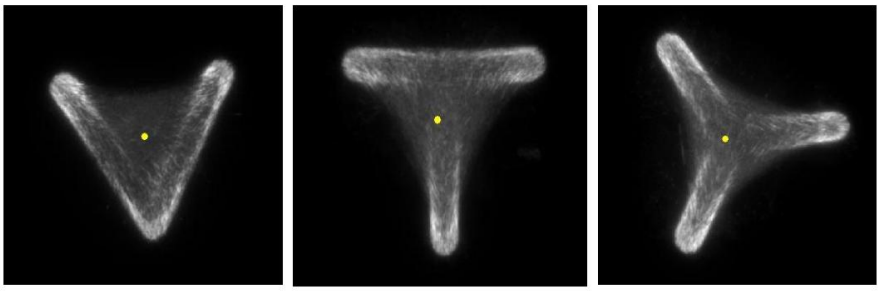

Figure 4.6.: *Focal adhesion converges to center of mass of ECM marked in yellow.*

We found that paxillin COM converges near the centrosome distribution center (as shown in figure 4.6 for all 3 shapes.) showing a strong spatial correlation between substrate adhesions and centrosome centering. This results may suggests an underlying mechanism which links centrosome positioning to the adhesion distribution and actin architecture.

On the other hand, cell adhesion sites work as microsensors to feel the microenvironment such as ECM geometry, which affects the force distribution. In addition physical basis of cell contractile forces are actin network. Therefore force distribution may complete correlation among actin network with paxillin and centrosome distribution.

4.4. Traction force distribution on different shapes

We have used Traction Force Microscopy (FTTC) method as described in chapter 2 for cell traction force quantification on 5 kPa substrate. Single cell induced displacement field of the substrate is shown for a single cell on each shape in figure 4.7 (upper Panel) (Typical displacement of an individual bead can reach values up to 2 μm). Vector length in figure 4.7 (upper Panel) corresponds to the relative magnitude of the displacement.

Typical force field of single cells on each pattern is shown in figure 4.7 (bottom panel). To make force distribution more clearly visible, we computed stress contour map. Figure 4.8 shows the single cell traction contour map. Color code in the cell

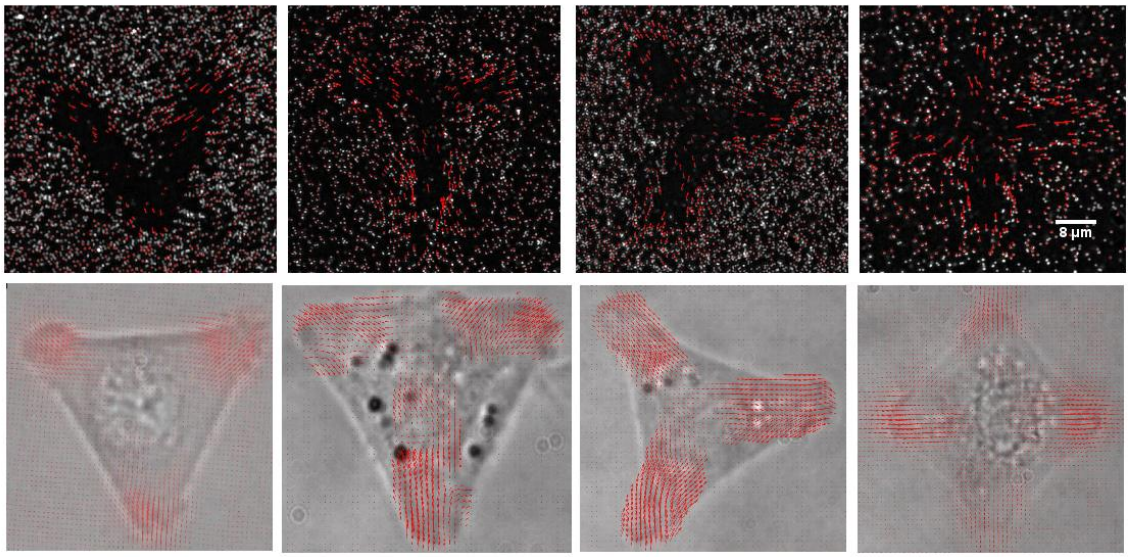

Figure 4.7.: *Displacement vector map of beads in YFP channel(top). Force vector map deduced from the displacement field overlaid on cell image cultured on protein coated micropatterns (down).*

traction contour map shows corresponding stress value(↑) in figure 4.8. It may be surprising that forces seem to lay beyond the pattern area. This is due to the limitted spatial resolution of calculated force map so that each point force has footprint of several microns [53].

From the single contour map it appears that the forces are exerted on each corner of the pattern. To give more clarity to our statement, we performed a statistical analysis by screening a large number of cells for each shape(V = 82; T = 53; Tripod = 79; plus = 45). To achieve statistics on a large number of cells, experiments were performed on different days while maintaining the same experimental conditions. A Matlab program has been developed to produce average stress map in which pattern images are used to correct translation and rotation for averaging calculation.

We found that for ⅄ and plus shape, forces are symmetrically distributed (see fig.4.9) at each corner of the envelope unlike V and T shapes, where force distribution is asymmetric. The reason might be related to the fact that V and T shapes have stress fibers both above adhesive and nonadhesive boarders, contrary to ⅄ and plus shapes. Indeed, we have shown in the previous chapter that stress fibers above

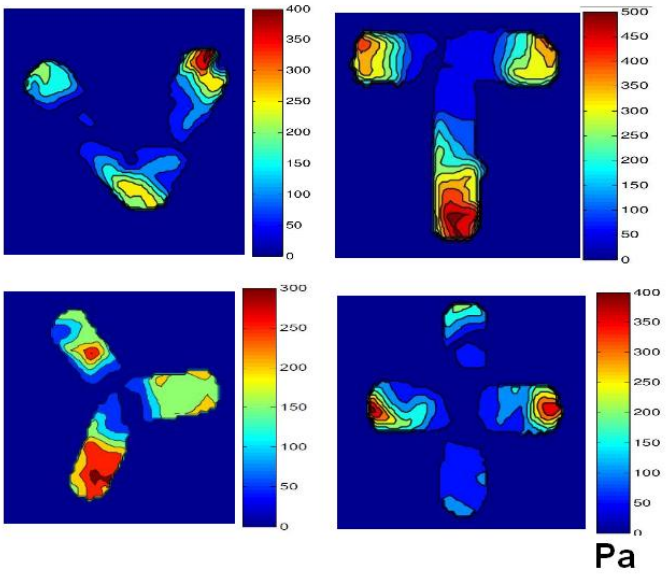

Figure 4.8.: *Stress contour map of single MEF cells cultured on fibronectin coated micropatterns for all 4 shapes (V, T,Tripod and plus respectively).*

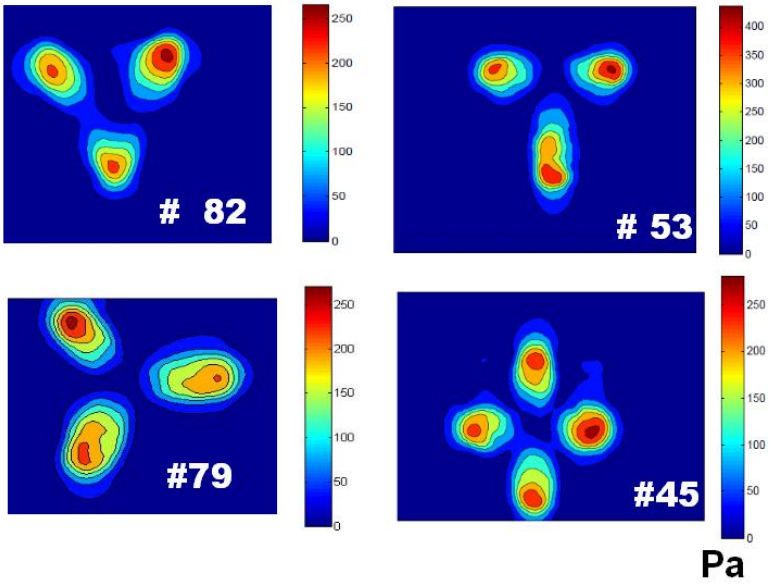

Figure 4.9.: *Stress contour map obtained by averaging over several cells.*

adhesive and nonadhesive boarder have different level of contractility and consequently affect local stress distribution. To understand better the force distribution asymmetry in response to ECM geometry, we then probed local force distribution and its orientation.

4.4.1. Local force distribution and orientation

In this sub-section we focus on the local force quantification (magnitude and orientation at each pattern corner). To simplify the problem we consider that forces are essentially applied in the corners of V, T, ⅄ and plus which is justified by the average stress map (see figure 4.9). We calculate average force over an area of 18μm diameter circle at each corner of all shapes. We remark that the forces, located at each pattern corner of of V and T shapes are off- centered with respect to ECM geometrical center(GC). For V shape forces are directed towards the lower part of the pattern whereas, in the case of T shape forces are pulled towards the upper part. In contrary, for ⅄ and plus where vectors are directed at the pattern center. It is to be noted here that ⅄ and plus are symmetric shapes. Moreover, in case of ⅄ and plus shapes pattern center of mass(COM) and pattern geometrical center(GC) coincides at center. Results obtained on symmetric and asymmetric shapes are discordant as clearly visible in case of V and T shapes than ⅄ and plus shape in figure 4.10. Highlights of the results are in different color : red mark in the middle shows the center of mass of each pattern, purple circle is the area over which forces are averaged, green arrow shows the average force orientation directed towards a point very close to the pattern COM.

From these observations, we may suggest that cell traction force convergence depends on the underlying ECM geometry. We observe that force orientation on V and T deviate from the geometrical center in the same direction as the centrosome position or the adhesion distribution. Therefore it may suggest an underlying mechanism relating to centrosome centering, focal adhesion distribution, actin organization and force distribution. Although observations need to be confirmed by further studies, our results indicate correlation between centrosome position and actin structures. Moreover actin generated force distribution is correlated with centrosome positioning.

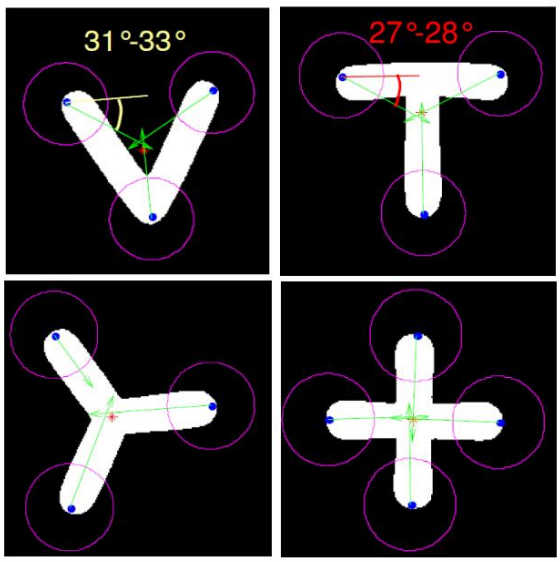

Figure 4.10.: *Average forces(green), calculated on each corner are directed towards the pattern center of mass, marked in red.*

4.5. Total contractile energy

In this section we calculate total Contractile energy on each micropattern (V, T, ⅄, Plus) and averaged over a large number (more than 50 cells for each shape) of cells. Though projected area are not exactly equal with deviation nearly 3 to 12% from the mean, with maximum area in ⅄ shape, we observe that total contractile energy on T shape is higher than other shapes. It seems that cells on T shapes are more contractile.

To further investigate cell contractility we calculate the percentage (adhesive) area difference on each pattern with and without cell. Average percentage area contraction of each stressed pattern with respect to relaxed pattern shows same baised behavior on T shape [see in figure 4.11 (left)], confirming higher level of contractility. We thought that the biomechanical regulation may reach to saturation for T shape because of geometrical stimulation. May be there is an interplay of geometry and envelope which leads to such behavior. It requires detailed analysis and understanding.

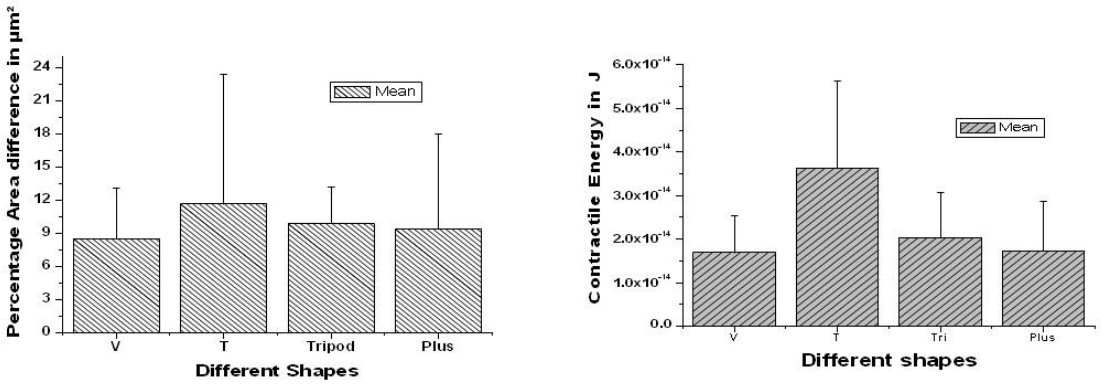

Figure 4.11.: *Average percentage area difference (left) for each pattern with and without cell; and error bar is the standard deviation for each individual case. Contractile energy averaged (right) over several MEF cells cultured on protein coated micropatterns for all 3 shapes.*

4.6. Conclusion and Discussion

In this chapter we see that centrosomes are distributed off-centered with respect to geometrical center of the pattern for the V and T shapes in contrary to ⅄ and plus shapes. Hence, centrosome positioning are influenced by ECM geometry. We also find that center of mass of the average paxillin distribution on each shape coincides with the COM of ECM. We observe that the forces are located on the upper part of the T shape and in the mower part of the tripod shape. We thus may say that mechanism of centrosome positioning correlated to FA distribution. Moreover actin generated forces are directed towards the centrosome distrubution center when we calculate average forces on each corner of the pattern. We propose that this result is an interplay among centrosome, actin cytoskeleton, actin generated forces and focal adhesions. We also observe a biased behavior on T shape in total contractile energy and percentage area measurements which seems to contradict the previous observation on square envelope. We would suggest that there is an increase of basal tension which may be due to an interplay of the geometry and ECM and envelope. However, present results here are under careful analysis and investigation.

5. Thermoresponsive micropatterned substrates for single cell studies

5.1. Introduction

Surface micropatterning is a powerful tool for the design of cell-based assays and sensors, or for fundamental studies of cellular response to environmental cues [102, 103, 104]. Such patterns have proven to be highly valuable for e.g. statistical analysis of the response of cells cultured in a well-controlled microenvironement [23]. Micropatterning has attracted many polymer physicist over the last few years to make the micro-structure design more suitable for cell biology research. There are different polymers which are sensitive to specific wavelength of light or temperature. These polymers can be used to enrich the biomedical device sensitivity and functionnality.

This chapter contains a description of a new approach to design micropattern for single cell studies. Here we describe the combination of surface chemistry and microfabrication techniques which allows to create substrates onto which adhesion can be tuned so as to obtain regular 2D arrays of immobilized cells. The work in this chapter has been done in collaboration with Dr. Lionel Bureau. He has done polymer brush synthesis and characterization. Next part which we have developed , is creating micropattern on the polymer brush and surface functionalization. Then in collaboration we showed adhesion and thermo-detachment of cell on the pattern .

The microfabrication technique which we have developed, is based on the use of poly(Nisopropylacrylamide) (PNIPAM) polymer brushes. The main interest of working with PNIPAM is that the polymer is sensitive to temperature (PNIPAM polymer chain in water becomes hydrophobic above the lower critical solution temperature of the polymer, around $32°C$). Many applications in bioengineering, especially in microfluidics have used PNIPAM temperature sensitivity to design switches or valves to control fluid flows. Grafted PNIPAM polymer turns out to be a promising surface modifier in order to control cell adhesion.

Patterned brushes of passive water soluble polymers, can be elaborated by two main routes:

1. uniform coating of the substrate grafted-onto brush by adsorption of a block-copolymer containing a protein-repellent part (often poly(ethyleneglycol)) stretching away from the underlying surface. Such a uniform brush is subsequently patterned by selective UV irradiation to create adhesive zones[105, 106].

2. polymer brushes grafted from the substrate, i.e. grown from a layer of polymerization initiators first grafted on the substrate. Patterning is achieved by micro-contact printing of the initiator, which ensures a growth of polymer chains restricted to the initiator-printed regions [107, 108].

These are two very important techniques to create adhesive pattern in the field of single cell studies.
On the other hand, it has been shown by Okano et al [109] that poly (Nisopropylacrylamide) (PNIPAM) brushes could be use for the cell detachment. PNIPAM polymer undergoes conformational change below Lower critical Solution Temperature (LCST) and swells, when temperature goes down from 37° to below 32°. The cell detachment has been shown when thickness of the brush are low enough [110, 111]. But if the polymer grafting is very thick , then irrespective of the temperature brushes becomes nonadhesive for the cell [112, 113].

In the present work we have developed a method to fabricate thermoresponsive micropatterned substrates which combines many of the advantages of the above-mentioned techniques and allows for single cell studies. Unlike all other work [110, 111, 112, 113] the dimension of the pattern can be achieved down to $4\mu m$. A key point in designing micropatterned surfaces is to obtain a high contrast between the regions onto which cells attach and the surrounding non-adhesive background. The use of background polymer coatings, and in particular polymer brushes, have become a favorite choice, for they exhibit excellent protein-repellency, hence efficient cell non-adhesiveness.
Here is a short description of the new approach with advanced properties, that have been developed by us.

5.2. Polymer brush synthesis on glass coverslip:

PNIPAM brushes are grafted from glass coverslips and oxidized silicon wafers by surface-initiated Atom Transfer Radical Polymerization (ATRP). All aqueous solutions were prepared in ultra-pure water. To create PNIPAM polymer brush, several steps are involved. The following diagram 5.1 explains the main required steps :

1. Glass or silicon substrates are cleaned in a sodium hydroxide aqueous solution and rinsed with water.

2. Samples are immersed in an aqueous solution of 3- aminopropyl- triethoxysilane (APTES) of proper concentration c_{APTES}.

3. After rinsing with water it is dried in a nitrogen stream.

4. Samples are immersed in solution mix of dichloromethane, containing triethylamine (TEA) and 2-bromo-2 -methylpropionyl bromide (BMPB).

5. Samples are rinsed with dichloromethane, ethanol and water.

6. A solution of N -isopropylacrylamide (NIPAM), 1,1,7,7 - Pentamethyldiethylenetriamine (PMDETA) and water is prepared.

7. Initiator-grafted samples are immersed in this solution for required amount of time during which polymerization occurred.

8. And finally the samples are rinsed with pure water.

The figure 5.1 below shows the preparation steps of grafting polymer brush on glass coverslip

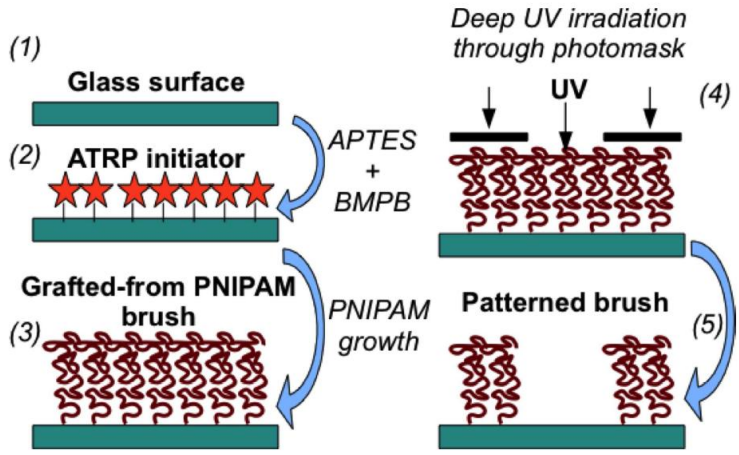

Figure 5.1.: Schematic diagram of PNIPAM polymer synthesis on glass coverslip. [step (2) grafting of an ATRP initiator on a glass surface ; Step (3)is NIPAM polymerization , step (4) polymer brush has grown are exposed to UV irradiation; Step (5) Prepared micro-structure]

5.3. PNIPAM brush characterization

Physical properties of brushes are characterized by ellipsometry

5.3.1. Brush thickness

PNIPAM brushes grown on silicon wafers are characterized by measuring their dry thickness, h_{dry} by ellipsometry. The dry thickness of a brush is given by

$$h_{dry} = Na^3/d^2 \tag{5.1}$$

where N is the number of monomer per chain, a is the monomer size, and d is the distance between anchoring sites. N is determined by the polymerization time, and d is fixed by the surface density of ATRP initiator, which depends on the concentration c_{APTES}. The value of a has been estimated from the data reported in reference [114]

We have used a custom-built ellipsometer in the rotating compensator configuration, at a wavelength of 632 nm and an angle of incidence of 70°. The dry thickness of the brushes grown on oxidized silicon wafers is determined assuming a Si/SiO2/PNIPAM multilayer, with a thickness of 2 nm and a refractive index of 1.46 for silicon oxide, and a refractive index of 1.47 for the PNIPAM layer [115].

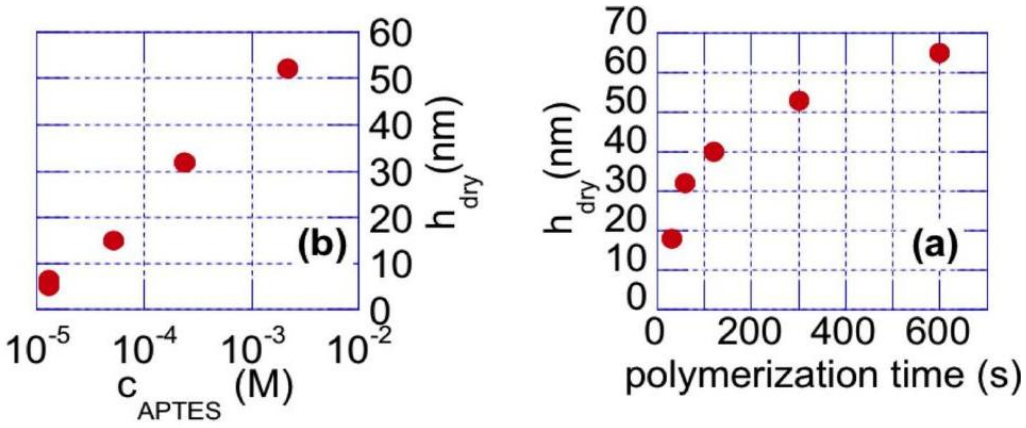

Figure 5.2.: Dry PNIPAM polymer brush dry thickness (h_{dry}) variation with polymerization time, for c_{APTES} =2.10^{-4}M. and h_{dry} vs c_{APTES} for 1 min polymerization.

Above figure 5.2 shows that with the increase of cAPTES or polymerization time, h_{dry} indeed increases. We measure dry thickness of the PNIPAM brushes at 5-6 different locations over a region of surface about $1cm^2$. Measurement shows the same results within $\pm 1nm$ range, yields brush growth homogeneity over a large scales. We have checked the h_{dry} immediately after grafting and after several days of immersion in water. No difference has been found. Hence, It can be concluded that the polymer layers are stable and covalently grafted to the underlying substrate

[116].

5.3.2. Effect of UV irradiation on polymer brushes

When dry PNIPAM brushes are exposed to deep UV light in air, it results in the ablation of the polymer from the surface. Ablation has been characterized under such conditions, by monitoring grafted brush thickness h_{dry} as a function of UV irradiation time (t_{UV}) on grafted silicon wafers which has the same surface property as glass. Figure 5.3 plot shows that starting from an initial brush thicknesses of a few tens of nm, a complete removal of the polymer is achieved for $t_{UV} \geq 300s$.

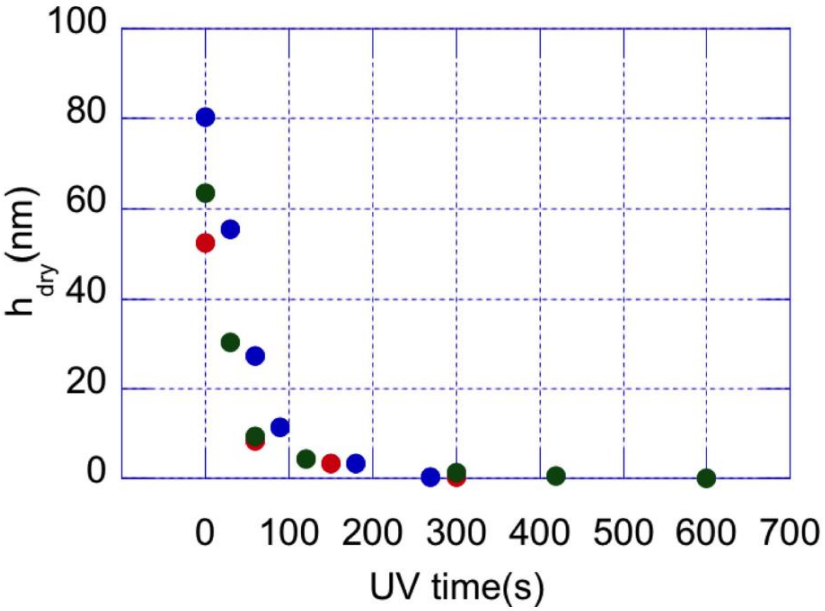

Figure 5.3.: Polymer brush thickness h_{dry} is controlled by UV irradiation time : Data are shown here for brushes of initial thickness 82 nm (blue),65 nm (green), and 54 nm (red). Complete removal of brush appears at t=300sec.

It shows that lower wavelength (below 200nm) is required for PNIPAM ablation. An exposure of a 75W UV lamp (l=365nm) at 2 cm for 15 mins results no dry thickness decrease of the grafted layers. It shows that 365nm UV exposure can used to sterilize the PNIPAM surface if required.

5.3.3. Patterning on synthesized polymer

To create required micropattern design on the grafted polymer glass surface, a deep UV irradiation technique has been used.

1. Dry PNIPAM-bearing coverslips were placed in direct contact with a chromium quartz photomask (Toppan Photomasks inc.,Texas USA)

2. UV irradiation of the surfaces through the photomask was achieved in a custom-built device housing a set of 4 low-pressure mercury lamps (Heraeus Noblelight GmbH, NIQ 60/35 XL long life lamp,λ = 185 and 254 nm, quartz tube, 60 W).

3. Samples were placed at a fixed distance of 9 cm from the UV tubes and irradiated for a duration between 5 and 10 minutes.

Patterns elaborated on PNIPAM-bearing coverslips using $t_{UV} \geq 300s$ can be observed by phase contrast microscopy. Fig.5.4 provides an illustration of different pattern shapes that can be observed.

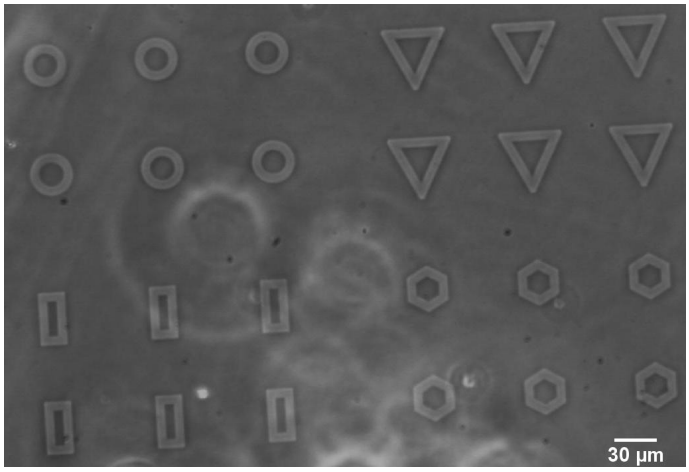

Figure 5.4.: Phase contrast image of annular, triangular, rectangular and hexagonal patterns obtained by UV photoablation of PNIPAM. The light grey regions have been irradiated by deep UV, where the polymer have been removed. Image size is 700x500 μm^2.

Contrast on such image arises from both the height and the refractive index difference between the PNIPAM background layer and the bare glass which has been

exposed to the UV-irradiated regions. Best spatial resolution of the patterns was obtained by placing the dry PNIPAM-bearing coverslips in direct contact with the photomask. This results in patterns obtained on PNIPAM being $1\mu m$ broader than the original shapes of the photomask.

5.3.4. Micro-textured surface functionalization

One of the main interest of micropatterning is to culture cells on the pattern. For that purpose it is necessary to create an ECM-like structure on the pattern by performing an ECM protein coating (fibronectin, laminin, collagen, vitronectin ...). To coat the pattern with protein, PNIPAM glass coverslips were first extensively washed with phosphate-buffered saline(PBS 1x),pH-7.4 . A $100\mu l$ drop of protein solution composed of fibronectin (Sigma) and fibrinogen-Alexa fluor 546 nm (Invitrogen) mixture in 10mM Hepes (pH 8.5) was deposited on a flat piece of parafilm at room temperature. Then the coverslips were directly placed on the drop and incubated for 1hr. After incubation samples were washed twice with PBS 1x and can be stored for 2 -3 days at $4°C$.

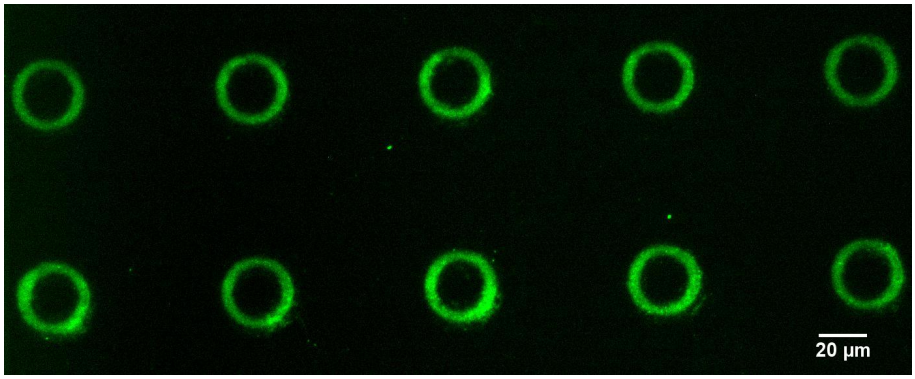

Figure 5.5.: PNIPAM micro pattern coated with fibronectin protein conjugated with fibrinogen in GFP channel .

The results shown in figure 5.6 have been obtained with high density brushes (cAPTES= $2.10^{-3}M$) of h_{dry} varying between 15 and 80 nm, and t_{UV}= between 5 and 10 minutes. No significant influence of these two parameters on the observed behavior have been noticed. We have created many different shape patterns with

the same photomask design. We find similar results regarding protein adsorption and cell adhesion when projected area for all the shapes were conserved. Protein can be coated freshly before cell seeding on the elaborated substrates. These substrates could be stored under ambient conditions for about three to four months before surface functionalization with ECM protein.

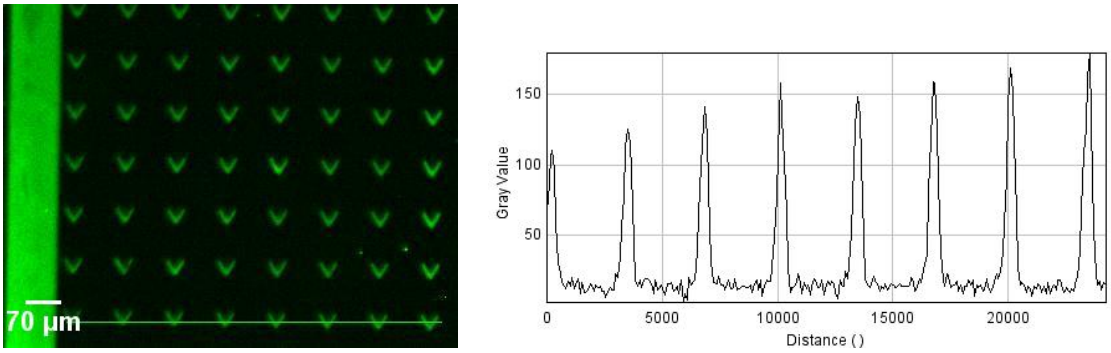

Figure 5.6.: Protein coated V shape (V arms of length 40 μm and width 10 μm) micropattern prepared PNIPAM polymer grafted glass coverslip : Images taken with a 4x objective on an Olympus IX70 microscope. Reduced contrast quality is due to the low NA of the objective. The plot profile of intensity is given by right image.

Figure 5.6 shows fibronectin conjugated with fibrinogen adsorbed onto V-shaped patterns in the UV irradiate part, protein is absorbed and the background which is free from protein is covered by PNIPAM brush. This shows that the high density brushes are excellent protein-repellent at room temperature.
Fluorescence intensity profile on the right side of the above figure along the green line drawn left V-pattern image shows high signal to noise ratio. Wide field image of stained fibronectin adsorbed on V-shaped patterns, shows a large scale homogeneity. Image size: $2200 - 1664 \mu m$ (taken with a 4x objective on an Olympus IX70 microscope. Reduced contrast quality is due to the low NA of the objective)

Pnipam grafted pattern on glass coverslip has been stored for 4/5 months and has been checked its biocompatibility efficiency by culturing cells on polymer brush patterns with and without protein coating, both results in a good cell spreading.

However, cell spreading time for protein coated pattern takes 30mins while without protein it takes 3 to 4 hrs.

5.4. Cell adhesion and fixation

5.4.1. Cell seeding on the pattern

To check cell adhesiveness of PNIPAM micropattern we have used Mouse Embryonic Fibrobasts (MEF) and Rat Embryonic Fibrobasts (REF52)as model systems. Cells were maintained at $37°C$ in a humidified atmosphere of $5\%CO_2$ and 95% air in Dulbeccos modified Eagle medium (DMEM) containing 10% bovine fetal serum, 0.2% peni-streptomycin. For REF52 cell high glucose DMEM has been used. On the micropattern cells have been deposited on the substrate (with and without protein coating) at a density of $50000 cells/cm^2$. Micropattern area is adapted to ensure full spreading of cells on each pattern ($900\mu m^2$). After 30 minutes non adherent cells localized in between the patterns are removed by gentle flushing with fresh media. After 2 hours of culture, spread cells were either observed; at room temperature during thermo-detachment experiments, or fixed in order to preserve their shapes. For image averaging, cells were fixed and immuno-staining has been performed.

The results shown below have been obtained with high density brushes (c_{APES} = 2.10–$3M$) of h_{dry} varying between 15 and 80 nm, and t_{UV} between 5 and 10 minutes. No significant influence of these two parameters on the observed behavior has been noticed. We have used phototomasks displaying various pattern shapes having the same projected area of $900\mu m^2$. Similar results regarding protein adsorption and cell adhesion have been obtained with freshly elaborated substrates and with samples stored under ambient conditions for three months before use.

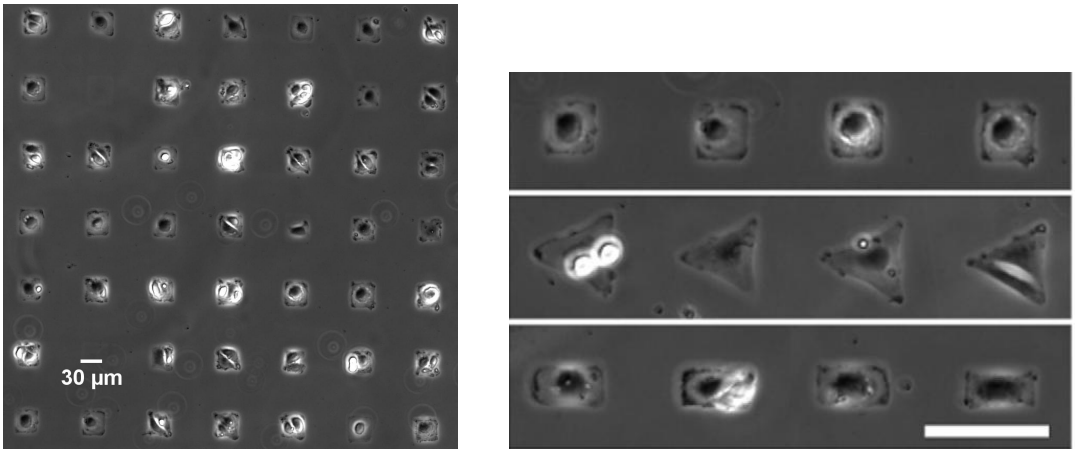

Figure 5.7.: Phase contrast image of cells arranged on PNIPAM brushes: on square (left) and square, triangular and rectangular (right) envelope pattern. scale bar is 80μm.

5.4.2. Cell adhesion depends on physical properties of polymer brush

The quality of cell patterns obtained at T= 37°C (Fig. 7) shows that good protein resistance is also maintained above the polymer LCST, since no cells are seen to adhere outside the defined adhesive zones. Besides, we have checked that, in contrast to the behavior exhibited on dense brushes, cells do adhere, at 37°C, on low-density brushes (c_{APES} = 10–5M) having the same chain length. Such an effect of brush density on cell adhesion agrees with a recent report [110] . It is consistent with recent theoretical works concluding that the protein resistance of brushes is mainly controlled by the osmotic penalty associated with protein insertion within the brush, such a penalty being lower or negligible at low grafting densities [117]. Schematic 5.8 describes cell adhesion dependency on different parameters.

Next we have checked the efficiency of cell adhesion, when plated on the glass coverslip bearing micropattern with and without protein coating. Though the less time is required to spread on the protein coated pattern but cells gets arranged nicely in both these two cases.

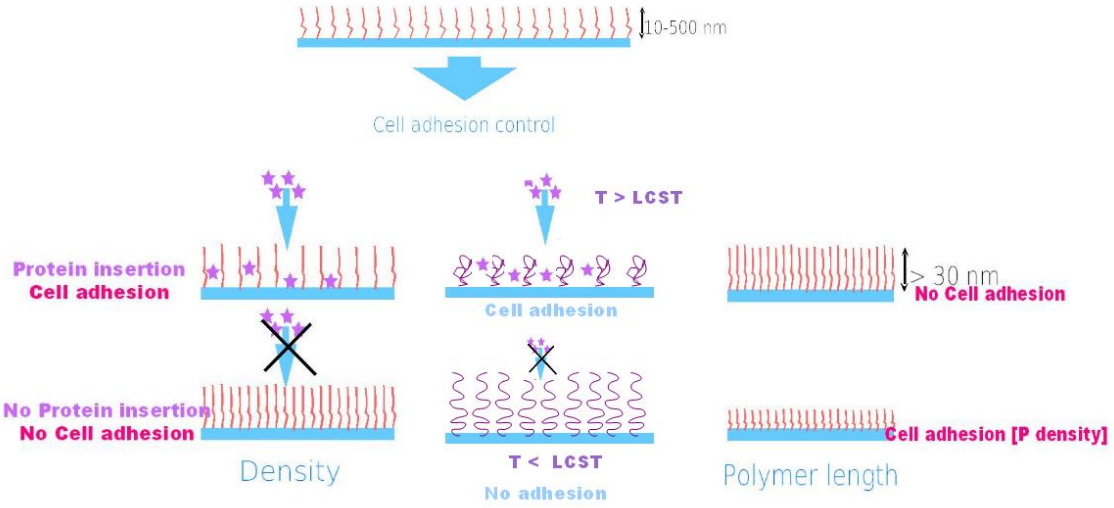

Figure 5.8.: Schematic diagram of cell adhesiveness dependence on the brush density, LCST and length.

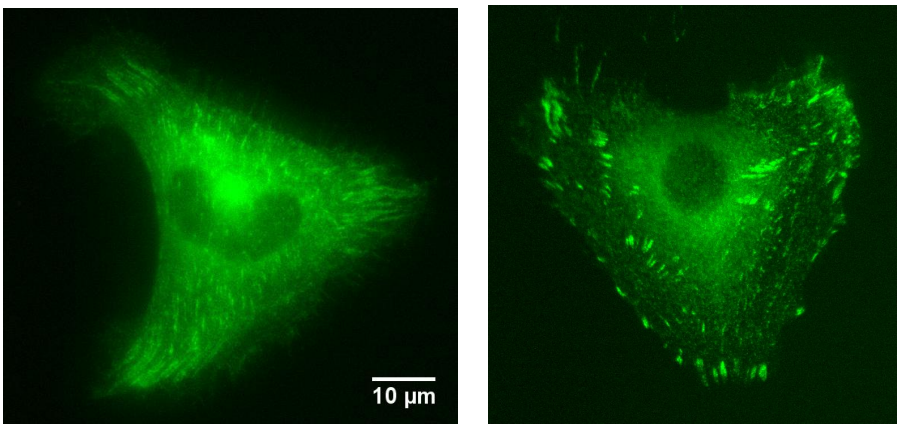

Figure 5.9.: REF cell transfected with GFP-Paxillin (green) adhered on protein (left) /and without protein (right) coated Pnipam micropattern .

Figure 5.9 shows the excellent cell adhesion efficiency with protein coated and non-coated pattern with REF52 cells in which paxillin-GFP is transfected as an adhesion marker.

5.4.3. Cell fixing and staining

This photo-ablated pattern shows high resolution up to $5\mu m$. Typical dimension used for the experiment is $10\mu m$ as shown in the image of figure 5.10. This patterning makes cell shape and internal organization reproducible. This technique is very useful for statistical analysis of cellular response based on image overlay. As shown by Thery et al.(CMC 2006) cell architecture can be maintained by controlling the geometry of the substrate. As a result, substrate geometry influence actin fibers organization in a reproducible manner [23, 106, 118].

We have used our PNIPAM patterned substrates to generate averaged actin maps. After seeding the cells on the PNIPAM patterned substrate, once cells are fully spread, the sample is fixed. Actin is labeled by immuno-staining (using phalloidin) to visualize actin redistribution in response to ECM shapes.

In order to probe actin cytoskeleton reproducibility on PNIPAM micropatterns we have used a software written in Matlab to average many actin images for a given shape. Before averaging, all the individual fluorescent images are normalized to the same integrated total signal value to prevent averaged images from intercellular variations. Averaged fluorescent staining images were automatically aligned,using the protein-stained micropattern images as reference positions.
Figure 5.10 shows single pattern image of different geometry . Single cell actin stained on each pattern shape are in green in figure 5.10. The heat map has been generated from the overlay of several single cell actin images. Averaged actin images unambiguously confirms the ability of our micropatterns to orient actin network organization: cells form preferentially contractile F-actin bundles, or stress fibers, along the boarder of the adhesive regions of the micropatterns.

5.4.4. Cell division on the pattern

Next, we have checked for the possibility of long term cultures on the substrates. We have maintained cells in culture up to 5 days, during which cell division occurred, indicating good biocompatibility of the patterned surfaces. Furthermore, we have

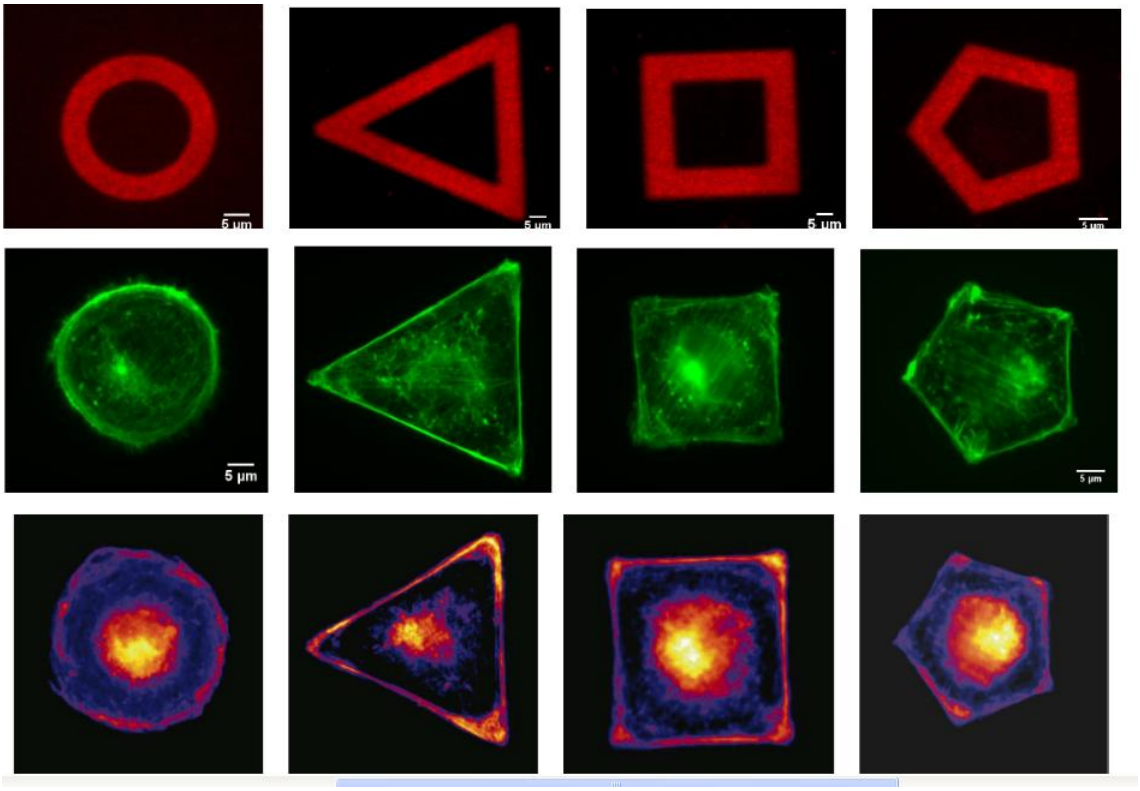

Figure 5.10.: Fibronectin and fibrinogen-A546 coating on micropatterned PNIPAM glass surface (red). Individual MEF cells plated on annulus, triangle or square,pentagon-shaped fibronectin micropatterns. Cells were fixed and stained with phalloidin to reveal F-actin filaments (green). Average distributions of actin (fire), built from the overlay of 10 images for each shape. The average distribution highlights the reproducibility of the distributions shown and enhances the spatial distribution of F-actin bundles along micropattern border regions.

observed that cell adhesion is also achieved without fibronectin pre-coating. Such a non protein-specific cell patterning method, along with the ability to reach long culture time, make the present surfaces a potentially powerful tool for stem cell culture. It also shows that our technique is a versatile one, for e. g. different protein coatings can be used on our surfaces, thus allowing to address more specific biological questions.

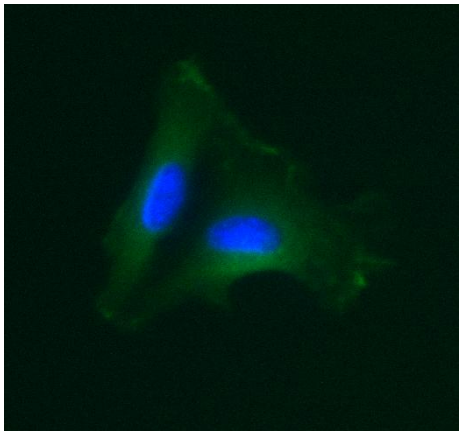

Figure 5.11.: Cell division on V shape pattern after 5 days: green paxillin; blue nucleus.

5.4.5. Temperature dependent properties of PNIPAM and cell detachment

PNIPAM polymer has the property to response to temperature stimulation. Although dense PNIPAM brushes are protein repellent irrespective of the temperature, their thermo sensitive property can still be used for local cell manipulation. We showed that by exploiting thermoresponsiveness and micropattern geometry cells can be detached from the substrate very easily without using any chemical reagents.

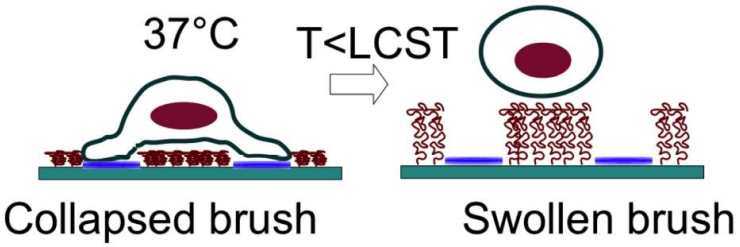

Figure 5.12.: Schematic diagram of cell detachment from PNIPAM polymer, induced by temperature.

Most importantly the way cells are detached are different from what has been described previously [109, 110, 111, 112, 113]. This cell detachment mechanism does not involve a temperature-induced change in the cell/PNIPAM affinity, but rather takes advantage of polymer swelling to generate forces. Cells thus detached from

the patterned substrates are subsequently re-cultured in a polystyrene petri dish and are observed to spread and divide on the surface. This shows that cells detachment achieved by the method we report here does not affect their viability.

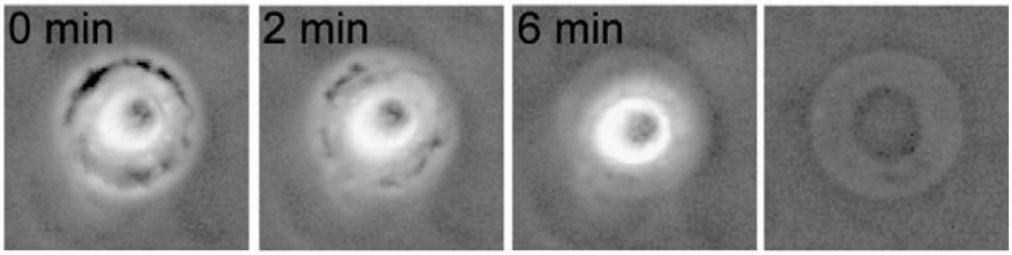

Figure 5.13.: Phase contrast image of thermally induced cell detachment : 0min , 2min 6min respectively. Initially adhered on circular shape pattern with brush thickness 75nm. Imposed temperature is $21°C$.

For the thermoresponsive experiments, time-lapse sequences are acquired while regulating the temperature of the room between $21°C$ and $30°C$. Phase contrast images of the detaching cells are taken using an Olympus CKX41 microscope equipped with a 10X air objective(NA 0.25) and a 12-bit monochrome camera.

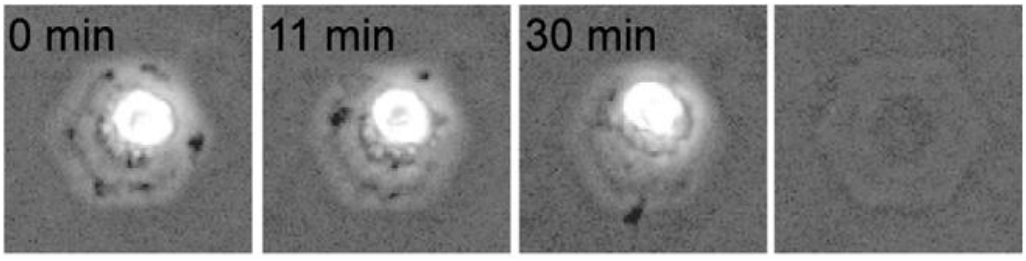

Figure 5.14.: Thermally induced cell detachment: 0min , 11min 30min respectively. Cell initially adhered on a hexagonal pattern with brush thickness 75nm . Imposed temperature is $26°C$.

The kinetics of cell detachment depends on the temperature imposed below the LCST. The lower is the temperature the faster is the detachment. We have checked that such a thermo-actuated detachment does not depend on the pattern shape, provided that the shape is chosen as follows: The pattern has to be such that cells

spread over a non adhesive PNIPAM region, while bridging two adhesion zones, as shown in cell detachment cartoon. Below the LCST of the polymer chains goes to swollen coil conformation [116]. PNIPAM has LCST at32°C when dissolved in water.

Here cells detaching slowly as temperature is lowered The time stamp gives the time elapsed since the surfaces are taken out of the incubator. Initially cells adhered on a circular pattern. Then the imposed temperature is 26°C by regulating thermalization chamber. Here the dry brush thickness used to exhibit thermoresponsive behavior are h_{dry} = 75nm.

5.5. Conclusion and Discussion

Creating thermoresponsive pattern on PNIPAM or its copolymer based substrate have been employed in several previous studies [119, 120, 121, 122]. However, these studies by T. Okano and other groups have focused on patterns of large dimensions. They study mainly focused on the cell sheets for tissue reconstruction applications. We focused on describing the design of micropatterned surfaces for single cell studies. The main attraction of using PNIPAM polymer, is based on thermoresponsive property of the polymer brushes. These brushes can readily be patterned at the micron scale via deep UV photolithography. We show that the use of high density polymer brushes of PNIPAM, bound to glass substrates via the so-called graftingfrom method, and patterned by direct photo-ablation, represents a reliable, fast and cost-effective technique to design thermosensitive micropatterned platforms. Compared to the existing well-established templating techniques, the method we report presents the following important features, and comes as an interesting alternative to e.g. coatings based on adsorbed ethylene-glycol copolymers [106].

5.5.1. Advantages

1. PNIPAM brushes are elaborated from common and inexpensive chemicals, and their molecular structure can be tuned at will. Furthermore, micron-scale

patterning is achieved in one single step, without requiring access to clean room facilities.

2. Robust and stable anti-adhesive brushes are covalently grafted at high density on common glass coverslips by surface-initiated ATRP.

3. Polymer chains being covalently bound to the substrate, such coatings show excellent usage and storage long-term stability.

4. High grafting density brushes display superior protein and cell repellency, obtained in an extremely reliable and reproducible way.

5. Photolithography yields sharp patterns, in contrast to microcontact-printing techniques which may be limited in resolution by surface diffusion of the printed species

6. This method is easy to implement and requires only basic laboratory equipment.

7. Although such high density brushes are cell-repellent at 37°C, PNIPAM chains still shift from a collapsed to a swollen state as the temperature is decreased below the polymer LCST (Lower Critical Solution Temperature) of 32°C. This temperature-controlled conformation change of PNIPAM, combined with a proper choice of the pattern shapes, make the polymer coating act as a thermoactuator which allows us to detach the studied cells by lowering the surface temperature. This adds a very attractive feature to the usual passive micropatterned platforms.

Patterned substrates can thus be produced within 2-3 hours only, in a highly reproducible way. Moreover, we have shown that a proper choice of the pattern shapes allows us to combine the cell non-adhesiveness of dense PNIPAM brushes with their thermoresponsiveness, which permits gentle cell detachment. These features make such PNIPAM based substrates a choice tool for single cell patterning and thermally-induced on-chip cell manipulation.

The empirical designing of the thermoresponsive micropattern is very useful for single cell studies. However further elucidation is required to optimize the design. It needs to elicit how the ability of swelling or collapsing of the polymer brushes depend on grafting density, how the detachment kinetics depends on the brush thickness.

6. Summary and Outlook:

Major part of this thesis is dedicated to investigate the extracellular matrix influence on intracellular organization and its associated cytoskeletal tension distribution using polyacrylamide micropatterning and traction force microscopy. The novelty of this work lies on correlating cell traction forces with cell internal architecture in a reproducible manner. Using single cell micropatterning on soft substrates, we have explored the role of the physical properties of the extracellular matrix such as geometry and stiffness on cell force distribution while keeping cell projected area constant. We thus were able to correlate different cell architectures such as actin cytoskeleton organization, focal adhesions and centrosome localization in response to various geometrical stimulations. This thesis also includes the development of a new micropatterning technique based on the utilization of thermoresponsive polymer brushes providing new insights in single cell manipulation.

When cells have been plated on soft micropatterns of different geometry, actin fibers were accumulated along both adhesive and non-adhesive boarder of the pattern envelope contrary to previous experiments performed on glass. For a set of three different shapes of a fixed envelope (square), we have statistically quantified cell contractile energy and their associated cytoskeletal architectures. Interestingly, we have shown for the first time that total forces and contractile energies are independent of the ECM geometry when averaged over a large number cells (more than 50 cells per shape) indicating a strong regulatory mechanism of mechanical balance within cell. Moreover, we have also been able to explore this regulatory mechanism by describing local force redistribution and their associated adhesive structures distribution in response to the underlying ECM geometry.

In a second part, we tried to compare cell traction forces obtained via two major techniques used in the field of cell mechanics: TFM and micropost arrays. Cellular traction forces have been compared on 2D micropatterned substrates with 3D micro-pillar arrays, having same arrangements of ECM geometry, on three different stiffnesses 7, 20 and 40 kPa respectively. In both these two methods, it has been observed that traction forces increase linearly with increasing substrate stiffness. In addition we also observed a linear correlation between force and focal adhesion growth. However, higher magnitudes of force developed on micropillars may be due to the discontinuity in long-range deformation propagation that in turns affect cell basal tension regulation.

Subsequently, we have studied centrosome positioning and its relation with actin generated forces using micro-patterned traction cytometry. Very surprisingly, we observed that for V and T shapes, centrosome were off centered with respect to the cell geometrical center were usually observed. In addition, we also have shown that paxillin distribution converges to the center of mass of the ECM geometry in correlation with centrosome distribution. Thus we may suggest that centrosome positioning highly depend upon adhesion spatial distribution which is as far as we know the first evidence of this correlation. Finally, we found that local traction forces (at each pattern corners) are directed towards the centrosome localization. This correlation in between actin generated forces, adhesion distributions and centrosome positioning suggests a potential role of actin in centrosome centering. We also have studied contractile energy in which it seems that T shape has a bias behavior. However, obtained results require better understanding and further investigations.

Finally, we proposed a new approach to create micropattern using thermoresponsive PNIPAM polymer brushes grafted on glass substrates. In previous studies, PNIPAM thermoresponsive property has been used for cell sheet engineering. In this thesis we have shown that PNIPAM micropatterns can be created by deep UV irradiation, by removing polymer from the surface, and thus designed for single cell studies. Using this technique, pattern resolution can be reached up to 4 μm (see

chapter5) and the created patterns could be easily functionalized with ECM proteins. We also have shown that the length(<30nm) and grafting density of the polymer has to be tightly adjusted to make cells adhere on the substrate. Ultimately, we have shown that a proper choice of the pattern shapes allows them to combine the cell non-adhesiveness of dense PNIPAM brushes with their thermoresponsiveness, which permits gentle cell detachment. Though this technique may provide different useful advantages in lab on chip developments and single cell manipulation. Following the dynamic of this detachment over time will give great insights in cell adhesion comprehension.

A. ANNEX

A.1. Hydrogel Preparation Protocols:

A.1.1. Bead Functionalization:

Materials:

- 0.2μm (stock solution is 2 % solid) DAPI beads or 0.2μm YFP beads [purchased from Bangs Laboratory, Inc (FC02F)]
- PLL-g-PEG in powder [purchased from VWR(20-3.3-2)]
- N-Hydroxysuccinimide (NHS) [purchased from Fluka Analytical (56480-25G)]
- 1-ethyl-3-(3-dimethylaminopropyl) carbodiimide(EDC) [purchased from sigma (E6383-5G)]
- HEPES buffer (10 mM pH 8.5, pH 7.4)
- MES buffer (10 mM pH 5.5)

Procedure:

1. 10μL beads (stock solution is 2 % solid) + 40uL MES buffer(10mM pH5.5) solution, mix well 50μl by vortexing.
2. Prepare NHS/EDC (0.4 mg/0.8 mg) in 200μL MES solution.
3. Prepare PLL-PEG solution by adding 4 mg powder in 250 μL HEPES buffer (10 mM pH 8.5).

4. Mix bead and EDC/NHS solution (solution 1 + 2).
5. Add peg solution in the bead-EDC/NHS solution (solution 3 + 4).
6. Incubate solution(5) in a rotator for 2hr @ RT (or 4°C rocking overnight).
7. Spin down the beads at 14000 rpm for 30 minutes, and remove solution. (Try to use a lower speed and short time at first if possible)
8. Re-suspend in HEPES (10 mM pH 7.4).
9. Spin down the beads and remove solution.
10. Re-suspend in 2 to 4× original beads volume in HEPES (10 mM pH 7.4).

A.1.2. Coverslip Treatment

Materials:

- 99.9% ethanol
- 10% Acetic acid
- Bind saline (stored at RT purchased from Plus one; code no - 17-1330-01)

Procedure:

1. Solution prepared in 99.9% ethanol by adding acetic acid of 3.2 % and bind saline of 0.38% and mix wel by votexing
2. 100μl of solution used to cover 20×20 coverslip.
3. By kimwipe, solution is smeared on the glass coverslip.
4. Keep for drying about 15 to 20 mins.
5. Functionalized coverslips can be stored for long term using for gel preparation.

A.1.3. Hydrogel Micropatterning :

Materials:

All chemicals purchased from Sigma.

- Acrylamide solution.
- N,N-methylene bisacrylamide solution.
- Tetramethylethylenediamine(TEMED)
- 98 % Ammonium persulfate (APS)
- DPBS, Ca and Mg free [PAA Laboratories (Cat no H15-002)]
- Fibronectin from bovine plasma (Purchased from Sigma)
- Fibrinogen (Purchased from Sigma F1141-IMG) (Purchased from Invitrogen)

Stock Solutions:

- 10 % APS prepared in water
- 0.2 M EDC prepared in water
- 0.15 M NHS prepared in water

Procedure:

1. Put enough amount of isopropanol and smear it on the quartz mask.
2. Sonicate the beads for 2 to 4 mins.
3. Add 3 μl of beads (for TFM measurements only) in 160 μl of gel premix(PBS/acrylamide/bis-acrylamide).
4. Put enough amount of n-hexan on the mask and keep rubbing on the mask with kimwipe.
5. Put 1-2 ml of n- hexen with pipette and smear it with kim wipe.

6. Add 1μl of TEMED in gel solution.
7. Add 1μl of APS in gel solution and vortex it.
8. 30 μl of solution drop put on the n-hexan smeared mask for 20×20 mm square saline treated coverslip.
9. Cover the mask to prevent evaporation. And also put a small piece of wet tissue to avoid dry environment.
10. Give 45Mins to 1 hr for polymerization at room temperature (RT) .
11. Illuminate with deep UV through the mask for 4mins.

EDC- NHS Coating

12. Put a piece of parafilm on a flat place.
13. Take out the mask and put enough water over the coverslip on the mask .
14. Prepare NHS and EDC mix (1:1) and put a drop of mix of 100 μl for 20×20 mm square coverslip on the parafilm sheet .
15. Detach the gel-coverslip from the mask by adding milliQ-water.
16. Dry the gel by air-flow (blow with nitrogen or clean air).
17. Put the coverslip (gel side down) directly on NHS/EDC solution on parafilm for 15 minutes at RT.
18. Move the coverslip 2 to 3 times during incubation to remove bubbles.

Protein Coating

19. Prepare protein solution 1 μl Fibrinogen and 3 μl of Fibronectin in 100μl of Hepes pH 8.5(20 μg/mL protein).

20. Put a small piece of parafilm on a flat place. Put the 100μl of protein solution drop on the parafilm.
21. Remove excess NHS/EDC solution by blotting the side of the coverslip against kimwipe.
22. Put the coverslip with gel side down on the solution.
23. Incubate at RT for at least 1 hr.
24. Wash the coverslip 2 times 1X PBS (not necessarily sterile).
25. Store at 4°C (can be kept for ≈ 2 days).

A.2. Micropatterning on PNIPAM polymer brush experimental protocols:

A.2.1. Patterning

- Synthesized polymer on glass coverslip kept under UV lamp.
- A quartz-chromium mask, containing experimental design placed on top of the coverslip with minimum gap.
- UV lamp illuminated for about 5-7 minutes.
- Patterns are created on the sample which can be stored 5-6 months.

A.2.2. Surface Functionalization

Surface can be functionalized with desired proteins.

1. Protein solution prepared in HEPES (10 mM of 8.5 pH) by adding 20 μg /ml in concentration (fibrinogen and fibronectin)
2. 100 μl of protein solution put on a flat piece of parafilm.
3. Coverslip deposited in the solution and incubated for 1 hr at RT.

A.3. Cell Culture

Materials:

1. Dulbecco's Modified Eagle Medium (DMEM) (Purchased from PAA Laboratories)
2. Fetal calf/ bovine serum (FCS/FBS) (Purchased from PAA Laboratories)
3. Primary and secondary antibody (Purchased from Invitrogen)
4. TritonX-100 (Purchased from Sigma T8787)
5. Trypsin EDTA 1× (Purchased from PAA Laboratories)
6. Fluoroshield (Purchased from Sigma T8787)

A.3.1. Classic culture

Mouse embryonic fibroblast (MEF) cells are generous gift of Dr. Olivier Destaing from Institute of Albert Bonniot, Grenoble.
Rat embryonic fibroblast (REF52) cells are kindly provided by Dr. Benoit Ladoux from Paris 7 University.

Mouse embryonic fibroblasts(MEF) are cultured in Dulbecco's Modified Eagle Medium (DMEM) supplemented with 10 % Fetal calf serum (FCS), 0.2 % penicillin streptomycine and 2 mM L-glutamine (GIBCO) and Sodium Pyruvate. Cells were maintained at 37°C and 5% CO2.

Rat embryonic fibroblasts (REF52) cells are cultured with high Glucose Dulbecco's Modified Eagle Medium (DMEM) with 10 % Fetal bovine Serum(FBS), and 0.2 % penicillin streptomycine. Incubator temperature was maintained at 37°C supplemented with 5 % CO2.

Some cells were frozen to maintain same passage for different set of experiments. Cells were stored in DMSO at 80° C for few months.

A.3.2. cell culture on pattern

1. Remove media for the classic petri or flask.
2. Cells are washed with 1× PBS.
3. Cells are trypsinized in the classic culture.
4. Culture media added maintaining 50,000/ cm^2 cells.
5. trypsinized cells are seeded on the prepared micropatterned coverslip (mounted on cell observation chamber only for TFM).
6. When cell starts adhering on the adhesive part of the substrate (after 30 - 45mins) extra cells are washed off.
7. When cells are fully spread after 2-3 hrs of intubation at 37°C , media is replaced with imaging media supplemented with 5 % CO2 without Phenol red.
8. Cell bearing coverslip is taken for respective experiments (traction force experiment or for staining).

---

* Before plating cells it is required to count the cell density.

* Cell adhesion time depends on the cell type and substrate rigidity.

* 2 hrs before starting experiments, microscope thermalization chamber is set to 37°C.

* In TFM experiments cells are killed by milliQ water.

A.4. Immuno-labeling:

Actin Staining :

1. Remove culture media from cell and rinse (for paxillin) with 1× PBS (pH 7.4).
2. Wash cells 2 times with 1× PBS (pH 7.4).
3. Fix in 4 % formaldehyde for 15 to 20 minutes at RT.
4. Rinse 2 times with 1× PBS (pH 7.4).
5. Permeabilize cells in 0.5 % Triton-X100 for 10 minutes.
6. Incubate in fluorescent-phalloidin (1ug/ml from 1mg/ml frozen stock) in HEPES (10mM pH 8.5) for 45 minutes to 1 hr.
7. Wash 2 times with 1× PBS (pH 7.4).
8. Mount in Fluoroshield with DAPI to stain nuclei if required for overnight and seal it.

Double Staining : Paxillin and Centrosome

1. Remove culture media from cell.
2. Fix in 4% formaldehyde for 15 to 20 minutes at RT (for paxillin) or add cold methanol(-20°C) by the side of the petridish (only for centrosome).
3. keep it at -20°C for about 5-6mins (for centrosome). Keep it at room temperature for 10 -20 minutes.
4. Remove methanol or formaldehyde.
5. Wash cells 2× with 1× PBS (pH 7.4).
6. Permeabilize cells in 0.5 % Triton-X100 for 10 minutes (only for paxillin)
7. Incubate in 100 μl of protein solution composed of 1.5% BSA primary antibody (1 μg/ml) in PBS for 45 minutes to 1 hr (paxillin) at RT.

Immuno-labeling:

8. Wash 2 times with 1 × PBS (pH 7.4).

9. Incubate in 100 μl of protein solution composed of 1.5% BSA secondary antibody (1 μg/ml) in PBS for 40 minutes (for centrosome) or 45 minutes to 1 hr (paxillin) at RT.

10. Wash 2 times with 1 × PBS (pH 7.4).

11. Mount in Fluoroshield with DAPI to stain nuclei if required for overnight and seal it.

References

[1] Viola Vogel, Michael Sheetz; Local force and geometry sensing regulate cell functions Nature Reviews Molecular Cell Biology Volume 7 April 2006 271.

[2] Benjamin Geiger, Alexander Bershadsky, Roumen Pankov and Kenneth M. Yamada; Transmebrane Extracellular Matrix Cytoskeleton Crosstalk; Nature Reviews; Molecular Cell Biology Volume 2 November 2001 793

[3] Alexander D. Bershadsky, Nathalie Q. Balaban, and Benjamin Geiger; Adhesion - Dependent Cell Mechanosensitivity ; Annual Review of Cell Developmental Biology 2003 19:67795 .

[4] Adam J. Engler, Shamik Sen, H. Lee Sweeney and Dennis E. Dische Engler; Matrix Elasticity Directs Stem Cell Lineage SpecificationCell 126, 677689, August 25, 2006

[5] Amnon Buxboim, Irena L. Ivanovska and Dennis E. Discher, Matrix elasticity, cytoskeletal forces and physics of the nucleus: how deeply do cells feel outside and in?; Journal of Cell Science 123, 297-308 2010 doi:10.1242/jcs.041186.

[6] Marie Versaevel1, Thomas Grevesse1 ang Sylvain Gabriele; Spatial coordination between cell and nuclear shape within micropatterned endothelial cells; Nature Communication 2012 DOI: 10.1038/ncomms1668.

[7] Wang HB, Dembo M, Hanks SK, Wang Y Focal adhesion kinase is involved in mechanosensing during fibroblast migration. Proc Natl Acad Sci USA 2001 98(20):1129511300.

[8] Goetz JG. Bidirectional control of the inner dynamics of focal adhesions promotes cell migration; Cell Adhesion and Migration 2009, 3:185-190.

[9] Lo CM., Wang HB., Dembo M., Wang YL., Cell movement is guided by the rigidity of the substrate. Biophys Journal 2000 79:144152,

[10] Thery M; Cell Micropatterning as a Tool to Decipher Cell Morphogenesis and Functions; Journal of Cell Science 2010 123: 4201-4213.

[11] Sui Huang and Donald E. Ingber; Shape-Dependent Control of Cell Growth, Differentiation, and Apoptosis: Switching between Attractors in Cell Regulatory Networks; Experimental Cell Research; 2000 261 91103 doi:10.1006/excr.5044.

[12] Jaalouk D.E. and Lammerding J., Mechanotransduction gone awry; Nature Reviews Molecular cell Biology 2009 volume 10 63.

[13] Riveline D., E. Zamir, N. Q. Balaban, U. S. Schwarz, B. Geiger, Z. Kam and A. D. Bershadsky; Focal contact as a mechanosensor: externally applied local mechanical force induces growth of focal contacts by a mDial-dependent and ROCK-independent mechanism; Journal of Cell Biology 2001 153:11751185.

[14] Yeung T., Georges, PC., Flanagan LA., Marg B., Ortiz M., Funaki M.,Zahir N., Ming W., Weaver V., Janmey PA.; Effects of Substrate Stiffness on Cell Morphology, Cytoskeletal Structure, and Adhesion; Cell Motility and the Cytoskeleton 2005 60:2434.

[15] Zamir E, Geiger B, Kam Z Quantitative Multicolor Compositional Imaging Resolves Molecular Domains in Cell-Matrix Adhesions. PLoS ONE 2008 3(4): e1901. doi:10.1371/journal.pone.0001901.

[16] Choquet D., D. F. Felsenfeld, and M. P. Sheetz; Extracellular matrix rigidity causes strengthening of integrin-cytoskeleton linkages; Cell 1997. 88:3948.

[17] Christopher S. Chen, John Tan, Joe Tien; Mechanotransduction at cell matrix

and cell-cell contacts; Annual Review of Biomedical Engineering 2004 vol 6: 275- 302.

[18] Matthew J. Paszek, Nastaran Zahir,Kandice R. Johnson,Johnathon N. Lakins,Gabriela Rozenberg,Amit Gefen, Cynthia A.Reinhart-King, Susan S. Margulies, Micah Dembo,David Boettiger, Daniel A. Hammer, and Valerie M. Weaver; Tensional homeostasis and the malignant phenotype; Cancer Cell 2005 DOI 10.1016/j.ccr.2005.08.010.

[19] J. Dai and M. P. Sheetz ; Mechanical properties of neuronal growth cone membranes studied by tether formation with laser optical tweezers; Biophysical Journal 1995 March 68(3): 988996 doi: 10.1016/S0006-3495(95)80274-2.

[20] Balaban N.Q., Schwarz U.S., Riveline D., Goichberg P., Tzur G., Sabanay I., Mahalu D., Safran S., Bershadsky A.D., Addadi L., Geiger B.; Force and focal adhesion assembly: a close relationship studied using elastic micropatterned substrates; Nature Cell Biology 2001 3, 466472.

[21] Harris, A. K., P. Wild, and D. Stopak. Silicone rubber substrata: a new wrinkle in the study of cell locomotion; Science 208(4440):177179, 1980.

[22] M Dembo, T Oliver, A Ishihara, and K Jacobson ;Imaging the traction stresses exerted by locomoting cells with the elastic substratum method; Biophysical Journal 1996 April; 70(4): 20082022.

[23] Thery M, Racine V, Piel M, Pepin A, Dimitrov A, Chen Y, Sibarita JB, Bornens M; Anisotropy of cell adhesive microenvironment governs cell internal organization and orientation of polarity; Proc Natl Acad Sci USA 2006 103: 1977119776.

[24] Chen C.S., Mechanotransduction a field pulling together? Journal of Cell Science 2008 121, 3285- 3292.

[25] Chretien, D. and Fuller, S.D. Microtubules switch occasionally into unfavorable configurations during elongation; Journal of Molecular Biology 2000 May 12;298(4):663-76.

[26] Michel Bornens; The Centrosome in Cells and Organisms; Science 2012 425 DOI: 10.1126/science.1209037.

[27] Jones J. C. R., Goldman A. E., Steinert P. M., Yuspa S., Goldman R. D; Dynamic aspects of the supramolecular organization of intermediate filament networks in cultured epidermal cells; Cell Motil. 1982 2:197213.

[28] Goldman R. D., Grin B., Mendez M. G., Kuczmarski E. R; Intermediate filaments: versatile building blocks of cell structure; Curr. Opin. Cell Biol. 2008 20:2834

[29] Oriolo A. S., Wald F. A., Ramsauer V. P., Salas P. J. Intermediate filaments: a role in epithelial polarity; Exp. Cell Res. 2007;313:22552264

[30] Robert Kirmse., Zhao Qin., Carl M. Weinert., Andrea Hoenger, Markus J. Buehler, Laurent Kreplak. Plasticity of Intermediate Filament Subunits; PLoS ONE 2010 Volume 5 .

[31] Kirmse R, Portet S, Mcke N, Aebi U, Herrmann H, Langowski J. A quantitative kinetic model for the in vitro assembly of intermediate filaments from tetrameric vimentin; J Biol Chem 2007 282(25):18563-18572.

[32] Herrmann H, Haner M, Brettel M, Ku NO, Aebi U Characterization of distinct early b assembly units of different intermediate filament proteins; J Mol Biol 1999 286: 14031420.

[33] Mogilner A. Oster G. Cell motility driven by actin polymerization; Biophys. J. 1996 71(6):3030-45.

[34] Tom Shemesh, Alexander D. Bershadsky, and Michael M. Kozlov; Physical Model for Self-Organization of Actin Cytoskeleton and Adhesion Complexes at the Cell Front; Biophysical Journal Volume 102 April 2012 17461756doi: 10.1016/j.bpj.2012.03.006.

[35] Balland M., Richert A., Gallet F., The dissipative contribution of myosin II in the cytoskeleton dynamics of myoblasts; Eur Biophys J 34: 255261, 2005.

[36] Hynes RO., Integrins: bidirectional, allosteric signaling machines, Cell 2002 20;110(6):673-87.

[37] Yonggang Pang, Xiaoli Wang, Dongkeun Lee, Howard P. Greisler; Dynamic quantitative visualization of single cell alignment and migration and matrix remodeling in 3-D collagen hydrogels under mechanical force; Biomaterials 2011 32 3776e3783.

[38] Alberts B, Johnson A, Lewis J, et al. Molecular Biology of the Cell, 4th edition ; Garland Science 2002.

[39] Je rome Solon, Ilya Levental, Kheya Sengupta, Penelope C. Georges, and Paul A. Janmey; Fibroblast Adaptation and Stiffness Matching to Soft Elastic Substrates; Biophysical Journal Volume 93 December 2007 44534461;doi: 10.1529/biophysj.106.101386.

[40] Manuel Thery, Anne Pepin, Emilie Dressaire,Yong Chen,2and Michel Bornens1; Cell distribution of stress fibres in response to the geometry of the adhesive environment; Cell Motility and the Cytoskeleton 2006.

[41] Kalpana Mandal, Martial Balland, Lionel Bureau; Thermoresponsive Micropatterned Substrates for Single Cell Studies; PLoS ONE, May 2012 Volume 7 Issue 5 e37548.

[42] Khaled W., Ermert H., Reichling S., Bruhns O.T., The inverse problem of elasticity: a reconstruction procedure to determine the shear modulus of tissue, in Proc. of 2005 IEEE Ultrasonics Symp, 735738, 2005.

[43] Sun C., Standish B., Yanga V.X., Optical coherence elastography: current status and future applications, Journal of Biomedical Optics 2011 16(4), 043001.

[44] D. Stopak and A.K. Harris, Connective tissue morphogenesis by fibroblast traction I. Tissue culture observations ; Dev. Biol. 1982 90:383398.

[45] Daniel J. Leahy, Implications of atomic-resolution structures for cell adhesion; Annu. Rev. Cell Dev. Biol.1997 13:363393.

[46] Abercrombie M, Dunn GA; Adhesions of fibroblasts to substratum during contact inhibition observed by interference reflection microscopy; Exp Cell Res. 1975; 92(1):5762.

[47] Ballestrem C, Hinz B, Imhof BA, Wehrle-Haller B.Marching at the front and dragging behind: differential alphaVbeta3-integrin turnover regulates focal adhesion behavior; J Cell Biol. 2001 Dec 24;155(7):1319-32.

[48] Clark E. A., King W. G., Brugge J. S., Symons M. and Hynes R. O.; Integrin-mediated signals regulated by members of the rho family of GTPases; J. Cell Biol 1998. 142, 573-586.

[49] Rottner K, Hall A, Small JV; Interplay between Rac and Rho in the control of substrate contact dynamics; Curr Biol. 1999 Jun 17;9(12):640-8.

[50] Beningo KA, Lo CM, Wang YL. Flexible polyacrylamide substrata for the analysis of mechanical interactions at cell-substratum adhesions; Methods Cell Biol.2002 69:32539 .

[51] Tan J.L., Tien J., Pirone D.M., Gray D.S., Bhadriraju K., Chen C.S. Cells lying on a bed of microneedles:an approach to isolate mechanical force; Proc. Natl Acad. Sci.2003 USA 100, 14841489.

[52] Goffin JM, Pittet P, Csucs G, Lussi JW, Meister JJ, Hinz B , Focal adhesion size controls tension-dependent recruitment J Cell Biol. 2006 Jan 16;172(2):259-68. Epub 2006 Jan 9.

[53] J. Stricker, B. Sabass, U. Schwarz, and M. Gardel.Optimization of traction force microscopy for micron-sized focal adhesions; J. Phys. Condensed Matter 2010 22:194104 doi:10.1088/0953-8984/22/19/194104.

[54] Zaidel-Bar R., Cohen M., Addadi L. Geiger B. Hierarchical assembly of cell-matrix adhesion complexes. Biochem. Soc. Trans. 2004 32(Pt3):416-20.

[55] Katsumi A., Wayne Orr A., Tzima E., Schwartz M.A., Integrins in Mechanotransduction, JBC 2004 volume 279 13 pp. 1200112004.

[56] Eli Zamir and Benjamin Geiger Components of cell-matrix adhesions ; J Cell Sci 2001 October 15 114, 3583-3590.

[57] Galbraith C.G., Sheetz M.P.: A micromachined device provides a new bend on fibroblast traction forces. Proc. Natl Acad. Sci.1997 USA 94, 91149118 .

[58] Juliet Lee, Michelle Leonard, Tun Oliver,Akira Ishihara, and Ken Jacobson, Traction Forces Generated by Locomoting KeratocytesThe Journal of Cell Biology 1994 December Volume 127, Number 6, Part 2, 1957-1964.

[59] Demosthene Mitrossilis, Jonathan Fouchard, Axel Guiroy, Nicolas Desprat, Nicolas Rodriguez, Ben Fabry,and Atef Asnacios; Single-cell response to stiffness exhibits muscle-like behavior; PNAS 2009 October 27 . 1824318248, doi 10.1073

[60] Jochen Guck, Revathi Ananthakrishnan, Hamid Mahmood, Tess J. Moon, C. Casey Cunningham and Josef K; The Optical Stretcher: A Novel Laser Tool to Micromanipulate Cells; Biophysical Journal 2001 Volume 81 Issue 2 767-784 doi:10.1016/S0006-3495(01)75740-2.

[61] James L Wilbur, Amit Kumar, Hans A Biebuyck, Enoch Kim and George M Whitesidesy Microcontact printing of self-assembled monolayers:applications in microfabrication; Nanotechnology 7 1996 452457.

[62] Milan Mrksich, Laura E. Dike, Joe Tien, Donald E. Ingber, and George M. Whitesides, Using Microcontact Printing to Pattern the Attachment of Mammalian Cells to Self-Assembled Monolayers of Alkanethiolates on Transparent Films of Gold and Silver Experimental cell research 1997 235, 305313 .

[63] Ammar Azioune, Nicolas Carpi,Qingzong Tseng,Manuel Thry, Matthieu Piel; Chapter 8Protein Micropatterns: A Direct Printing Protocol Using Deep Uvs , Methods in cell Biology , volume 97, 2010, Pages 133146 .

[64] Azioune A, Storch M, Bornens M, Thry M, Piel M; Simple and rapid process for single cell micro-patterning; Lab on Chip 2009 Jun 7;9(11):1640-2.

[65] Harris AK, Stopak D, Wild P. Fibroblast traction as a mechanism for collagen morphogenesis. Nature 1981 290:249-251

[66] Marganski WA, Dembo M, Wang YL (2003) Measurements of cell-generated deformations on flexible substrata using correlation- based optical flow. Meth Enzymol 361:197211

[67] Yang Z, Lin JS, Chen J,Wang JH. Determining substrate displacement and cell traction fields–a new approach. J Theor Biol 2006 242:607-616.

[68] U.S. Schwarz, N.Q. Balaban, D.Riveline, A. Bershadsky, B. Geiger and S.A. Safran; Calculation of Forces at Focal Adhesions from Elastic Substrate Data: The Effect of Localized Force and the Need for Regularization; Biophysical Journal 2002 1 September Volume 83 1380-1394, doi:10.1016/S0006-3495(02)73909-X

[69] Butler, J.P., Toli-Nrrelykke, I.M., Fabry,B., Fredberg, J.J.; Traction fields, moments, and strain energy that cells exert on their surroundings; Am. J. Physiol. Cell Physiol 2002 282, C595C605.

[70] du Roure O, Saez A, Buguin A, Austin RH; Force mapping in epithelial cell migration; Proc Natl Acad Sci U S A, 2005 102:2390-2395.

[71] Pelham RJ Jr, Wang Y. 1997. Cell locomotion and focal adhesions are regulated by substrate flexibility. Proc. Natl. Acad. Sci. USA 94:1366165.

[72] James H-C. Wang 1, and Bin Li; The principles and biological applications of cell traction force microscopy Microscopy: Science Technology Applications and Education 2007.

[73] Valentina Peschetola, Valrie M. Laurent, Alain Duperray, Luigi Preziosi, Davide Ambrosi, Claude Verdier; Traction forces of cancer cells; Computer Methods in Biomechanics and Biomedical Engineering 2011 14, S1 159-160; DOI 10.1080/10255842.2011.593954.

[74] Burton, K. Taylor, D. L.; Traction forces of cytokinesis measured with optically modified elastic substrat.; Nature 1997 385 450454 .

[75] Sabass B., Gardel, M.L., Waterman, C.M., Schwarz, U.S.: High resolution traction force microscopy based on experimental and computational advances. Biophysical Journal 2008 94 207220 ; doi:10.1529/biophysj.107.113670.

[76] Dembo M,Wang YL. Stresses at the cell-to-substrate interface during locomotion of fibroblasts. Biophysical Journal 1999 76:2307- 2316.

[77] Marie Versaevel, Thomas Grevesse1 and Sylvain Gabriele; Spatial coordination between cell and nuclear shape within micropatterned endothelial cells; Nature communications 2012 DOI: 10.1038.

[78] Justin R. Tse and Adam J. Engler; Preparation of Hydrogel Substrates with Tunable Mechanical Properties; Current Protocols in Cell Biology 2010 DOI: 10.1002/0471143030.cb1016s47.

[79] Eric A. Klein,Liqun Yin,Devashish Kothapalli,Paola Castagnino,Fitzroy J. Byfield, Tina Xu,Ilya Leventa, Elizabeth Hawthorne, Paul A. Janmey,and Richard K. Assoian; Cell-Cycle Control by Physiological Matrix Elasticity and In Vivo Tissue Stiffening; Current Biology 2009 19, 15111518; DOI 10.1016/j.cub.2009.07.069.

[80] Eric A. Klein, Liqun Yin, Devashish Kothapalli,Paola Castagnino,Fitzroy J. Byfield, Tina Xu, Ilya Levental, Elizabeth Hawthorne, Paul A. Janmey and Richard K. Assoian1; Cell-Cycle Control by Physiological Matrix Elasticity and In Vivo Tissue Stiffening; Current Biology 2009 19 DOI 10.1016/j.cub.2009.07.069.

[81] Masha Prager-Khoutorsky, Alexandra Lichtenstein1, Ramaswamy Krishnan, Kavitha Rajendran,Avi Mayo1, Zvi Kam, Benjamin Geiger and Alexander D. Bershadsky1; Fibroblast polarization is a matrix-rigidity-dependent process controlled by focal adhesion mechanosensing ; Nature Cell Biology 2011 DOI: 10.1038/ncb2370.

[82] M. Ghibaudo, A. Saez, L. Trichet, A. Xayaphoummine, J. Browaeys, P. Silberzan, A. Buguin, and B. Ladoux; Traction forces and rigidity sensing regulate cell functions; Soft Matter 2008 4:18361843, 2008.

[83] Alexander D. Bershadsky, Nathalie Q. Balaban and Benjamin Geiger; adhesion-dependent cell mechanosensitivity ; Annu. Rev. Cell Dev. Biol 2003. 19:67795

[84] Daniel A. Fletcher and R. Dyche Mullins; Cell mechanics and the cytoskeleton; Nature 2010 doi:10.1038;nature08908.

[85] Burridge K., and M. Chrzanowska-Wodnicka; Focal adhesions,contractility, and signaling; Annu. Rev. Cell Dev. Biol 1996 12:463518.

[86] Galbraith, C. G., and M. Sheetz. Forces on adhesive contacts affect cell function; Curr. Opin. Cell Biol 1998 10:566571.

[87] Qingzong Tseng, a Irene Wang, Eve Duchemin-Pelletier,Ammar Azioune, Nicolas Carpi,Jie Gao, Odile Filhol,Matthieu Piel,Manuel Thery and Martial Balland; A new micropatterning method of soft substrates reveals that different tumorigenic signals can promote or reduce cell contraction levels; Lab Chip 2011 11 DOI: 10.1039/c0lc00641f.

[88] Geiger B., A. Bershadsky, R. Pankov, and K. M. Yamada. Transmembrane crosstalk between the extracellular matrix and the cytoskeleton. Nat. Rev. Mol. Cell Biol. 2001 2:793805.

[89] Andrew D. Rape, Wei-hui Guo, Yu-li Wang;The regulation of traction force in relation to cell shape and focal adhesions; Biomaterials 2011 32 2043e2051; doi:10.1016/j.biomaterials.2010.11.044.

[90] Saez A, Buguin A, Silberzan P, Ladoux B ,Is the mechanical activity of epithelial cells controlled by deformations or forces?; Biophysical Journal 2005 89:L524.

[91] Wesley R. Leganta, Amit Pathak, Michael T. Yang, Vikram S. Deshpande, Robert M. McMeeking, and Christopher S. Chen; Microfabricated tissue gauges to measure and manipulate forces from 3D microtissues, PNAS 2009 June 23 volume 106 no 25 1009710102 doi 10.1073 .

[92] Britta Trappmann, Julien E. Gautrot, John T. Connelly,Daniel G. T. Strange, Yuan Li,Michelle L.Oyen, Martien A. Cohen Stuart, Heike Boehm6, Bojun Li, Viola Vogel,Joachim P. Spatz, Fiona M.Watt,and Wilhelm T. S. Huck; Extracellular-matrix tethering regulates stem-cell fate; Nature Materials Advance Online Publication DOI: 10.1038/NMAT3339.

[93] Kimura K, Kimura A; A novel mechanism of microtubule length-dependent force to pull centrosomes toward the cell center; Bioarchitecture 2011 March 1(2):74-79.

[94] Shinji Deguchi, Tsubasa S Matsui, Kazushi Iio; The position and size of individual focal adhesions are determined by intracellular stress-dependent positive regulation.; Cytoskeleton 2011 68(11):639-51. DOI: 10.1002/cm.20541.

[95] Martin, S.G., and Chang, F. New end take off: Regulating cell polarity during the fission yeast cell cycle; Cell Cycle 2005 (Georgetown,Tex) 4, 10461049.

[96] Courtney R. Terenna, Tatyana Makushok,Guilhem Velve-Casquillas,Damien Baigl,Yong Chen,Michel Bornens,Anne Paoletti,Matthieu Piel and Phong T. Tran1;Physical Mechanisms Redirecting Cell Polarity and Cell Shape in Fission Yeast; Current Biology 2008 November 25 18 17481753, DOI 10.1016/j.cub.2008.09.047.

[97] Olivier M Rossier1,Nils Gauthier Nicolas Biais1,Wynn Vonnegut, Marc-Antoine Fardin, Philip Avigan,Evan R Heller,Anurag Mathur, Saba Ghassemi, Michael S Koeckert,James C Hone and Michael P Sheetz; Force generated by actomyosin contraction builds bridges between adhesive contacts ; European Molecular Biology Organization 2010.

[98] Chen CS, Alonso JL, Ostuni E, Whitesides GM, Ingber DE ; Cell shape provides global control of focal adhesion assembly; Biochem Biophys Res Commun 2003 307: 355361.

[99] Christophore A. Lemmon, Lewis H. Romer; A Predictive Model of Cell Traction Force Based on Cell Geometry; Biophysical Journal 2010 Volume 99 doi:10.1016/j.bpj.2010.09.024.

[100] Shang-You Tee, Jianping Fu, Christopher S. Chen, and Paul A. Janmey; Cell Shape and Substrate Rigidity Both Regulate Cell Stiffness; Biophysical Journal 2011 Volume 100 doi: 10.1016/j.bpj.2010.12.3744.

[101] Britta Trappmann, Julien E. Gautrot, John T. Connelly, Daniel G. T. Strange, Yuan Li, Michelle L. Oyen, Martien A. Cohen Stuart, Heike Boehm, Bojun Li, Viola Vogel,Joachim P. Spatz, Fiona M.Watt, andWilhelm T. S. Huck1; Extracellular-matrix tethering regulates stem-cell fate; Nature materials 2012 DOI: 10.1038/NMAT3339

[102] Singhvi R, Kumar A, Lopez GP, Stephanopoulos GN, Wang DI, et al. Engineering cell shape and function. Science 1994 264: 696698.

[103] Falconnet D, Csucs G, Grandin HM, Textor M Surface engineering approaches to micropattern surfaces for cell-based assays; Biomaterials 2006 27: 30443063.

[104] Thery M ; Micropatterning as a tool to decipher cell morphogenesis and functions; J Cell Sci 2010 123: 42014213.

[105] Pan Z, Yan C, Peng R, Zhao Y, He Y, et al.Control of cell nucleus shapes via micropillar patterns; Biomaterials 2012 33: 17301735.

[106] Ma H, Hyun J, Stiller P, Chilkoti A non-fouling oligo(ethylene glycol)- functionalized polymer brushes synthesized by surface-initiated atom transfer radical polymerization; Adv Mater 2004 16: 338341.

[107] Azioune A, Storch M, Bornens M, Thery M, Piel M ; Simple and rapid process for single cell micro-patterning; Lab Chip 2009 9: 16401642.

[108] Gautrot JE, Trappmann B, Oceguera-Yanez F, Connely J, He X, et al. Exploiting the superior protein resistance of polymer brushes to control single cell adhesion and polarization at the micron scale. Biomaterials 2010 31: 50305041.

[109] Okano T, Yamada N, Okuhara M, Sakai H, Sakurai Y Mechanism of cell detachment from temperature-modulated, hydrophilic-hydrophobic polymer surfaces. Biomaterials 1995 16: 297303.

[110] Nagase K, Kobayashi J, Okano T ; Temperature-responsive intelligent interfaces for biomolecular separation and cell sheet engineering. J R Soc Interface 2009 6: S293S309.

[111] Schmaljohann D, Oswald J, Jorgensen B, Nitschke M, Beyerlein D, et al. Thermo-responsive pnipaam-g-peg films for controlled cell detachment; Biomacromolecules 2003 4: 17331739.

[112] Mizutani A, Kikuchi A, Yamatao M, Kanazawa H, Okano T Preparation of thermoresponsive polymer brush surfaces and their interaction with cells; Biomaterials 2008 29: 20732081.

[113] Nagase K, Watanabe M, Kikuchi A, Yamato M, Okano T ;Thermoresponsive polymer brushes as intelligent biointerfaces: Preparation via atrp and characterization; Macromol Biosci 2011 11: 400409.

[114] Ishida N, Biggs S ; Direct observation of the phase transition for a poly(nisopropylacryamide) layer grafted onto a solid surface by afm and qcm-d; Langmuir 2011 23: 1108311088.

[115] Plunkett KN, Zhu X, Moore JS, Leckband DE Pnipam chain collapse depends on the molecular weight and grafting density; Langmuir 2006 22: 42594266.

[116] Malham IB, Bureau L; Density effects on collapse compression and adhesion of thermoresponsive polymer brushes; Langmuir 2010 26: 47624768.

[117] Halperin A, Kroger M Collapse of thermoresponsive brushes and the tuning of protein adsorption; Macromolecules 2011 44: 69867005.

[118] Peng R, Yao X, Ding J Effect of cell anisotropy on differentiation of stem cells on micropatterned surfaces through the controlled single cell adhesion; Biomaterials 2011 32: 80488057.

[119] Liu H, Ito Y Cell attachment and detachment on icropatternimmobilized poly(nisopropylacrylamide) with gelatin; Lab Chip 2002 2: 175178.

[120] Takahashi H, Nakayama M, Itoga K, Yamato M, Okano T ; Micropatterned thermoresponsive polymer brush surfaces for fabricating cell sheets with well-controlled orientational structures; Biomacromolecules 2011 12: 14141418.

[121] Yamato M, Konno C, Utsumi M, Okano T ;Thermally responsive polymer-grafted surfaces facilitate patterned cell seeding and co-culture. Biomaterials 2002 23: 561567.

[122] Williams C, Tsuda Y, Isenberg BC, Yamato M, Shimizu T, et al. Aligned cell sheets grown on thermo-responsive substrates with microcontact printed protein patterns; Adv Mater 2009 21: 21612164.

124

Publications :

1. **Thermoresponsive micropatterned substrates for single cell studies**. Kalpana Mandal, Martial Balland, Lionel Bureau.- *PLoS one, May 31, 2012* .

2. **Geometrical cue influences cell internal tension distribution locally and globally**. Kalpana Mandal, Irne Wang, Martial Balland. - *In preparation.*

3. **Spatial correlation between actin generated forces and centrosome positioning.** Kalpana Mandal, Irne Wang, Martial Balland. - *In preparation.*

4. **Direct comparison of cell traction force on 2D micropattern with 3D micropillar.** Kalpana Mandal, Irene Wang, Martial Balland, Benoit Ladoux. - *In preparation.*

List of Figures